Methods to Develop Composite Action in Non-Composite Bridge Floor Systems: Fatigue Behavior of Post-Installed Shear Connectors

by

Hulya Kayir, B.S.C.E.

Thesis

Presented to the Faculty of the Graduate School of

The University of Texas at Austin

in Partial Fulfillment

of the Requirements

for the Degree of

Master of Science in Engineering

The University of Texas at Austin

May 2006

Methods to Develop Composite Action in Non-Composite Bridge Floor Systems: Fatigue Behavior of Post-Installed Shear Connectors

APPROVED BY
SUPERVISING COMMITTEE:

Michael D. Engelhardt

Richard E. Klingner

Dedication

To all the members of my wise, supportive, knowledgeable, and loving family

Acknowledgements

I would first like to express my deep gratitude to my academic advisors Prof. Michael D. Engelhardt and Prof. Richard E. Klingner, for their help, suggestions and encouragement throughout this study and during the writing of this thesis. I am grateful to Prof. Young-Kyu Ju and Gunup Kwon for their tremendous help. I would also like to thank the Texas Department of Transportation for their support.

The experimental work that went into this thesis would not have been possible without the help of the Ferguson Structural Laboratory staff: Blake Stasney, Dennis Fillip, Mike Wason, Mike Bell, and Eric Schell. I am grateful to them for sharing with me their expertise and patiently answering questions. I would also like to thank Joan Hanson, Roberto Bustamante, Ty Womble, and Austin Evetts for their assistance in the laboratory.

Special thanks to my professors at Purdue University for providing me with a solid background in civil engineering.

May 2006

Methods to Develop Composite Action in Non-Composite Bridge Floor Systems: Fatigue Behavior of Post-Installed Shear Connectors

Hulya Kayir, M.S.E.

The University of Texas at Austin, 2005

CO-SUPERVISOR: Michael D. Engelhardt

CO-SUPERVISOR: Richard E. Klingner

This thesis is a continuation of the work reported by Schaap (2004) and Hungerford (2004) as a part of TxDOT Project 0-4124. TxDOT Project 0-4124 aims to investigate structurally efficient, cost-effective, and practical ways to post-install shear connectors to increase the load carrying capacity of bridges originally designed as non-composite. Using a direct-shear test setup, the structural effectiveness of alternative post-installed shear connectors was evaluated through cyclic tests. Additional tests were conducted to examine the load-slip behavior of these post-installed shear connectors under monotonically increasing shear loads. The installation processes of each shear connection

method were also evaluated and their feasibility in a field application was determined.

This thesis presents results from 8 static tests, 20 high-cycle fatigue tests, and 10 low-cycle fatigue tests, conducted on post-installed shear connectors and the cast-in-place welded shear stud. Two post-installed shear connectors were determined to be structurally efficient and constructible and are recommended to be further tested in full-scale beam tests.

Table of Contents

xi

xii

List of Tables

xv

List of Figures

xxiii

CHAPTER 1
Introduction

1.1 OVERVIEW

An increasing number of bridges in the United States have design load capacities close to or below the loads expected to be imposed on them. As bridges age, it becomes uneconomical to maintain those whose capacity is significantly less than the expected load. In the United States, more than 80,000 bridges face replacement due to insufficient load-carrying capacity, size or geometry. Some 6000 of these bridges are located in the state of Texas alone (National Bridge Inventory 2006).

It is undesirable to replace bridges that are structurally sound and well-maintained, simply because they cannot meet projected demands. It would be more efficient and economical to keep such bridges in service by finding cost-effective ways of increasing their load capacities. For steel girder bridges, one way of doing this is by making their concrete decks act compositely with their underlying steel girders.

Composite construction has been used in bridges and buildings since the 1930's. It implies connecting one or more components of a structure so that they resist loads as a single unit, with a load-carrying capacity greater than what could be achieved if the components acted separately. In bridge construction, the steel girder and the concrete slab can be made to act together in flexure by installing

shear connectors between the girder and the slab (Viest et al. 1997), increasing the flexural capacity of the bridge by more than 50 percent [1].

In new bridge construction, composite action is typically achieved by welding shear connectors (shear studs) to the top flange of the steel girder and casting the slab on top. In non-composite bridges, on the other hand, composite action is achieved by using post-installed shear connectors. While such connectors are not common, they can be a promising, cost-effective alternative to the demolition of a bridge with an insufficient load rating. This study focuses on finding cost-effective, straightforward and practical ways to create composite action in bridges originally designed to be non-composite.

1.2   OBJECTIVES OF TxDOT PROJECT 0-4124

TxDOT Project 0-4124 aims to investigate structurally efficient, cost-effective, and practical ways to post-install shear connectors to increase the load carrying capacity of bridges originally designed as non-composite. The work required to fulfill the objectives of this study comprises eight tasks, shown in Figure 1.1 and listed here:

- Review the available technical literature to gain insight on composite beam design, shear connector behavior, and American Association of State Highway and Transportation Officials (AASHTO) composite design provisions.
- Survey typical bridges in the state of Texas that display non-composite behavior to develop a prototype bridge for the modeling of experiments.
- Select shear connectors to be tested based on structural effectiveness, constructability and cost.

---

[1] Engelhardt, M.D. and Klingner, R.E. (2002), Proposal for Project 0-4124, 2002

2

- Test single shear connectors under static loading: Identify shear connectors that display strength and stiffness comparable to those of a typical cast-in-place welded stud. Select shear connectors for further evaluation.
- Test the selected shear connectors in high-cycle fatigue: Select shear connectors to be further evaluated under full-scale composite beam testing.
- Test a full-scale composite beam to obtain information on load-deformation response, ultimate strength, and constructability.
- Make design recommendations for using post-installed shear connectors in steel bridges originally designed as non-composite.
- Submit a project report with study results and recommendations.

```
┌─────────────────────────────────────┐
│         Literature Review            │
└─────────────────────────────────────┘
                  ↓
┌─────────────────────────────────────┐
│   Survey of Typical Existing Bridges │
└─────────────────────────────────────┘
                  ↓
┌─────────────────────────────────────┐
│ Identify Methods for Post-Installing │
│              Shear Connectors        │
└─────────────────────────────────────┘
                  ↓
┌─────────────────────────────────────┐
│   Single Shear Connector Tests-Static│
└─────────────────────────────────────┘
                  ↓
┌─────────────────────────────────────┐
│  Single Shear Connector Tests-Fatigue│
└─────────────────────────────────────┘
                  ↓
┌─────────────────────────────────────┐
│    Full-Scale Composite Beam Tests   │
└─────────────────────────────────────┘
                  ↓
┌─────────────────────────────────────┐
│      Recommendations for Design      │
└─────────────────────────────────────┘
                  ↓
┌─────────────────────────────────────┐
│            Project Report            │
└─────────────────────────────────────┘
```
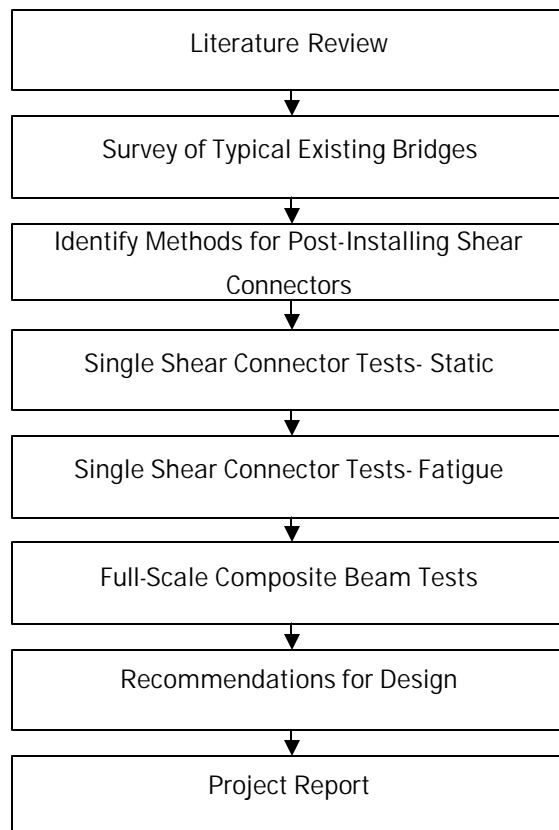
Figure 1.1: Research Tasks for TxDOT Project 0-4124

1.3   OBJECTIVES OF THIS THESIS

The primary objectives of this thesis are to evaluate the performance of candidate post-installed shear-connection methods under cyclic loads, and to recommend at least one for testing in the full-scale bridge deck. In composite bridge design not only static loading, but also cyclic loading is a concern due to the presence of moving vehicle loads. Therefore, post-installed shear connectors must have a long fatigue life. This thesis focuses on the fatigue life of shear connectors loaded in shear under service loads and overloads.   Secondary objectives include the following:

- Determine the load-slip behavior of shear connectors under static loading;
- Compare load-slip data to results of Schaap (2004) and Hungerford (2004);
- Summarize fatigue data collected by earlier researchers on cast-in-place welded shear studs;
- Compare the fatigue performance of post-installed shear connectors to that of welded shear studs;
- Evaluate the constructability of each considered shear-connection method; and
- Identify and recommend a shear-connection method that is structurally sound and constructible.

1.4   SCOPE OF THIS THESIS

This thesis is a continuation of the work reported by Schaap (2004) and Hungerford (2004) as a part of TxDOT Project 0-4124. Those studies, which focused on the responses of single shear connectors under static loading, recommend that particular post-installed shear-connection methods be studied

further under fatigue loading. That is the work described here. This thesis also addresses the ultimate static strength and load-slip behavior of those shear-connection methods.

This thesis consists of seven chapters plus several appendices. Chapter 2 provides a summary of AASHTO specifications on the design of shear connectors in composite bridges and background information necessary to assess the fatigue performance of these connectors. Chapter 3 summarizes the research of Schaap (2004) and Hungerford (2004) on field surveys, the static load-slip behavior of post-installed shear connectors, and the criteria used to recommend particular connectors for further study. In Chapter 4, the test setup is described; the mechanical properties of materials used in this study are provided; the installation process for each candidate shear connector is given; and testing procedures for static and cyclic tests are explained. Chapters 5, 6, and 7 respectively include data collected for cyclic and static tests; significance of those data; and a summary, conclusions, and recommendations for connection methods to be used in the full-scale beam tests.

CHAPTER 2

Background and Literature Review on the
Fatigue Behavior of Shear Connectors

2.1 INTRODUCTION

Fatigue is a primary cause of failure of metals that resist cyclic loading. Under fatigue loads a structural component can fail at stress levels well below its static ultimate strength, sometimes without warning. This is due to the propagation of a fatigue crack through the cross section of the component, which in time reduces the component's load carrying capacity, or can reach a critical size to initiate brittle fracture.

Shear connectors in composite bridge floor systems are subject to loading from moving vehicle loads, and are susceptible to fatigue. Therefore, it is essential in the design of composite bridges to ensure that shear connectors have adequate fatigue endurance as well as strength (Oehlers and Bradford 1999).

In this chapter, background information is provided on current design methods for shear connectors in composite bridges. Literature that has been published on the fatigue behavior of shear connectors is also summarized.

2.2 AASHTO PROVISIONS FOR SHEAR CONNECTORS IN COMPOSITE BRIDGES

AASHTO provides guidelines for the design of bridges in the U.S. Until recently only allowable stress design (ASD) and load factor design (LFD) were used in AASHTO provisions and made available through the publication, *AASHTO Standard Specifications for Highway Bridges*. Since 1994, *AASHTO LRFD Bridge Design Specifications* has also been published utilizing load resistance factor design (LRFD). Both sources have specifications for the design

6

of composite beams and shear connectors. From this point on, AASHTO Standard Specifications for Highway Bridges will be referred to as AASHTO ASD or AASHTO LFD in this thesis, depending on the type of design method discussed. AASTHO LRFD Bridge Design Specifications will be referred to as AASHTO LRFD.

In this section, the most recent requirements for the design of shear connectors in composite bridges are presented. Design requirements using AASHTO LRFD, AASHTO ASD and LFD will be discussed AASHTO specifications referenced in this thesis are AASHTO Standard Specifications for Highway Bridges 17th Edition (AASHTO 2002) and AASHTO LRFD Bridge Design Specifications 3rd Edition Interim 2005 (AASHTO LRFD Interim 2005).

2.2.1 Provisions for Shear Connectors in AASHTO Standard Specifications on Highway Bridges

Design requirements for shear connectors in AASHTO are the same for both ASD and LFD. Section 10.38 of AASHTO ASD deals with the design of composite girders and it is also referenced in Section 10.50 of AASHTO LFD. In Section 10.38 shear connectors are required to satisfy fatigue load and static load criteria separately. Shear connectors are typically first designed for fatigue loads and then checked for ultimate strength.

The design for shear connectors starts with an initial selection of the number of shear connectors needed in a bridge cross section. Next, the allowable range of horizontal shear force on a single welded stud (with a height-to-diameter ratio greater than or equal to 4), is calculated using Equation 2.1 (AASHTO ASD 10.38.5.1.1).

$$Z_r = \boldsymbol{a}\, d^2 \tag{2.1}$$

Where: α = 13,000 for 100,000 fatigue cycles

10,600 for 500,000 fatigue cycles

7,850 for 2,000,000 fatigue cycles

5,500 for over 2,000,000 fatigue cycles

d = diameter of stud (in.)

This equation is the result of the work done by Slutter and Fisher (1966); a study described in detail later in this chapter.

Since AASHTO provisions consider the effects of fatigue at service loads; the response of a composite bridge is calculated using elastic theory. This leads to the horizontal shear present per unit length of the beam, S_r, also known as shear flow, to be determined using Equation 2.2 (AASHTO ASD 10.38.5.1.1).

$$S_r = \frac{V_r Q}{I} \tag{2.2}$$

Where: V_r = range of shear at cross section due to live and impact loads
(kips)

Q = first moment of area of the transformed concrete section under compression, about the neutral axis of the composite section (in^3)

I = moment of inertia of the transformed composite section (in^4)

Once the shear strength of a welded stud and shear flow are determined, the spacing of shear connectors at a bridge cross section can be calculated with Equation 2.3 (AASHTO ASD 10.38.5.1.1).

$$s = \frac{\sum Z_r}{S_r} \leq 24 \; in. \qquad \qquad \textbf{(2.3)}$$

Where: s = required spacing (center-to-center) of shear connectors (in.)

ΣZ_r = the sum of the allowable range of horizontal shear on all connectors at cross-section (kips)

After the spacing of shear connectors are determined under fatigue provisions, this value must also be checked for ultimate strength requirements. These requirements utilize plastic theory. The force in the slab is taken as the smaller of either the ultimate strength of the steel in tension (Equation 2.4) or the ultimate strength of the concrete in compression (Equation 2.5) (AASHTO ASD 10.38.5.1.2).

$$P_1 = A_s F_y \qquad \qquad \textbf{(2.4)}$$

$$P_2 = 0.85 f_c' b t_s \qquad \qquad \textbf{(2.5)}$$

Where: P_1 = ultimate strength of steel (kips)

P_2 = ultimate strength of concrete in compression (kips)

A_s = area of steel including cover plates (in^2)

F_y = specified minimum yield strength of steel (ksi)

f_c' = 28 day compressive strength of concrete (ksi)

b = effective flange width (in.)

t_s = thickness of concrete slab (in.)

To determine the number of shear connectors required, the ultimate strength of single connector, S_u, is needed and is given in Equation 2.6 (AASHTO ASD 10.38.5.1.2). This equation was developed by Ollgaard et al. (1971) and suggests that the static strength of a shear connector depends on its diameter, the strength of concrete, the elastic modulus of concrete, and the tensile strength of the shear connector.

$$S_u = 0.4d^2\sqrt{f_c'E_c} \quad \leq 60{,}000A_{sc} \tag{2.6}$$

Where: d = diameter of stud

f_c'= 28 day compressive strength of concrete (ksi)

A_{sc} = area of shear connector (in^2)

E_c = modulus of elasticity of concrete (lb/in^2) given as in

Equation 2.7:

$$E_c = w^{3/2}33\sqrt{f_c'} \tag{2.7}$$

Where: w = unit weight of concrete (lb/ft^3)

Finally, the minimum required number of shear connectors at a cross section is calculated using Equation 2.8 (AASHTO ASD 10.38.5.1.2).

$$N_1 = \frac{P}{j\,S_u} \tag{2.8}$$

Where: N_1 = minimum number of connectors between points of

maximum positive moment and adjacent end supports

P = lesser of P_1 or P_2 (kips)

f = reduction factor = 0.85

General requirements are also given in AASHTO for shear connectors and are the same for both ASD and LFD design. Shear connectors are required to be mechanical anchors and "… shall be capable of resisting both horizontal and vertical movement between the concrete and the steel" (AASHTO ASD 10.38.2.2).   A minimum embedment depth of 2 in. is specified for shear connectors, with a minimum clear cover requirement of 2 in. (AASHTO ASD 10.38.2.3). Edge distance and longitudinal spacing requirements are also given in Section 10.38.2.4. The edge to edge clear distance between the girder flange and the shear connectors must be greater than 1 in. Also, adjacent shear connectors must be at least 4 in. apart on center (AASHTO ASD 10.38.2.4).

The location of shear connectors is discussed in AASHTO ASD Section 10.38.4.2. Shear connectors are to be placed in either positive moment regions or throughout the entire length of a bridge. In the case of a continuous span bridge, shear connectors may be placed in the negative moment regions if the reinforcing steel in the concrete is considered as part of the composite section (AASHTO ASD 10.38.4.2).

2.2.2 AASHTO LRFD Bridge Design Specifications on Shear Connectors

AASHTO LRFD follows the same design procedures as AASHTO ASD and LFD for shear connectors. A number of shear connectors in a cross section is chosen and the spacing (pitch) is determined based on fatigue provisions. The selected number of shear connectors is then checked for ultimate strength requirements. General provisions for shear connector design in AASHTO LRFD are the same as in AASHTO ASD.

AASHTO LRFD provisions enforce the use of somewhat different equations for determining the strength of a shear stud under fatigue and static loads compared to AASHTO ASD. Equation 2.9 shows the shear resistance of a single connector, Z_r, for fatigue loading, given in AASHTO LRFD Section 6.10.10.2. This equation is same as Equation 2.1, except with a lower limit, below which the connector is not expected to fail. Z_r has units of kips as in Equation 2.1.

$$Z_r = \boldsymbol{a}d^2 \geq \frac{5.5d^2}{2} \tag{2.9}$$

$$\boldsymbol{a} = 34.5 - 4.28\log N \tag{2.10}$$

Where: d = diameter of stud (in.)

N = number of fatigue load cycles specified in AASHTO LRFD Article 6.6.1.2.5 for a bridge with a design life of 75 years.

11

The unfactored shear strength of a shear connector, Q_n, is given in AASHTO LRFD Section 6.10.10.4.3 and is presented here as Equation 2.11.

$$Q_n = 0.5 A_{sc} \sqrt{f_c' E_c} \leq A_{sc} F_u \qquad \textbf{(2.11)}$$

Where: F_u = specified minimum tensile strength of a stud (ksi)

Note that Equation 2.11 is identical to Equation 2.6.

2.3   FATIGUE BEHAVIOR OF SHEAR CONNECTORS

This section summarizes literature published over the last several decades on the fatigue behavior of shear connectors. Early studies led to the development of current AASHTO fatigue design provisions for shear connectors. More recent publications have been geared towards optimizing or refining current design provisions.

In the following subsections, testing procedures, main results and conclusions of previous research on high-cycle fatigue and low-cycle fatigue behavior of shear connectors are presented. Testing procedures and results of all research discussed here served as a guideline and benchmark for experiments conducted as a part of this thesis.

2.3.1   Previous Research on Shear Connectors under High Cycle Fatigue

In AASHTO provisions prior the 1970's (AASHO at the time), fatigue did not govern the design of shear connectors in composite bridges. A composite member was designed to reach its ultimate flexural capacity before the shear connectors yielded. That is, shear connectors were designed for the interface shear computed based on elastic analysis of the transformed section, following the shear diagram for the member. That is, the shear flow was computed at ultimate load using Equation 2.2. Consequently, fatigue did not control shear connector design. The resulting design, however, was conservative and required a large

number of shear connectors to be placed along the span of a bridge (Slutter and Fisher 1966).

As design provisions proved to be uneconomical and inefficient, many researchers started focusing on ways to change the design of composite bridges so that the number of shear connectors could be reduced. This was accomplished by using plastic analysis to determine the interface shear at ultimate loads (Equations 2.4 and 2.5). This reduced the number of shear connectors needed for static ultimate loads on the bridge. However, this resulted in the need to consider the effect of fatigue loading on shear connectors. Since, the design provisions at the time relied solely on static strength tests, new research was required to assess the behavior of shear connectors under cyclic loading.

2.3.1.1 *Methods used for Testing Shear Connectors under High-Cycle Fatigue*

High-cycle fatigue is associated with the application of cyclic loads at service levels and fatigue failure after a high number of loading cycles. The types of tests that have typically been used to investigate the fatigue endurance of shear connectors are beam tests and push-out tests. Most fatigue tests have been conducted using push-out tests and their results are the basis for current AASHTO provisions. Although beam tests more accurately represent actual conditions on a bridge, the fatigue behavior of individual shear studs cannot be monitored. Further, beam tests are more costly than push-out tests. Push-out tests, on the other hand, can be constructed faster and closer inspection of the behavior of individual shear studs is possible (Slutter and Fisher 1966). This point, however, was challenged by Oehlers and Foley (1985) and later Gattesco and Giuriani (1996), who argued that push-out specimens do not provide a good indication of individual stud strength. They attribute this mainly to the boundary conditions used for the concrete and steel as well as the use of average values to determine

individual connector strength. Furthermore, they argue that the type of boundary conditions used in tests can influence the fatigue behavior of a shear connector.

In a push-out specimen two concrete slabs are typically attached to the flanges of a steel beam with shear connectors. Load is applied to the steel beam in cycles until the connectors fail in fatigue. Variations of push-out specimens have also been used. For example, specimens used by Slutter and Fisher (1966) consisted of only one concrete slab attached to a flange of a steel beam with four shear studs. In these tests, load was applied to the edge of the concrete block. Badie et al. (2002) used one L-shaped concrete slab attached to a steel beam.

Push-out tests have varied also in the number of shear studs used in each test. Typically four shear studs are welded on each side of a steel beam. Mainstone and Menzies (1967) chose to use only two studs on each side while Badie (2002) used eight shear studs for one group of specimens.

Almost all researchers prevented bond at the steel-concrete interface of test specimens. This was done to eliminate any additional composite action due to adhesion.

Typical instrumentation used for fatigue tests have consisted of strain gages, dial gages, and displacement transducers to measure slip and separation between concrete and steel and individual connector behavior. Lehman et al. (1965), Mainstone and Menzies (1967), and Badie (2002) applied an initial monotonic loading cycle to specimens prior to fatigue loading. Slip and separation were measured via dial gages and was typically used for comparison with data from supplementary static tests. Load and slip values were also taken intermittently throughout some tests (i.e., Roberts and Dogan 1997). Researchers such as Mainstone and Menzies (1967) and Badie (2002) took specimens that did not fail at the end of cyclic loading and tested them statically up to failure. Load-slip data was recorded during the monotonic loading of these specimens. Strain

gages have mainly been used in beam tests where they are attached under the top beam flange below shear studs. This helped researchers qualitatively determine when a shear stud failed (i.e., Toprac 1964).

Most tests for high-cycle fatigue have been load controlled (except Roberts and Dogan 1997 used displacement control), with typically a single stress range and loading frequency used for each specimen. The range of loading frequencies has been between 0.1 Hz used by Ryu (2003) and 8 Hz used by Slutter and Fisher (1966).

2.3.1.2 *Factors Influencing the Fatigue Life of Shear Connectors*

The main objective of most past research discussed here was to determine the factors that influence the fatigue endurance of shear connectors. For example, Lehman et al. (1965) conducted fatigue tests on 3/4-in. diameter studs in lightweight concrete to compare results to those for regular concrete. Slutter and Fisher (1966) investigated the effect of stress range, minimum stress, and load reversal on the fatigue life of 3/4-in. and 7/8-in. diameter studs. Similarly, Mainstone and Menzies (1967) looked into the effect of four different ratios of minimum to maximum shear. Badie (2002) focused on the testing of larger diameter studs (7/8-in. and 1-1/4-in. diameter) and their response to fatigue loads.

Slutter and Fisher (1965) and Lehman et al. (1965) found that stress range is the most important variable affecting the fatigue life of a shear connector. Stress range is defined as the difference between the maximum and minimum stress acting on a connector, where the average stress is calculated based on the effective tensile stress area of a stud. Minimum stress was observed to have an influence only for reversed loading cases (Slutter and Fisher 1966). Johnson (2000), citing the work of Oehlers (1990), states that the maximum load applied to a shear connector has a small influence below load levels that are about 60% of

the connector's static shear strength. Loading frequency was reported to be insignificant to the fatigue life of shear connectors (Nakajima 2003).

Slutter and Fisher (1966) found no significant difference between the behavior of 3/4-in. and 7/8-in. diameter studs. Badie et al. (2002), found 1-1/4-in. diameter studs to have longer fatigue lives compared to 7/8-in. diameter studs. They also determined that 1-1/4-in. diameter studs did not fail at stress ranges below 16 ksi and 7/8-in. diameter studs did not fail at stress ranges below 15 ksi.

Concrete strength was found to not have a significant effect on fatigue life (Slutter and Fisher 1966). Mainstone and Menzies (1967) determined that the deformation and strength of concrete to an extent influences the stresses at the weld of a stud. They believe the influence will be increased for a more flexible connector. The study by Lehman et al. (1965) showed no significant difference between the fatigue behavior of shear connectors (3/4-in. diameter) in lightweight and regular concrete.

Lehman et al. (1965) indicate that no direct relationship can be drawn between the slip and fatigue life of a shear connector, however, distinct slip characteristics can be observed under fatigue loading. They report an initial gradual increase in slip followed by leveling of the slip curve with little increase up to failure. A sudden increase in the rate of slip was observed as specimens reached failure, which they believe can be used as a failure criterion in both beam and push-out tests. Roberts and Dogan (1997) indicate that the sudden increase in slip occurs simultaneously with the propagation of fatigue cracks through a connector, which leads to a reduction in stiffness. For a constant stress range, Mainstone and Menzies (1967) observed reduction in the range of slip with increasing load ratio (increasing mean load).

Early beam tests suggested that no direct relationship exists between the static and fatigue strength of shear connectors (King et al. 1965, and Toprac

16

1965). This was later determined also by Slutter and Fisher (1966) and became the basis for AASHTO provisions, where the static strength of a connector is treated separately from its fatigue strength. This concept was later challenged by Mainstone and Menzies (1971), Oehlers and Foley (1985), and Oehlers (1990) who found that the ultimate strength of a connector decreases once fatigue loads are applied.

Slutter and Fisher (1966) suggested that most connectors in a bridge experience loading in one direction. Mainstone and Menzies (1967) and Oehlers (1995), on the other hand, believe that reversed loading occurs along the span of a bridge except at supports. As the center of each span experiences complete load reversal, the maximum load at the supports is twice the maximum load at midspan (Mainstone and Menzies 1967). They also state that a shear connector in a bridge is subjected to both horizontal shear forces and tensile forces. The tensile forces are due to "… vertical uplift forces which result from the tendency of the slab to assume locally different curvatures from those of the steel" (Mainstone and Menzies 1967). This point was later proved by Nakajima (2003) as a result of push-out tests. Shear connectors subjected to reversed loading cycles were determined to have longer fatigue lives compared to unidirectional tests (Slutter and Fisher 1966). Nakajima (2003) conducted both unidirectional and reversed load tests on 1/2-in. diameter studs and found that reversed loading becomes critical only if the connector material is pushed beyond its elastic limit.

2.3.1.3 *Failure Mode of Shear Connectors*

According to Oehlers and Foley (1985), for a given stress range, the propagation rate of a fatigue crack through a connector can be assumed to be almost constant. They indicate that the fatigue life of a connector depends on its

17

uncracked area. Once the applied maximum load in a fatigue cycle exceeds the residual strength of the uncracked portion of a connector, failure occurs.

Failure in push-out specimens has usually been defined as one or more of the concrete slabs separating completely from the steel beam. Lehman et al. (1967) report complete failure usually in only one of the concrete slabs. Deterioration and fracture of shear studs was observed in the second concrete slab as well; however; complete separation was not usually achieved.

Two main types of fatigue failure have been observed as a result of experiments. The most common failure mode is the fatigue failure at the interface between the weld pool and beam flange; in some cases removing some of the beam material. The second failure mode is described as the failure at the weld collar-stud shank interface.   In some cases this was observed for high stress ranges (Lehman et al. 1965). It has also been observed at higher stress ranges that shear studs closer to the applied load failed in fatigue first.   The remaining connectors sheared off as the applied load exceeded their ultimate static strength. For lower stress ranges, on the other hand, load was more evenly distributed and all studs failed in fatigue (Slutter and Fisher 1966). Mainstone and Menzies (1971) also found that for tests with high maximum load the fracture of studs were due to shear. When maximum load was low and loading range was high, little deformation of the stud or concrete was associated with fracture. Badie et al. (2002) experienced failure of the base plate due to the testing of 1-1/4-in. diameter studs. They concluded that if large diameter studs are to be used, the flange thickness needs to be increased to prevent such a failure. Stud failure reported by all researchers was accompanied with local damage in the surrounding concrete.

2.3.1.4 Test Results

Stress range (S)-number of cycles to failure (N) data reported by Thurlimann (1959), Slutter and Fisher (1966), Lehman et al. (1967), Mainstone and Menzies (1967), Badie (2002), and Ryu et al. (2003) are presented in Figure 2.1. This figure only includes data from uni-directional push-out tests conducted for high-cycle fatigue on 3/4-in. and 7/8-in. diameter studs. Data from push-out tests were used, since they are more conservative compared to beam tests. Both stud diameters are presented due to their similar behavior as suggested by Slutter and Fisher (1966). Stress ranges used by these researchers ranged between 8 ksi and 25 ksi with fatigue lives ranging from 6000 to over 10 million cycles. Specimens that did not experience fatigue failure are shown as runout tests with arrows adjacent to the corresponding data points. This S-N plot was used as a benchmark for high-cycle tests performed as a part of this thesis.
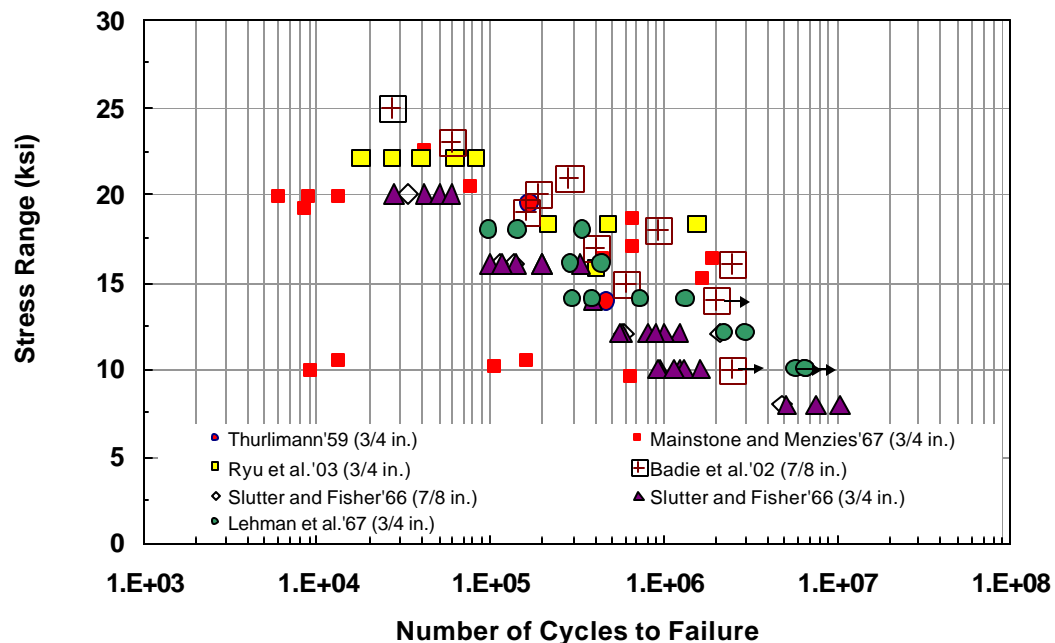
Figure 2.1: S-N data for push-out tests

19

King et al. (1962) and later Slutter and Fisher (1966) found that push-out tests give a lower bound for connector failure, as compared to beam tests, and can therefore be considered conservative. Mainstone and Menzies (1967) did not find push-out tests to underestimate beam test results. However, Roberts and Dogan (1997) later confirmed that fatigue strength of shear connectors to be significantly higher for beam test, agreeing with Slutter and Fisher (1966).

As a result of push-out tests conducted by Slutter and Fisher (1966) the relationship between the number of fatigue cycles, N, to failure for a given stress range, for a small diameter shear connector is presented as Equation 2.13. This equation conservatively ignores data obtained from reversed load tests.

$$LogN = 8.072 - 0.1753 S_r \qquad \textbf{(2. 13)}$$

Where: S_r = range of shear stress (ksi)

Based on the fact that push-out tests underestimate results from beam tests, Slutter and Fisher (1966) used push-out test results to derive a conservative design equation for shear connectors. The derived equation has been the basis for current AASHTO (both ASD and LRFD) design provisions for small diameter shear connectors (less than or equal to 7/8-in.) and is presented here as Equation 2.12.

$$Z_r = \boldsymbol{a} d_s^{\,2} \qquad \textbf{(2.12)}$$

Where: Z_r = allowable range of shear force per stud

α = 13,800 for N = 100, 000 cycles

10,600 for N = 500, 000 cycles

7,850 for N = 2,000,000 cycles

The design recommendations made by Slutter and Fisher (1966) enabled the uniform spacing of shear connectors along the length of a bridge. This was followed by a significant reduction in the number of shear connectors used in design and reduction in construction costs.

While most research focused on the fatigue endurance of shear connectors, some researchers such as Oehlers and Foley (1985) and Oehlers (1990) focused on the strength of shear connectors after applications of fatigue loads. Contradicting the earlier belief of researchers such as Slutter and Fisher (1966), they believe that the fatigue and static behavior of shear connectors are related. The analytical work of Oehlers and Foley (1985) and the experimental work of Oehlers (1990) showed that the fatigue life of a shear connector decreases the as soon as fatigue loads are applied. They propose changing the design of shear connectors in bridges to account for the reduction in static strength due to fatigue.

2.3.2 Previous Research on Shear Connectors under Low Cycle Fatigue

Factors that influence the fatigue life of shear connectors have been widely studied in the past several decades. Research suggests that the endurance of shear connectors to cyclic loads depends mostly on the stress range applied to them. However, almost all research has focused on loading cases in which shear connectors deform within their elastic range. Only in recent years, studies have focused on cases where connectors are loaded into their inelastic range. These studies show that loading shear connectors into their inelastic range results in a low number of cycles to reach failure; a phenomenon called low-cycle fatigue. Although a composite bridge would typically undergo high-cycle fatigue under service loads, researchers are starting to believe that shear connectors could experience low-cycle fatigue due to recurring overloads; especially in the case of partial composite interaction. Oehlers and Foley (1985) suggest that "the peak load or an occasional overload does not affect the rate of fatigue crack propagation, but it does affect the endurance [of a shear stud] by limiting the amount of fatigue cracking that can occur before the stud fractures."

Currently, partial composite interaction is not allowed in bridge design codes due to the associated increase in connector deflections. Gattesco et al. (1997) believe that increased deflections could force connectors into their inelastic range, in the case of overloads. However, they stress the practical and economical advantages of partial composite interaction and have led the research in low-cycle fatigue testing of shear connectors. As mentioned earlier, Oehlers and Foley (1985) and Oehlers (1990) conducted theoretical and experimental research on the relationship between the fatigue and static strength of shear connectors. Oehlers and Seracino (1998) indicate that with the application of fatigue loads, the stiffness of a shear connector decreases, eventually reducing the state of the bridge to partial composite interaction. Therefore, they believe that the research by Gattesco et al. (1997) does not only apply to bridges with partial composite interaction, but also to bridges with full interaction.

Gattesco et al. (1997) suggested that inelastic behavior of shear connectors change the structural response of a bridge in two ways:

1. Reduction in load amplitude: As the number of loading cycles increase the load amplitude experienced by shear connectors reduces with time (Figure 2.2 (b)). This is a result of load redistribution.

2. Load reversal: This usually occurs when connectors, typically at beam supports, yield while the rest of the beam behaves elastically. Load reversal is experienced if the recovered slip required by the beam is greater than the slip a yielded connector can recover by unloading (Figure 2.2 (c) and Figure 2.3).
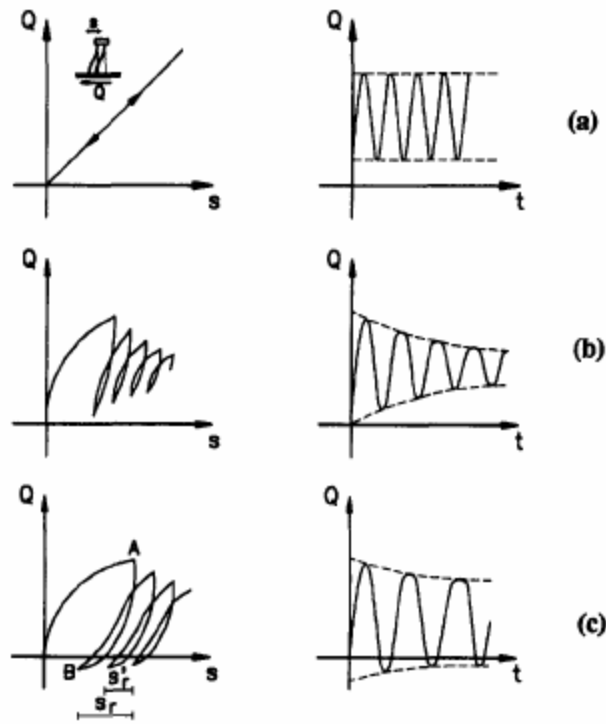
Figure 2.2: Load (Q)-Slip (s) and Load (Q)-Time (t) curves of a shear connector in a structure: (a) Elastic behavior; (b) Inelastic behavior; (c) Inelastic behavior with reversed loading (Gattesco et al. 1997)

Due to the difficulty in capturing the effects of load redistribution between shear connectors, researchers believe high-cycle and low-cycle fatigue should differ in the way they are studied. While high-cycle fatigue is usually studied using load control, low-cycle fatigue is typically studied using a displacement control approach. With displacement controlled tests the "slip-history" of a shear connector gains importance (Gattesco et al. 1997). The following is a summary of experimental programs conducted by Gattesco et al. (1997) and Gattesco and Giuriani (1996) on the low-cycle fatigue of shear connectors.
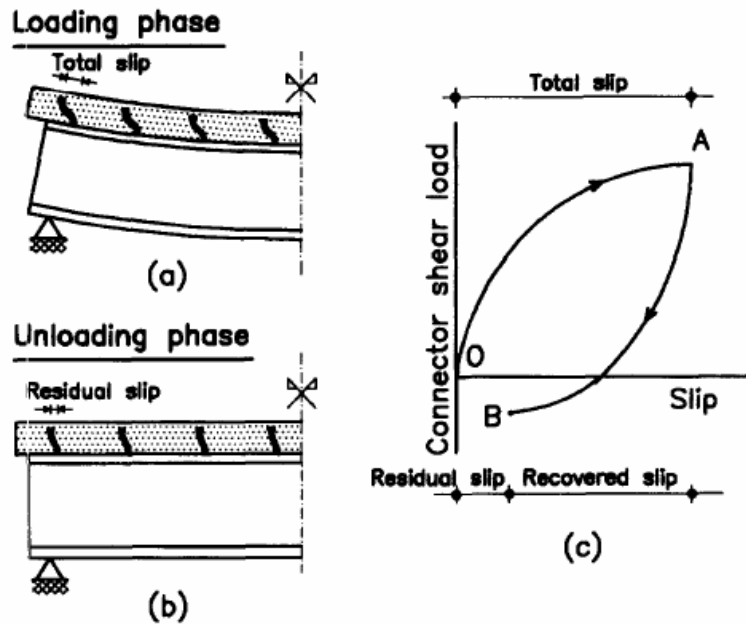
Figure 2.3: Connector load-slip relationship (Gattesco and Giuriani 1996)

N. Gattesco and E. Giuriani (1996)

The main goal of the tests performed by Gattesco and Giuriani (1996) was to investigate the behavior of shear connectors under reversed shear loading. The authors devised a direct-shear test setup to eliminate the issues related to push-out tests. The advantages of a direct-shear test setup are discussed in Chapter 3. Tests were performed by applying blocks of loading cycles with varying ranges of shear. Load cycles were applied at a rate of 500 N/s and the accumulated damage was monitored after each loading cycle. Each block of cycles ended when the slip increment, Δs, reached either a null or a constant value. For unidirectional tests, Δs was found to increase during initial cycles and later tend to a constant value. On the other hand, for reversed load tests, a more rapid deterioration was reported

of the stud shank and the concrete in front of the stud. In this case, Δs was observed to grow with each loading cycle.

Over 300 cycles, the authors also reported a 15 to 25 % reduction in the slope of the unloading branch of the load-slip curve. This suggests that the recovered slip increases with each cycle. This is expected due to the accumulation of damage and loss of stiffness of the connector and concrete after each loading cycle (Gattesco and Giuriani 1996).

Gattesco et al. (1997)

The purpose of experiments by Gattesco et al. (1997) was to assess the performance of shear connectors under low-cycle fatigue. The authors believe that especially for long-span composite beams with partial composite interaction, slip at the steel-concrete interface can reach values that would force shear connectors into inelastic deformations. This would cause some connectors in the composite beam to fail after only a small number of cycles.

To determine the low-cycle fatigue endurance of shear stud connectors, the authors used a displacement control approach where they determined the fatigue life of a connector with a given slip history. The slip history used for the connectors was determined analytically in a previous study by Gattesco and Giuriani (1990). The authors believe the amount of deformation a shear connector experiences beyond its elastic range depends on the amount the whole beam deforms, which reaches a constant value after a certain number of cycles. The numerical analysis by Gattesco and Giuriani (1990) showed that the maximum and minimum slip of a connector occurred after 20 cycles of loading. The initial maximum and minimum values of slip before 20 cycles were found to be 2/3 of the corresponding final maximum and minimum slip values ($2/3s_{max}$ and $2/3s_{min}$). The ratio of maximum to minimum slip was found to be 0.5. The

approximated envelope for the maximum and minimum slip and slip history are shown in Figure 2.4.
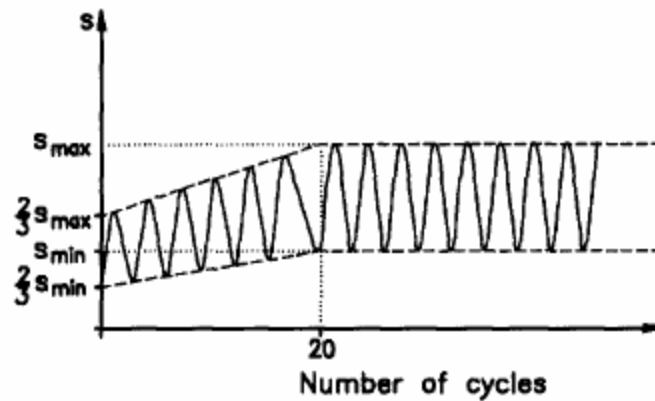
Figure 2.4: *Approximated envelope of maximum and minimum slip (Gattesco et al. 1997)*

Gattesco et al. (1997) conducted eight direct shear tests with 3/4-in. diameter shear studs under low-cycle fatigue. A direct-shear test setup was used instead of a push-out test. For each test only one shear connector was tested quasi-statically at 0.1 Hz and slip values were monitored by two LVDT's. Reduction in maximum applied shear load was also recorded to show the effects of increasing stud damage. The maximum induced slip values and corresponding number of cycles to failure are shown in Table 2.1.

Table 2.1: Maximum slip used for each specimen and corresponding number
of cycles to failure (Gattesco et al. 1997)

Specimen Number	Maximum slip (mm)	Number of cycles
1	0.80	38,338
2	1.00	18,400
3	1.00	13,200
4	1.25	5,274
5	1.50	3,040
6	2.00	3,230
7	2.00	1,440
8	3.00	432

The authors found that as the maximum slip value exceeded 1mm, the fatigue life of the connectors were lower than 10,000 cycles. The corresponding shear load at every displacement cycle was also found to reduce at the beginning of each test due to concrete damage around the stud. Fatigue failure was observed through the stud shank (Gattesco et al. 1997).

CHAPTER 3

Previous Work on TxDOT Study 0-4124

3.1 INTRODUCTION

This thesis documents the continuation of investigations started by Schaap (2004) and Hungerford (2004) on TxDOT Study 0-4124 on "Methods to Develop Composite Action in Non-Composite Bridge Floor Systems." The purpose of the work done by these researchers was to first identify possible post-installed shear connectors to create composite action in non-composite bridges. Once candidate connectors were identified, they were evaluated based on their static load-slip behavior in shear, as well as on constructability, practicality, and cost. To familiarize the reader with the previous work leading up to this thesis, this chapter provides a brief summary of the work completed by those researchers

The following sections include a summary of previous field surveys conducted, description of shear connectors identified as possible retrofit methods, test specimens and setup, summary of test results, and previous recommendations for further testing. The reader can refer to the theses by Schaap (2004) and Hungerford (2004) for additional information on all items discussed here.

3.2 DEVELOPMENT OF EXPERIMENTAL PROGRAM

A first step in the overall research program was to conduct a field survey of typical bridges that might be candidates for strengthening by the addition of shear connectors. The purpose of the survey was to collect data on the overall characteristics and condition of the bridges. This section summarizes the field survey conducted by Schaap (2004) and Hungerford (2004), their observations,

and the friction tests they performed to quantify the level of friction present at the steel girder-concrete slab interface of candidate bridges.

3.2.1 Survey of Candidate Bridges

A field survey of six bridges located north of San Antonio, Texas was conducted based on visual inspection. These bridges were originally designed and constructed as non-composite and were identified by TxDOT as candidates for retrofitting for composite action. Observations were made on the geometry of these bridges as well as their general condition. Information collected on the bridges included:

- age of bridge
- type and dimensions of structural elements
- support conditions and expansion joints
- general condition of slab and girder
- condition of slab-girder interface
- visual indications of deterioration and distress

The bridges had 4 or 9 spans with span lengths varying from 50 to 60 ft. Slab thicknesses were observed to vary between 8 to 9 in. Girders were steel rolled wide flange shapes, with transverse spacing varying from 6.75 ft. to 8 ft. and with depths of 28 in. to 36 in. Based on the information gathered on the geometrical properties of these bridges, the researchers created a prototype bridge representative of a typical non-composite TxDOT bridge. This provided the researchers with a model on which test specimens were based. The prototype also aided in finite element analyses and construction cost comparisons. The prototype bridge was designed as a 50 ft. simply supported non-composite bridge with cross sectional properties shown in Figure 3.1 (Hungerford 2004).
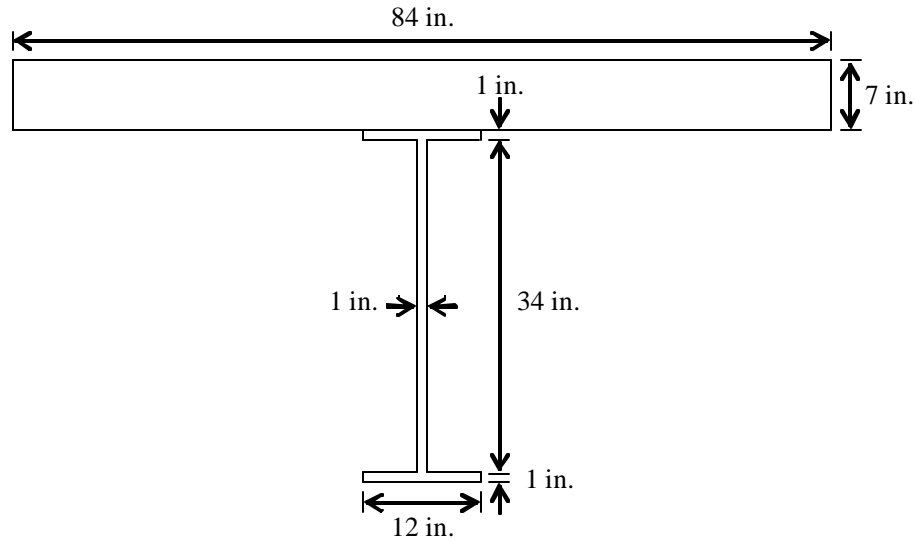
Figure 3.1: Cross section of prototype bridge (Hungerford 2004)

As a result of inspections all bridges were found to be in relatively good condition. They were all built in the late 1950's or 60's. In some cases, corrosion of steel girders and spalling of concrete slab were observed. Typical locations where corrosion was observed was at diaphragms, expansion joints, girder flanges embedded in concrete, and in some cases the slab-girder interface.

3.2.2   Friction Tests

The shear force transfer mechanism of several retrofitting options investigated in this study depends on the friction present at the girder-slab interface. Although the coefficient of static friction (μ) between rolled steel and concrete is stated as 0.7 (Section 11.7.4.3 of the American Concrete Institute Code 318-02), weathering can adversely affect the surface conditions of the steel and concrete and reduce the friction between them. It was important to the

30

researchers to have data on coefficient of friction still available in these candidate bridges. Field friction tests were conducted to establish a value for μ as well as to assess the effectiveness of retrofitting options that depend on friction. As a result of field tests, a conservative value for μ was suggested to be 0.4 (Schaap 2004, Hungerford 2004).

3.3   TYPES OF SHEAR CONNECTORS INVESTIGATED

The shear connectors tested by Schaap (2004) and Hungerford (2004) transfer horizontal shear between the concrete slab and the steel girder utilizing at least one of three force-transfer mechanisms: bearing, friction, and adhesion. A total of 13 post-installed shear connection methods were investigated of which 11 were tested under static loading. In this section the 11 connection methods (Figure 3.2) and the standard cast-in-place welded shear stud are introduced and their recommended installation process in a non-composite bridge is described.

Figure 3.2: Post-installed shear connectors investigated by Schaap (2004) and
Hungerford (2004)

3.3.1 Cast-in-Place Welded Stud (CIPST)

The welded stud is the most common shear connector used in modern composite bridge construction. It is a headed round steel bar that is welded to the top flange of a steel girder with a stud welding gun. The welding end of the stud is melted by an electric arc created between the flange and the stud. A porcelain ferrule is provided with each stud that controls the flow of molten metal and concentrates the heat in the weld area. The result is a weld that is stronger than the stud material (Viest et al. 1958).

Once the studs are welded, the concrete slab is cast (Figure 3.3). The stud then transfers horizontal shear by bearing against the concrete. The shear stud is subject to both bending and shear. The head of the stud also prevents the uplift of the slab relative to the girder. The cast-in-place shear stud was used as a

benchmark by the researchers with which all other post-installed connectors were compared.
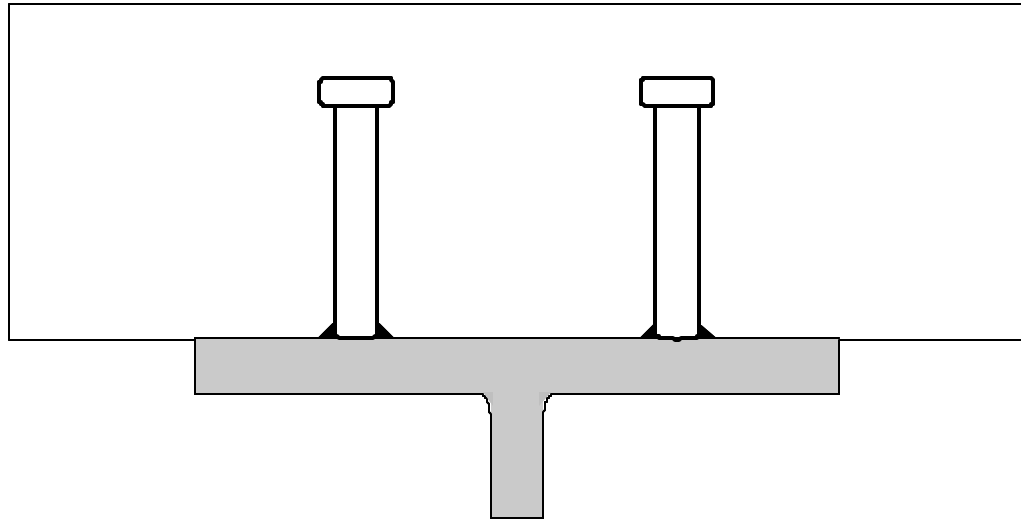
Figure 3.3: Cast-in-place Welded Stud

3.3.2 Post-Installed Welded Stud (POSST)

This method also uses the welded shear stud; however; the stud is installed after the concrete slab is in place. This requires coring a hole through the concrete slab to allow enough space for a shear stud and stud welding gun to fit. Once the hole is cored, the top flange of the girder is cleaned and the stud is welded. The hole is then filled with non-shrink grout (Figure 3.4). After the grout cures, the stud transfers horizontal shear loads between the slab and the girder by bearing (Schaap 2004).
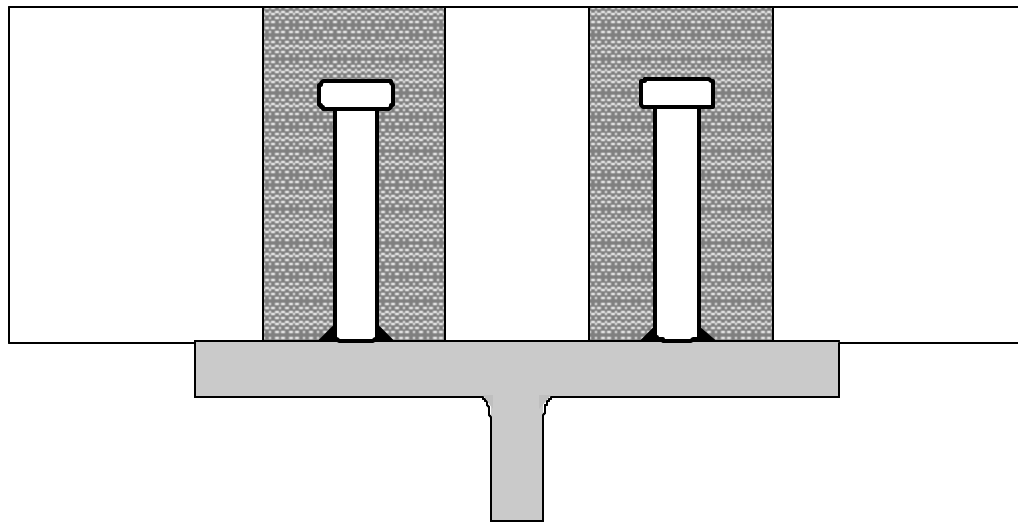
Figure 3.4: Post-Installed Welded Stud

3.3.3   Stud Welded to Plate (STWPL)

This method is a variation on the POSST method, as shown in Figure 3.5. The POSST method entails welding a stud directly to the top flange of an existing girder. The stud in the STWPL method, on the other hand, is welded to a separate plate that is then fillet welded onto the side of the girder. A smaller diameter hole is required in the slab than that for the POSST method, since the stud is shop-welded to a separate steel plate. This also permits the hole in the slab to be drilled from either above or below the bridge prior to welding the steel plate. After the connector is in place, the hole is filled with non-shrink grout. As in other methods using the shear stud, shear forces are transferred by bearing of the stud on the concrete (Schaap 2004).
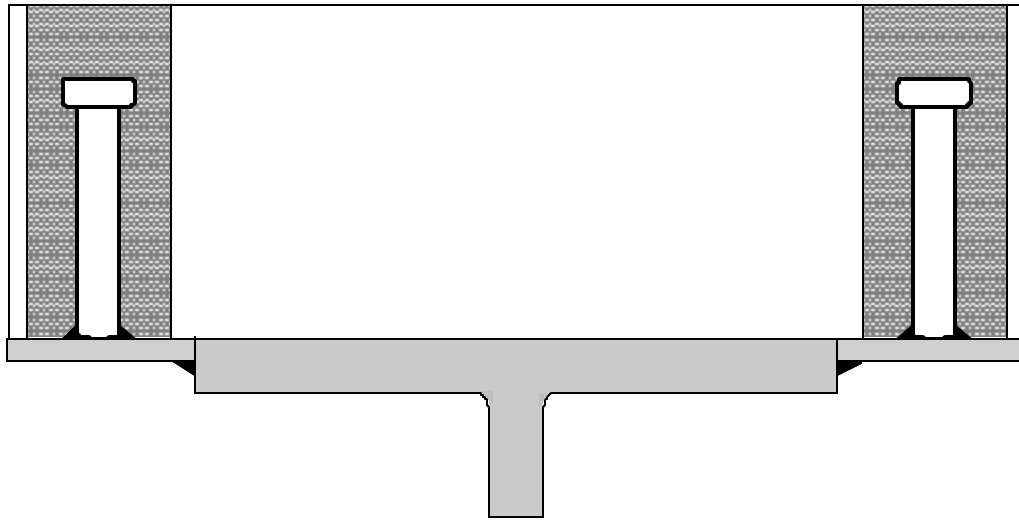
Figure 3.5: Stud Welded to Plate

3.3.4   Double-Nut Bolt (DBLNB)

The connector used in this method is a high strength ASTM A325 or A490 bolt. The installation of this connector requires drilling holes through both the concrete slab and the steel girder. The connector is then inserted in the hole and is held in place by two nuts. A bottom nut is placed and tightened while the two top nuts prevent the rotation of the connector. Once the connector is in place the hole is filled with non-shrink grout (Figure 3.6). Shear forces between the bolt and the girder are first resisted by friction. Once this friction is overcome, the bolt comes into bearing with the girder flange. Horizontal shear between the bolt and the concrete is transferred by bearing.

35
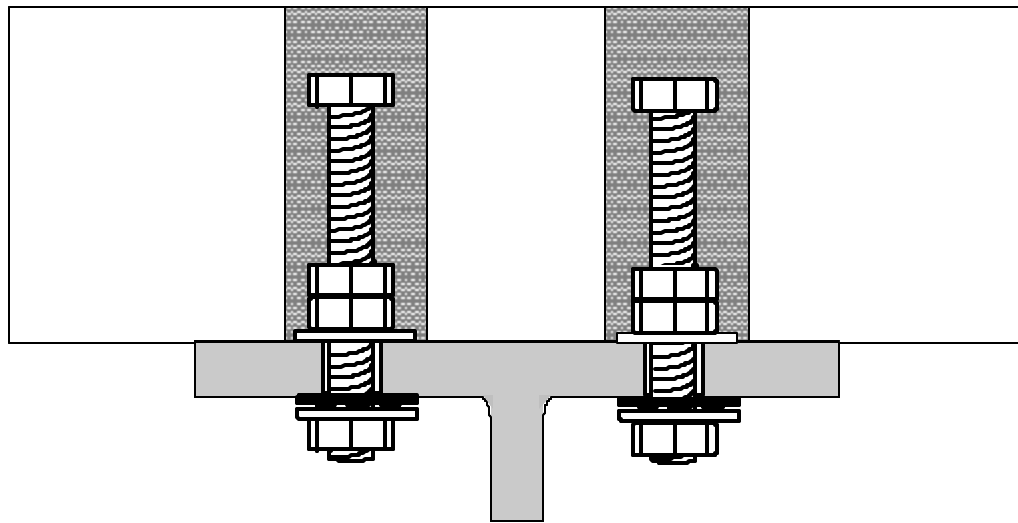
Figure 3.6: Double-Nut Bolt

3.3.5   High-Tension Friction Grip Bolt (HTFGB)

With this method, the concrete slab and the steel girder are clamped together with a high-strength A325 or A490 bolt. Shear force between the concrete and the steel is initially transferred through friction.   Once friction is overcome, shear force is transferred through bearing.

To install this connector, two different size holes are match-drilled through the concrete slab. The smaller of the two holes can be drilled from under the bridge after a hole is drilled through the top girder flange.   The bolt is inserted from the top of the bridge and tightened from underneath up to the required pretension. The remaining hole at the surface of the slab is later filled with non-shrink grout (Figure 3.7) (Schaap 2004).
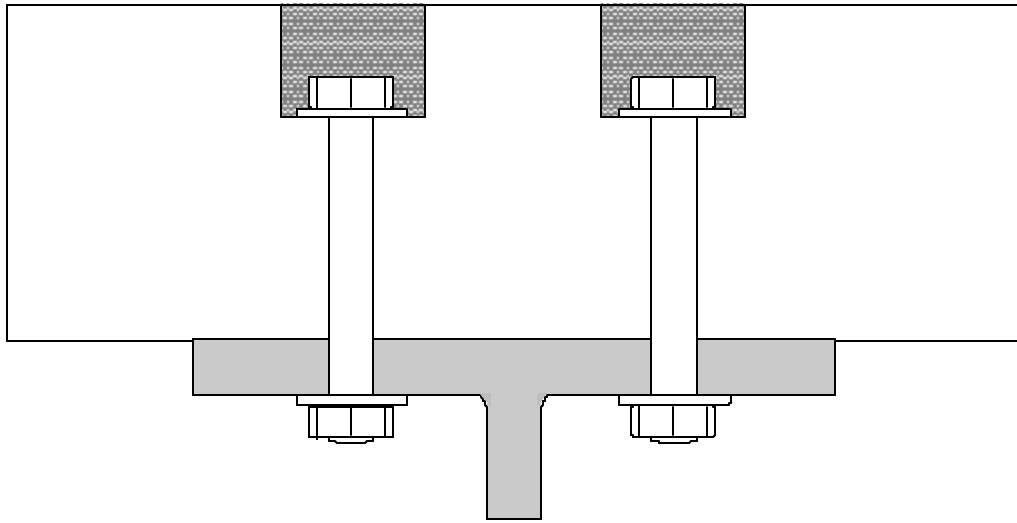
Figure 3.7: High-Tension Friction Grip Bolt

3.3.6   Expansion Anchor (KWIKB)

For this connector, holes are drilled through both the girder flange and the concrete slab from the bottom of the bridge. The anchor is then tapped into the hole and tightened (Figure 3.8). The expansion anchor is another connector that initially utilizes friction to transfer shear forces between the slab and the girder. Once friction at the steel-concrete interface is overcome with increasing load, the connector moves in the hole and transfers shear forces through bearing (Schaap 2004).
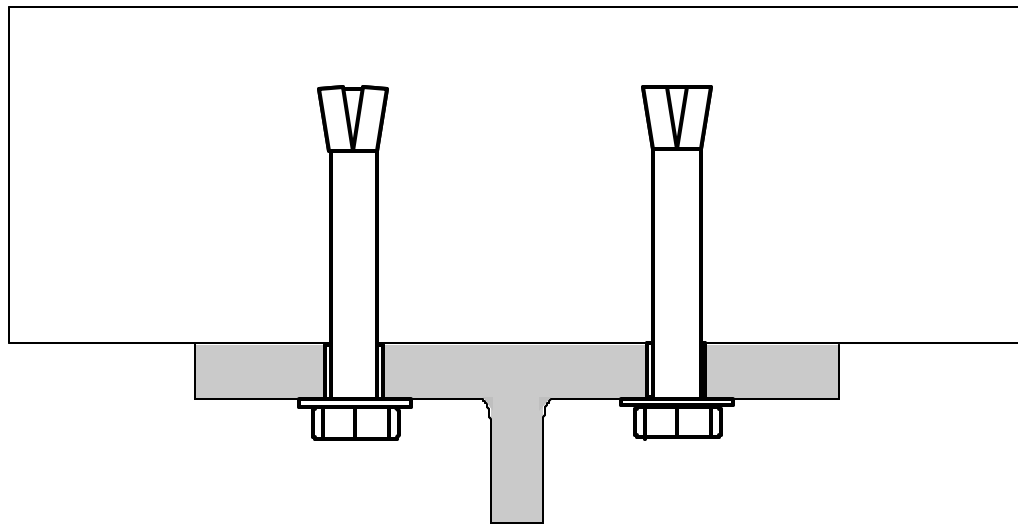
Figure 3.8: Expansion Anchor

3.3.7   Undercut Anchor (MAXIB)

The undercut anchor, like the expansion anchor, transfers shear forces initially through friction followed by bearing. The connector is installed by first drilling holes through the girder then the slab from under the bridge. The hole in the slab is later undercut using a special undercutting drill. The connector is set with a special setting device and the nut is tightened until the required pretension is reached (Figure 3.9) (Schaap 2004).
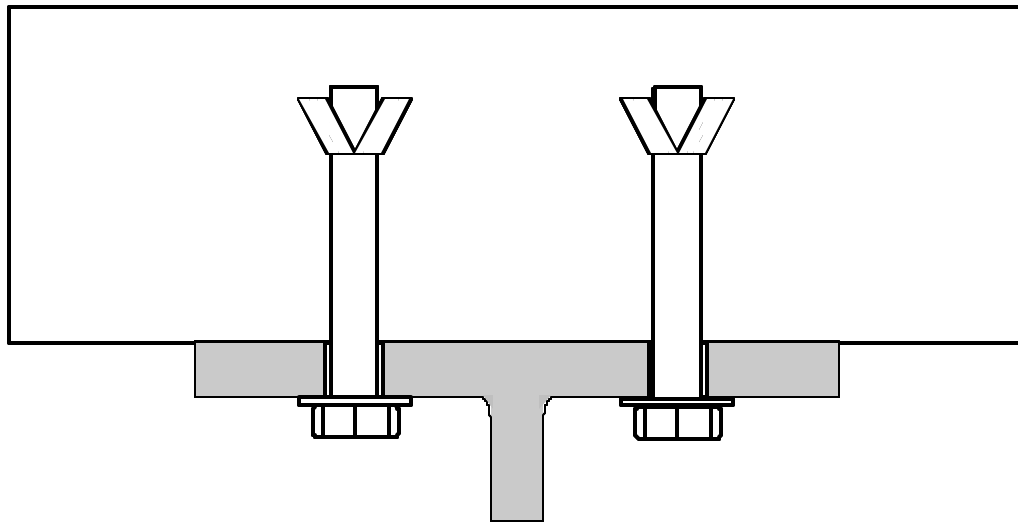
Figure 3.9: Undercut Anchor

3.3.8 Welded Threaded Rod (POSTR)

As shown in Figure 3.10, this method is another variation on the POSST method. A hole is cored through the concrete slab and a fully threaded rod is welded onto the steel girder. Prior to grouting, a sheath is placed around the rod to prevent grout from filling the threads. The hole is grouted leaving room for a washer and a nut. The sheath is later removed and the nut is tightened. As a result, the rod transfers shear forces first by friction, and then by bearing once friction is overcome (Hungerford 2004).
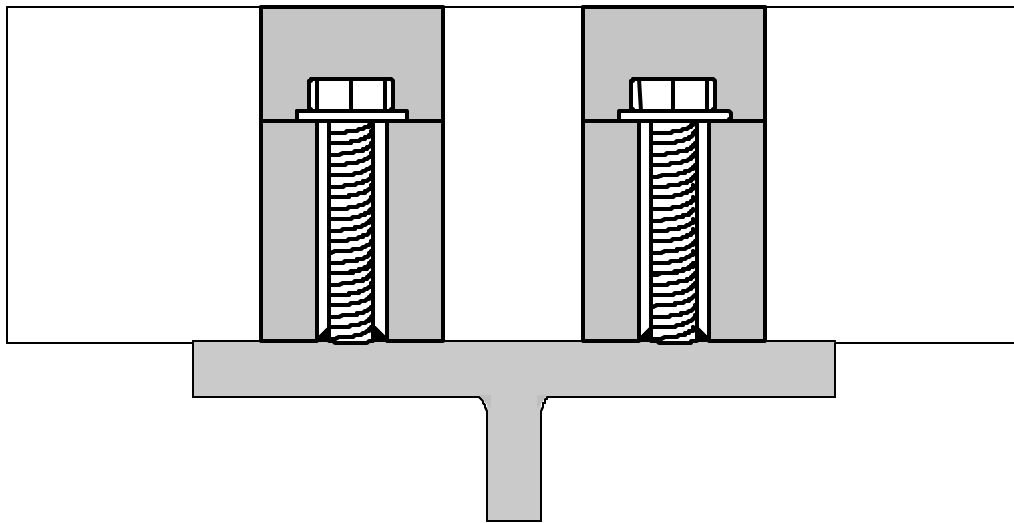
Figure 3.10: Welded Threaded Rod

3.3.9   HAS-E Adhesive Anchor (HASAA)

With this method, a hole is drilled from under the bridge, through the steel flange and into the concrete slab. Adhesive is injected overhead into the hole in the slab and then a fully threaded rod is inserted (Figure 3.11). Once the adhesive cures, the connector is tightened from under the bridge. The adhesive anchor initially uses friction to transfer shear force, followed by bearing. In testing this method, an adhesive and threaded rods manufactured by Hilti Corp. were used. The Hilti adhesive was designated HY 150 and the threaded rod was designated as HAS-E (Hungerford 2004).
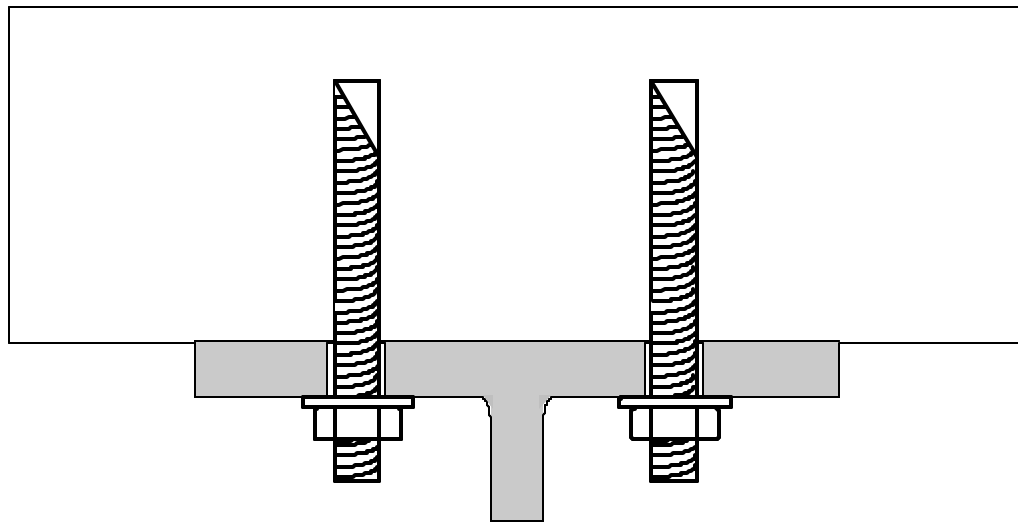
Figure 3.11: HAS-E Adhesive Anchor

3.3.10 HIT-TZ Adhesive Anchor (HITTZ)

Similar to the HAS-E anchor this anchor uses friction followed by bearing to transfer shear forces from the bridge girder to the slab. The difference between these two connectors is the way forces are transferred from the connector to the adhesive. The Hilti HAS-E anchor relies on the bond between its threads and the adhesive. The HIT-TZ anchor, on the other hand, transfers forces to the adhesive through wedging action due to its special threads. The installation process of the HIT-TZ follows the same steps as the HAS-E anchor (Figure 3.12) (Hungerford 2004).
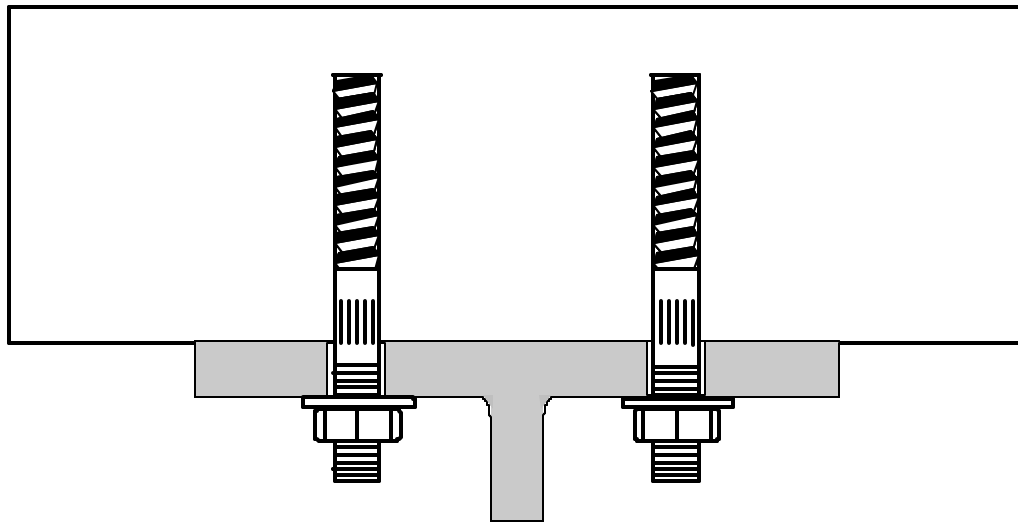
Figure 3.12: HIT-TZ Adhesive Anchor

3.3.11 Concrete Screw (WEDGB)

This connector requires a hole to be drilled through both the steel girder and concrete slab from under the bridge. The concrete screw is then simply driven into the hole and screwed into place (Figure 3.13). Shear forces are transferred through bearing only, after the connector slips into contact with the steel girder as load is increased (Hungerford 2004).
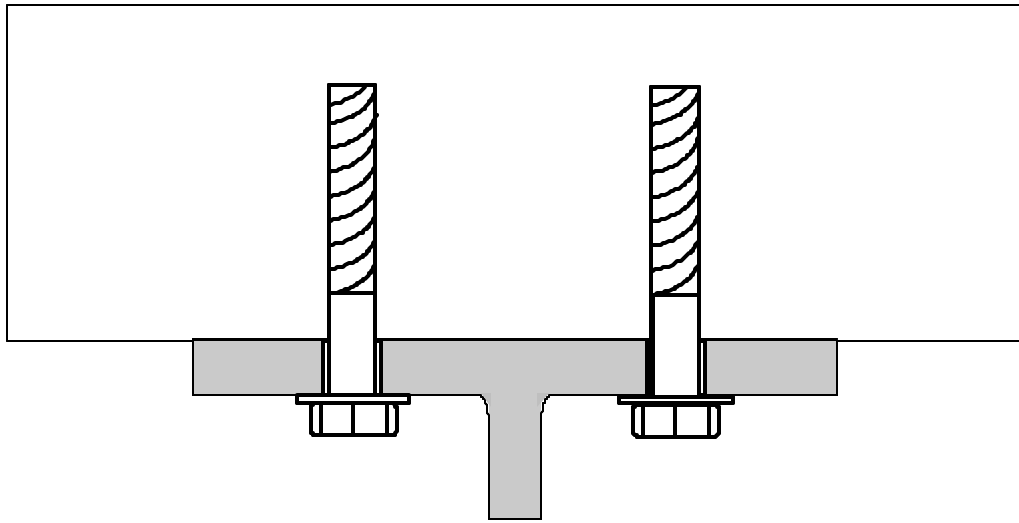
Figure 3.13: Wedge-Bolt Concrete Screw

3.3.12 Epoxy Plate (3MEPX)

The Epoxy Plate (Figure 3.14) is the only method that directly utilizes adhesion to transfer shear between the slab and the girder. A steel plate is temporarily held up by anchors and is welded to the edge of the top girder flange. The perimeter of the plate is then sealed with epoxy. Epoxy is injected to fill the gap between the slab and the plate until epoxy ejects through predrilled exit holes. The epoxy is then left to cure for at least 24 hours (Hungerford 2004).
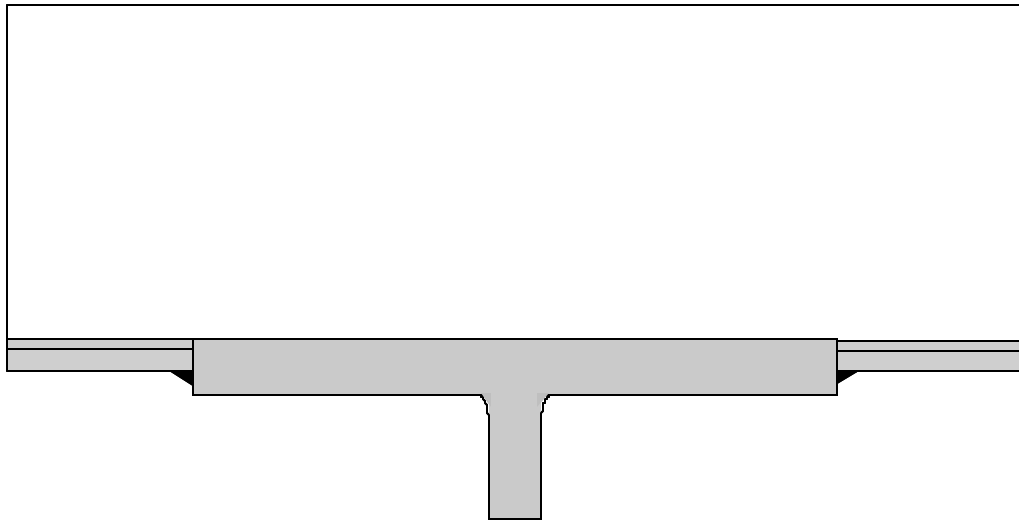
Figure 3.14: Epoxy Plate

3.4   TESTING PROCEDURE AND SETUP

Each connection method in this study was subjected to a screening process based on structural performance, constructability, practicality, and cost. Those that showed promise in each category were recommended for further investigation under fatigue tests.

To assess the load-slip behavior of each connector under static loads, the researchers investigated two possible testing methods: push-out tests and direct-shear tests. The push-out test is widely used among researchers to test shear connectors. A test specimen consists of two slabs connected to the flanges of a single steel girder with welded shear studs (Figure 3.15a). The load is applied at the center of the steel girder until the studs fail in shear. With this type of test, the load-slip behavior of a group of connectors is obtained. To deduce results for the behavior of a single connector, load and slip values need to be averaged. Depending on support conditions used, additional friction at the steel-concrete interface or tensile forces on the connectors are typically introduced which may

44

misrepresent conditions in an actual composite beam. With a direct shear test setup, on the other hand, a group of connectors as well as individual connectors can be tested. The main advantage of the direct shear test is that it can be designed to minimize eccentricity between the applied load and the concrete. With this method the load is applied closer to the steel-concrete interface as shown in Figure 3.15b. Due to limitations associated with a push-out test, the direct-shear test setup shown in Figure 3.16 was chosen for the testing of individual shear connectors (Hungerford 2004).

a)

b)
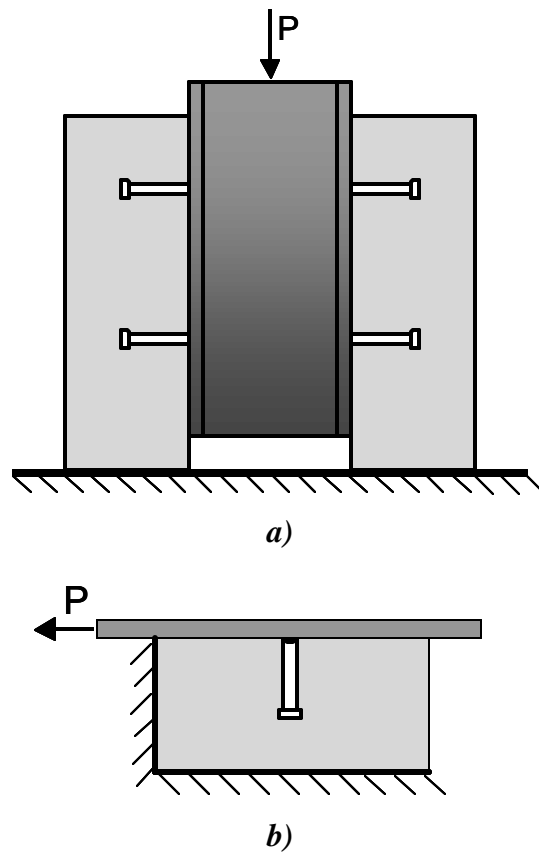
Figure 3.15: a) Push-out test b) Direct-shear test
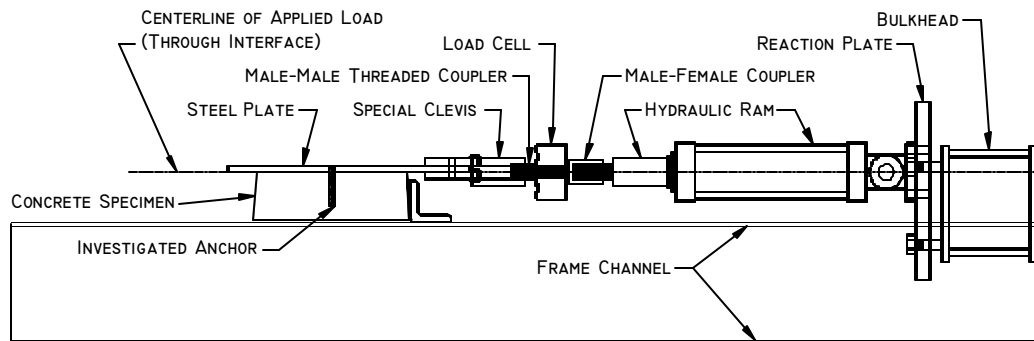
Figure 3.16: Side view of the direct-shear test setup used by Schaap (2004) and Hungerford (2004) (Schaap 2004)

3.5 TEST SPECIMENS

Test specimens were designed to enable the testing of a single connector in shear. The specimens were made up of a concrete block and a steel plate attached at the center by a shear connector (Figure 3.16). The steel plate represented a portion of the top flange of the prototype bridge girder, and the concrete block had the thickness of the prototype bridge slab. Edge effects were taken into consideration during the design of the specimens (Schaap 2004, Hungerford 2004).

3.6 TEST RESULTS

In the testing of shear connectors under static loading, the load-slip behavior of each connector was measured. Various parameters that characterize the behavior of the shear connector were then derived from the load-slip curve. This included items such as the initial slip load (for connectors that utilized friction for initial load transfer), the ultimate shear strength of the connector, and the value of slip when the ultimate strength of the connector was achieved. In addition, the strength of the connector at 0.2 in. slip was also taken as a measure of shear connector performance. This value, or values close to 0.2 in., have been

suggested by previous researchers as a reasonable basis for assessing shear connector strength, to limit the overall deflection of the composite girder when its composite flexural strength is achieved. Consequently, the shear strength of each connector was compared to the shear strength of the cast-in-place welded shear stud at a corresponding slip of 0.2 in. (Schaap 2004, Hungerford 2004).

Three static tests were performed for each type of shear connector and average load-slip curves were reported. All of the bolt type connectors tested had a diameter of 3/4-in. Strength evaluations showed that seven shear connection methods performed at least as well as the cast-in-place welded stud at the slip limit of 0.2 in.: POSST, STWPL, DBLNB, HTFGB, WEDGS, 3MEPX, and HASAA. The average load-slip curves of selected connection methods are shown in Figure 3.17. The 3MEPX method is not shown in this figure, because it experienced no slip until failure at an average load of 58 kips. The seven connection methods were further evaluated for constructability and practicality. The HTFGB was identified as the most difficult connection method to install whereas the WEDGB and HASAA methods proved to be the simplest. The 3MEPX was potentially the most costly connection method studied (Schaap 2004, Hungerford 2004).
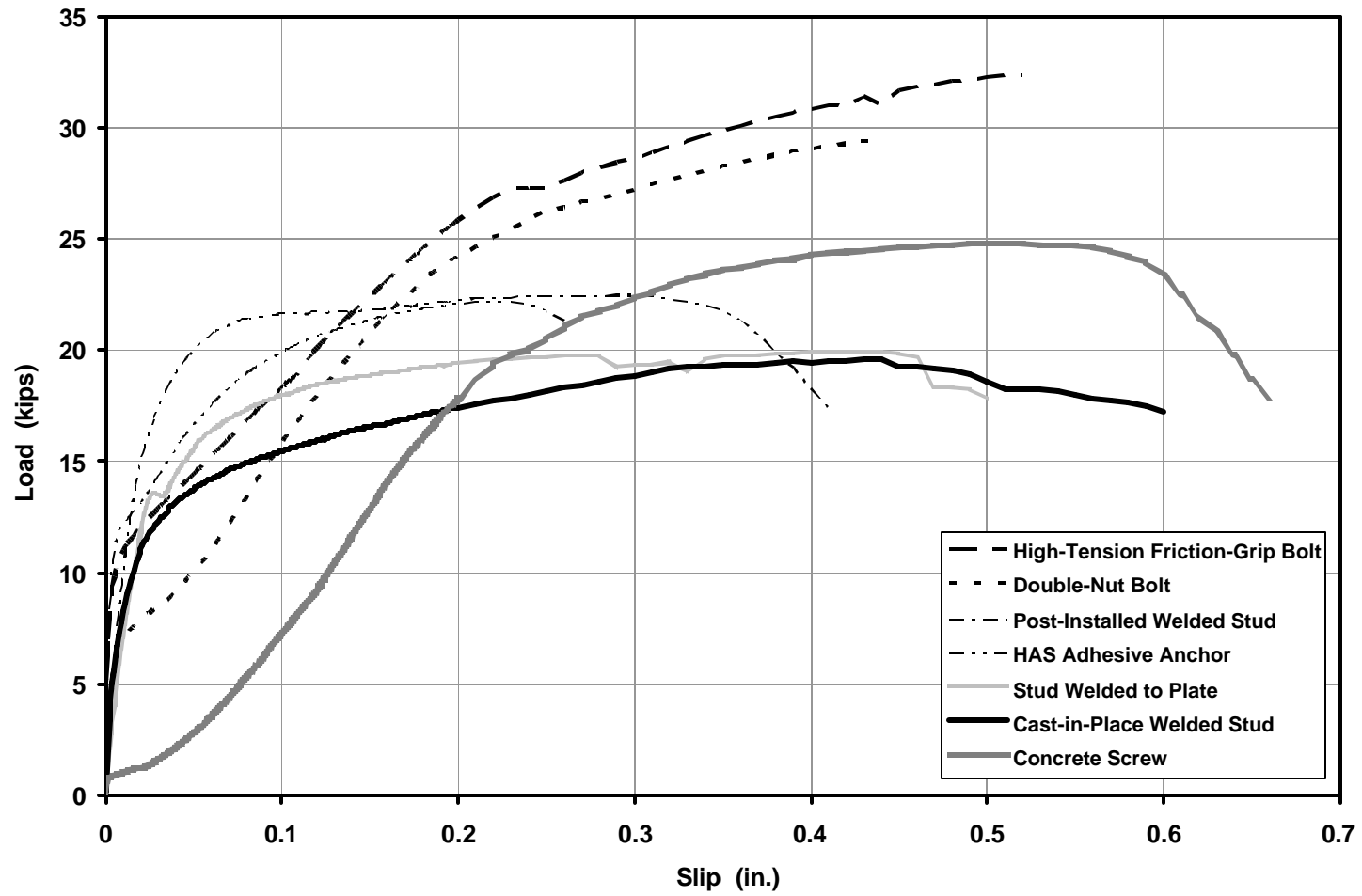
Figure 3.17: Comparison of load-slip curves

The figure contains the following legend entries:
- High-Tension Friction-Grip Bolt
- Double-Nut Bolt
- Post-Installed Welded Stud
- HAS Adhesive Anchor
- Stud Welded to Plate
- Cast-in-Place Welded Stud
- Concrete Screw

Axis labels: Load (kips) on the vertical axis (0 to 35); Slip (in.) on the horizontal axis (0 to 0.7).

48

3.7 PREVIOUS CONCLUSIONS AND RECOMMENDATIONS FOR FURTHER TESTING

The main purpose of investigations led by Schaap (2004) and Hungerford (2004) was to identify and evaluate shear connection methods to be used as retrofitting options for non-composite bridges. Three static tests per connection type, including several variations on the main connection methods, were tested with a total of 50 tests. As a result of those evaluations, the methods recommended for further evaluation by fatigue testing were: POSST, STWPL, DBLNB, HTFGB, HASAA, WEDGS (Concrete Screw with sheath), and 3MEPX (Schaap 2004, Hungerford 2004).

CHAPTER 4

Procedures Used for Fatigue Testing

4.1   INTRODUCTION

AASHTO provisions require shear connectors in a composite bridge to be strong enough to withstand shear loads while enduring many cycles of loading by moving vehicles.   Thus, retrofitting options investigated for this study were judged not only on their cost and constructability, but also on their performance under static and fatigue loading.

Previous research on TxDOT Project 0-4124 focused on identifying possible types of post-installed shear connectors and selecting those with sufficient shear strength. As discussed in Chapter 3, this resulted in the selection of seven shear connectors for further assessment under fatigue loads.   This chapter describes the experimental process used for that assessment.

The purpose of this study was to investigate the fatigue performance of a single shear connector at two distinct load levels: below the yield stress (high-cycle fatigue) and above the yield stress (low-cycle fatigue) of the connector material. Those that showed significantly better high-cycle fatigue performance than cast-in-place welded shear studs in high-cycle fatigue were then tested in low-cycle fatigue. Static tests were also performed to gather information on the load-slip behavior of each connector. All single connector tests were performed using a direct shear test setup rather than a conventional push-out test setup as recommended by Schaap (2004) and Hungerford (2004).

This chapter includes detailed descriptions of the test setup, equipment, instrumentation, specimen and material properties, installation procedures of the seven connection methods investigated, and the testing program.

4.2 TEST SETUP

The test setup consisted of a direct shear test assembly, loading equipment, and instrumentation. In this section, each is described.

4.2.1 Direct Shear Test Assembly

The same direct shear test assembly used for this study (Figure 4.1 through Figure 4.3) was previously used by Schaap (2004) and Hungerford (2004), and was selected over the more conventional push-out setup for the reasons discussed in Chapter 3. The direct shear test assembly is composed of several components, shown in Figure 4.1 and described below.
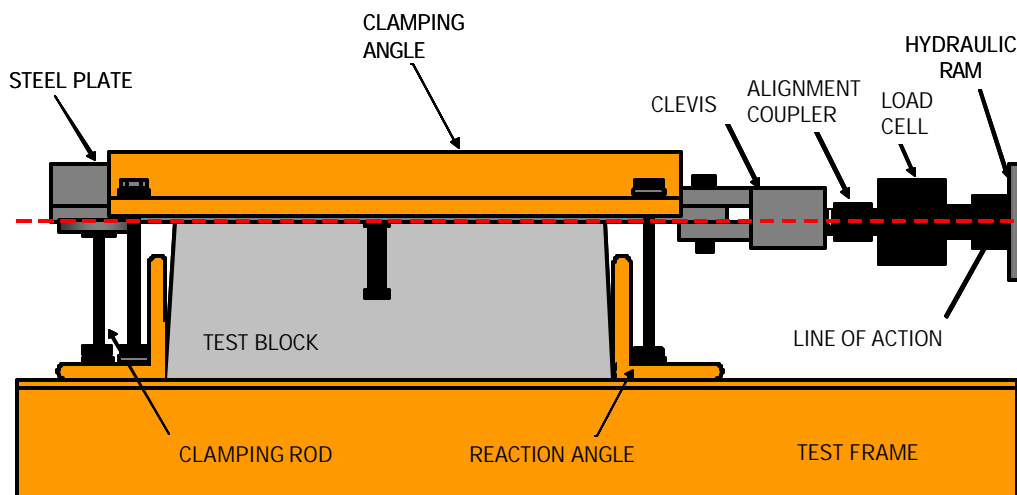
Figure 4.1: Side view of direct shear test assembly (bulkhead and base plate not shown)

51

Test frame: The test frame consists of two 23 ft-long, MC 18x58 channels bolted to 24- x 14- x 1-9/16- in. plate bulkheads at each end. For the purpose of this study, only one side of the test frame was used.

Hydraulic ram: The base plate of the hydraulic ram is bolted to the bulkhead using four 1-3/8 in. diameter high strength bolts, and supported by a rod eye that allows rotation in a vertical plane.

Load cell: The load cell is attached to the male threaded shaft of the hydraulic ram with an adapter having a 2-in. diameter female threaded section on one side and a 2-in. diameter male threaded section on the other.

Alignment Coupler: A 1-1/4 in. diameter coupler connects the load cell to the custom-made clevis, and allows additional movement between the clevis and the load cell during cyclic tests. Because the coupler is not designed for compressive loads, it tends to break after several million cycles of reversed load.

Custom-made clevis: This clevis is bolted through a 1-5/16-in. hole in the steel plate of the specimen using a 1-1/4-in. diameter ASTM A490 bolt. The line of action of the clevis coincides with the steel-concrete interface as shown in Figure 4.1.

Base plate: The specimen rests on the base plate, which is welded on its edges to the test frame.   The dimensions of the base plate are shown in Figure 4.2. The 7 in. x 20 in. open sections were intended to provide space for the protruding stirrups of each specimen.
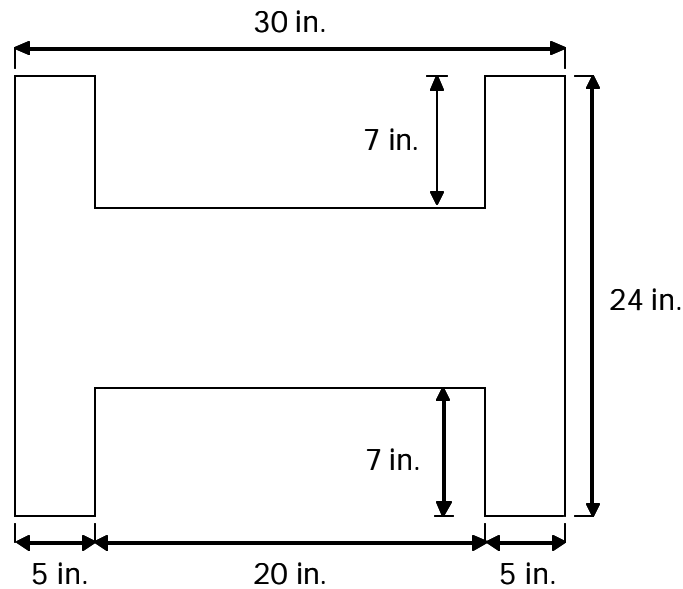
Figure 4.2: Base plate with dimensions

Reaction Angles: Two 6- x 6- x 1 in. reaction angles were welded in front of and behind the base plate to prevent the specimen from moving horizontally. The gaps between the specimen and reaction angles were filled in with hydrostone before each test.

Clamping Angles: Two 6- x 6- x 1-in. angles, connected with 3/4-in. diameter threaded rods, clamp the specimen down and prevent it from moving vertically.

Clamping rod: A 3/4-in. diameter threaded clamping rod prevents the back of the steel plate of the specimen from lifting during testing. Two 3-1/2 in. square steel plates, one with a 3/4-in. diameter hole and the other with a 3/4-in. x 2-in. slotted hole, were used as washers on each side of the test plate. To prevent any friction due to clamping, strips of Teflon© (tetrafluoroethylene) were glued to the washer plates, permitting the clamping plates to slide independently during loading.

53

Figure 4.3: Direct shear test assembly (with bulkhead)

In addition to the test setup components described above, a portable crane was used to rotate the hydraulic ram in a vertical plane to align the clevis with the steel plate of the specimen, and to lift and handle the test specimens.

4.2.2 Loading Equipment

Loading equipment for static and cyclic tests consisted of a hydraulic pump, a loading ram, and a load cell. The hydraulic pump was a 30-gpm MTS pump. This capacity was required to support sinusoidal loading of ±1 in. at frequencies as high as 6 Hz. The hydraulic ram used had a capacity greater than 100 kips in tension, and was attached to a 100-kip load cell having a precision of 0.005 kips.

4.2.3 Instrumentation

Loading of the test specimens was controlled by an MTS 407 single-channel servo-controller with automatic shutoff based on specified load, displacement or error limits (MTS 2000).

For static tests, the controller facilitated load monitoring, and its shutoff mechanism provided additional safety in the case of connector failure. The controller was found to be most useful, however, for cyclic tests, easily permitting automatic cycling between specified loads or displacements at a specified frequency. For the high-cycle fatigue tests, run under load control, the mean load, half the loading amplitude, loading frequency, and type of waveform were specified. For the low-cycle fatigue tests, run under displacement control, the corresponding displacement values were specified. During testing, the instantaneous load or displacement value, accumulated number of cycles, and the error between command and feedback signals were displayed on the controller monitor. For load-controlled tests, the controller was programmed to shut off hydraulic pressure once either connector failure or a predetermined number of cycles was reached. For displacement-controlled tests, hydraulic pressure was shut off manually following connector failure.

The relative slip between the concrete block and steel plate (slip of the connector) was measured with two Sensotech Model Linear Variable Differential Transformers (LVDT). These LVDT's were actually direct-current differential transformers (DCDT) which initially convert a DC current into an AC current, and then back to a DC output current. The LVDT's had a total stroke of ± 1 in. and a precision of 1/10000 in.
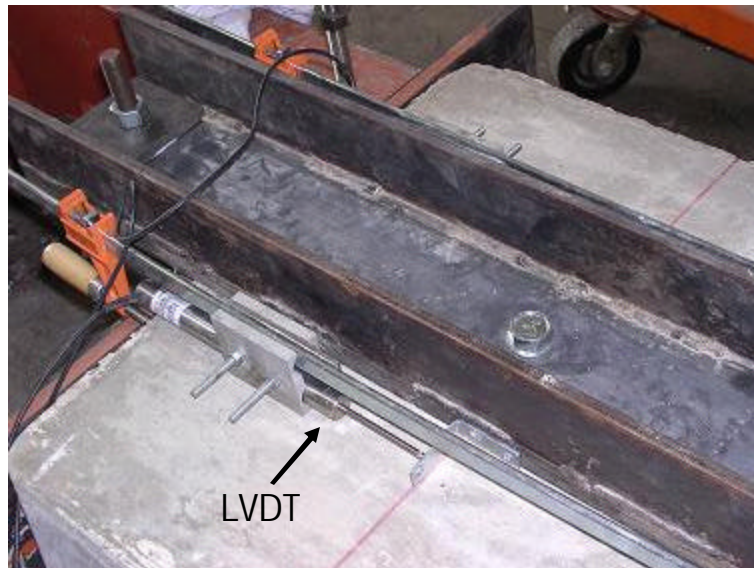
Figure 4.4: LVDT setup (second LVDT not shown)

The LVDT's were attached to carpenter's clamps using spacer blocks, and then clamped onto the concrete block spanning parallel to the steel plate of a specimen on both sides. Two 2-in. brackets were glued onto the steel plate in line with the location of the shear connector. The LVDT pins rested on the brackets and took increasing displacement readings in the direction of loading (Figure 4.4). A schematic of the instrumentation setup is shown in Figure 4.5. For high-cycle fatigue tests the controller was programmed to apply the user-specified loading range onto the connector, and the displacement signals from the LVDT's were logged directly onto a computer through a data acquisition system. For low-cycle fatigue tests, the controller was programmed to apply a user-specified displacement range using the LVDT signals, which were subsequently retrieved from the controller and passed to the data acquisition system.
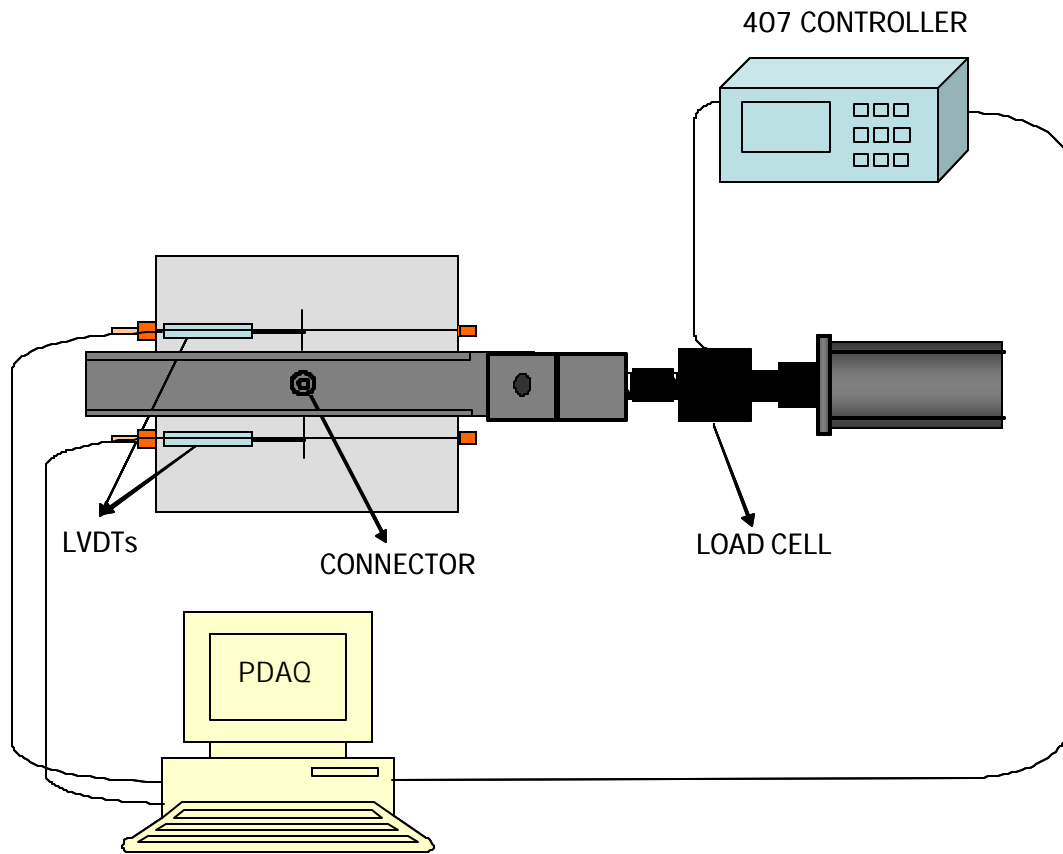
Figure 4.5: Instrumentation for load controlled tests

The time-varying load and displacement data were logged onto a computer using Iotech Personal Data Acquisition Program (PDAQ). For static tests, data were recorded at 1-2 Hz; for cyclic tests, they were recorded as fast as 17 Hz. During cyclic tests, the load cycling rate was reduced to 0.5 Hz during data recording, which resulted in a maximum of 34 load and displacement readings to be recorded every cycle. Displacement readings were accurate up to 1/1000 in.

4.3 TYPES OF SHEAR CONNECTORS INVESTIGATED

Based on their evaluation of the results of static testing of retrofit shear connectors, Schaap (2004) and Hungerford (2004) recommend seven types of

retrofit shear connectors for further evaluation under fatigue loading, in comparison with the Cast-In-Place Welded Stud:

1)   Post-Installed Welded Stud;

2)   Stud Welded-to-Plate;

3)   Double-Nut Bolt;

4)   High-Tension Friction-Grip Bolt;

5)   Adhesive Anchor;

6)   Concrete Screw, and

7)   Epoxy Plate

Throughout this thesis, these shear connectors will often be referred to by their corresponding abbreviations which are given in Table 4.1

Table 4.1: Abbreviations of shear connection methods discussed in this thesis

Connection Method	Abbreviation
Cast-in-Place Welded Stud	CIPST
Post-Installed Welded Stud	POSST
Stud Welded to Plate	STWPL
Double-Nut Bolt	DBLNB
High-Tension, Friction Grip Bolt	HTFGB
Adhesive Anchor	HASAA
Concrete Screw	WEDGB
Epoxy Plate	3MEPX

Previous static test results and selection criteria for all investigated shear connectors are presented in Chapter 3. In this section, the properties of the connectors used in each connection method are described.

4.3.1 Cast-in-Place Welded Stud (CIPST), Post-Installed Welded Stud (POSST), Stud Welded-to-Plate (STWPL)

For the Cast-in-Place Welded Shear Stud (CIPST) and Post-Installed Welded Headed Stud (POSST) methods, AISI Grade C1015 headed shear studs were used as shear connectors. The shear studs were 3/4-in. in diameter and 5-3/16 in. long, with specified minimum yield and ultimate tensile strength of 50 ksi and 60 ksi respectively. Manufacturer tested strength values were not obtained for the studs. All studs were obtained from a single heat of steel, to eliminate inherent variability from heat to heat.

Figure 4.6: Headed shear stud

The shear studs were welded onto the test plates with a stud gun by Dennis Steel in Austin, TX. The studs had an additional length of 3/16 in. to comply with welding standards provided by the Stud Welding Associates (Ohio). The resulting length was 5 in. also equal to the embedment depth. Figure 4.7 shows a typical specimen steel plate with a welded shear stud. These test plates were used for CIPST and POSST methods. Specimens for the Stud Welded to Plate (STWPL) method were not constructed for this study. It was concluded that they would display the same characteristics as POSST specimens; therefore, separate construction was deemed unnecessary. Test results obtained for the POSST method were assumed to also apply to the STWPL method.

Figure 4.7: Headed stud welded to plate

To test the effect of weld type and quality on strength and fatigue endurance, two headed studs were fillet-welded onto steel plates rather than gun welded. The fillet welding was performed by a certified weld technician at The University of Texas at Austin's Ferguson Laboratory. The fillet welds were 5/16 in. Shielded Metal Arc Weld with E7018 electrode (SMAW E7018). The steel plate was heated to 150°F before welding.

4.3.2   Double-Nut Bolt (DBLNB)

The connector for this method was chosen as an ASTM A193 B7 threaded rod. An ASTM A193 B7 rod is typically considered to be equivalent to an ASTM A325 bolt and has a specified tensile strength of 120 ksi. This material was chosen for its potential for better fatigue performance than the ASTM A490 bolts used by Schaap (2004) and Hungerford (2004), because its threads are rolled rather than cut.

Figure 4.8: Double-Nut bolt

For this study, a 12-ft. long threaded rod was purchased and cut into 8-in. long sections, ensuring uniform material properties in each connector. Four 3/4-in. diameter ASTM A563 Grade DH heavy hex nuts and ASTM F436 steel washers completed the installation, as shown in Figure 4.8. A single nut was placed on one face of the steel plate (away from the concrete block) and was tightened. Two additional nuts were placed on the opposite side of the plate to prevent twisting during tightening. A fourth nut was placed at the end of the connector (end of the bolt inside the concrete block) to represent a bolt head and restrict possible uplift of the steel plate.

4.3.3 High Tension Friction Grip Bolt (HTFGB)

In this study, a standard ASTM A325 bolt is referred to as a High-Tension Friction Grip Bolt (HTFGB). This bolt has a specified minimum yield and ultimate tensile strength of 105 ksi and 120 ksi respectively. The ASTM A325 bolt used for this method was 3/4-in. in diameter and 7-in. long. To tighten the bolt, ASTM A563 Grade DH heavy hex nuts were used along with 1-15/32 in. diameter ASTM F46 steel washers (Figure 4.9).

Figure 4.9: High-Tension Friction Grip Bolt

4.3.4   Adhesive Anchor (HASAA)

The Adhesive Anchor (HASAA) method consists of 2 components: A 3/4-in. diameter Hilti HAS-E threaded rod and HIT-HY 150 fast-curing adhesive. For this study, a rod with a total length of 10 in. was used (Figure 4.10).   A 6-3/4 in. threaded length of the rod is separated from a 3-1/8 in. threaded length by a 5/8 in. diameter and 1/8 in. long unthreaded length.   The HAS-E threaded rod is made of ISO 898 Class 5.8 zinc plated steel with a specified minimum yield and tensile ultimate strength of 58 ksi and 72.5 ksi respectively.
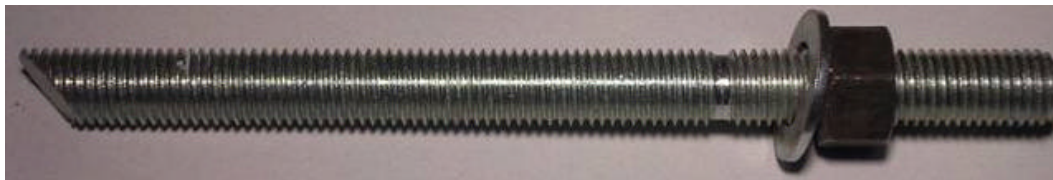
Figure 4.10:   HAS-E threaded rod

HY 150 adhesive is composed of resin, hardener, cement, and water. Application temperatures can range from 25°F to 104°F. The adhesive is mixed and injected using a Hilti HIT-MD 2000 dispenser and a HIT-M dispensing nozzle which are shown in Figure 4.11 and Figure 4.12.

Figure 4.11: Hilti HY 150 Adhesive (Hilti 2006)

Figure 4.12: Hilti MD2000 Adhesive Dispenser (Hilti 2006)

The adhesive anchor method requires three main installation steps. The adhesive is first injected into a predrilled bolt hole; the rod is inserted; and the adhesive is then left to cure (50 min. at 68°F). After the adhesive cures the bolt is tightened to the specified pretension. Additional information regarding temperature effects on cure time and bond strength is available from the manufacturer.

One concern about this connector was the required embedment depth for this type and size of rod. The manufacturer-specified embedment depth is 6-5/8 in. which is too deep for bridges with slabs 7-in. thick or thinner. Because

previous static tests on this connector by Schaap (2004) and Hungerford (2004) showed adequate results with a 5-1/2 in. embedment depth, the latter embedment depth was used in this study as well.

4.3.5 Concrete Screw (WEDGB)

The Wedge-Bolt® concrete screw, a product of Power Fasteners, is a one piece mechanical screw of heat-treated, high-strength carbon steel with specified yield and ultimate strengths of 130.5 ksi and 145 ksi respectively. For this study, a 3/4-in. diameter screw with a 6-in. length was used. Shown in Figure 4.13 is the concrete screw made up of a hex washer head, a 2-1/4 in. unthreaded length followed by a threaded length of 3-3/4 in., and a chamfered tip.

Figure 4.13: Power Fasteners Wedge-Bolt® concrete screw

The bolt is simply installed by screwing it into a clean pre-drilled hole using only a socket or impact wrench. The bolt is then tightened without exceeding the specified maximum torque. The 6-in. long, 3/4-in. diameter screw used in this study required a 5-3/4 in. embedment depth. This depth includes a 3/4 in. tolerance left for debris at the bottom of the drilled hole.

Figure 4.14: Power Fasteners Wedge-Bit®

The Wedge-Bolt® is recommended to be used in conjunction with a matched tolerance drill bit. A 3/4-in. diameter carbide steel SDS-Plus Wedge-Bit® with an overall length of 8 in. and a usable length of 6 in. was used for this study.

4.3.6 Epoxy Plate (3MEPX)

3M DP-460 NS Scotch-Weld® Epoxy is a non sag, two part epoxy and is available in 27-, 200-, and 400-mL cartridges. Shown in Figure 4.15 is a 27-mL cartridge used in this study. The epoxy has a 60-minute working time with a full cure time of 7 days at 73°F. It is applied on surfaces with a 3MEPX® Plus Applicator, shown in Figure 4.16.

Figure 4.15: 27- mL 3M DP-460 NS Scotch-Weld® Epoxy (3M 2006)

Figure 4.16: 3MEPX® Plus Applicator with cartridge

The epoxy requires both steel and concrete surfaces to be prepared before application. The steel plate must be scoured and cleaned with isopropyl alcohol, and the coarse aggregate in the concrete needs to be exposed through grinding to achieve a strong bond with the epoxy.

4.4 DESCRIPTION OF TEST SPECIMENS

The test specimens used in this study are slightly modified versions of those used by Schaap (2004) and Hungerford (2004). Their properties and geometry used by these researchers are described in Chapter 3. The specimens were designed to accommodate the testing of a single shear connector subjected to static and fatigue loading.

The test specimens consisted of 3 main components: a concrete block; a steel plate; and a shear connector. The concrete block had a thickness representative of the prototype bridge slab and the steel plate represents one-half of a typical girder flange. The steel plate was connected to the center of the concrete block with the shear connector. A typical test specimen with a welded shear stud is depicted in Figure 4.17. The procedures and the materials used to construct the specimens are described in detail in the following sections.

WELDED STIFFENER
PLATE

STEEL PLATE

TEST BLOCK
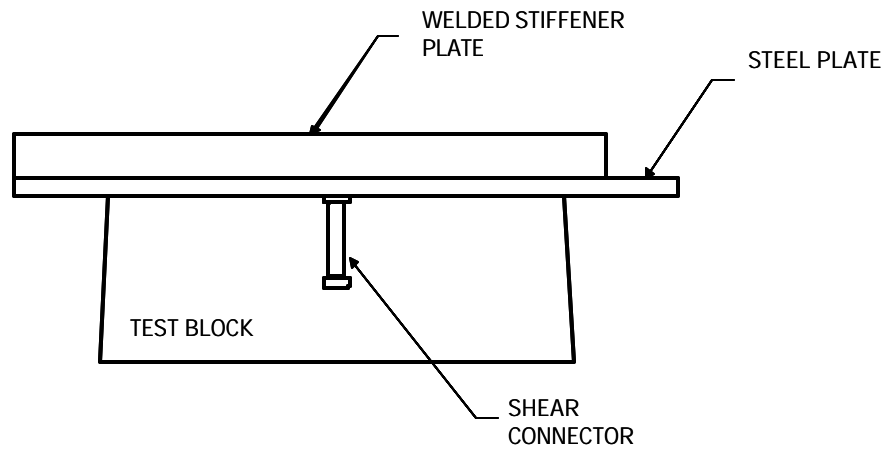
SHEAR
CONNECTOR

Figure 4.17: Typical test specimen (with welded shear stud)

4.4.1 Reinforcement

The size and layout of steel reinforcement was based on the prototype bridge developed by Schaap (2004) and Hungerford (2004), and discussed in Section 3.2.1. Two layers of Grade 60, #4 and #5 size reinforcing steel were used in the specimens along with #3 bars in the form of 4- x 9.5-in. closed stirrups with 4-in. hooks. A clear cover of 1.5 in. was provided for the bottom layer of reinforcement using plastic-dipped reinforcing chairs, tied to the cages to prevent separation during the casting of concrete. A clear cover of 1.5 in. was also left for the top reinforcement. The typical reinforcement layout used for test specimens is shown in Figure 4.18.

In addition to representing the reinforcement layout of the prototype bridge, the reinforcement in the test specimens provided confinement for the concrete around the shear connectors. The stirrups extended out of the concrete blocks to assist in lifting and handling.

67
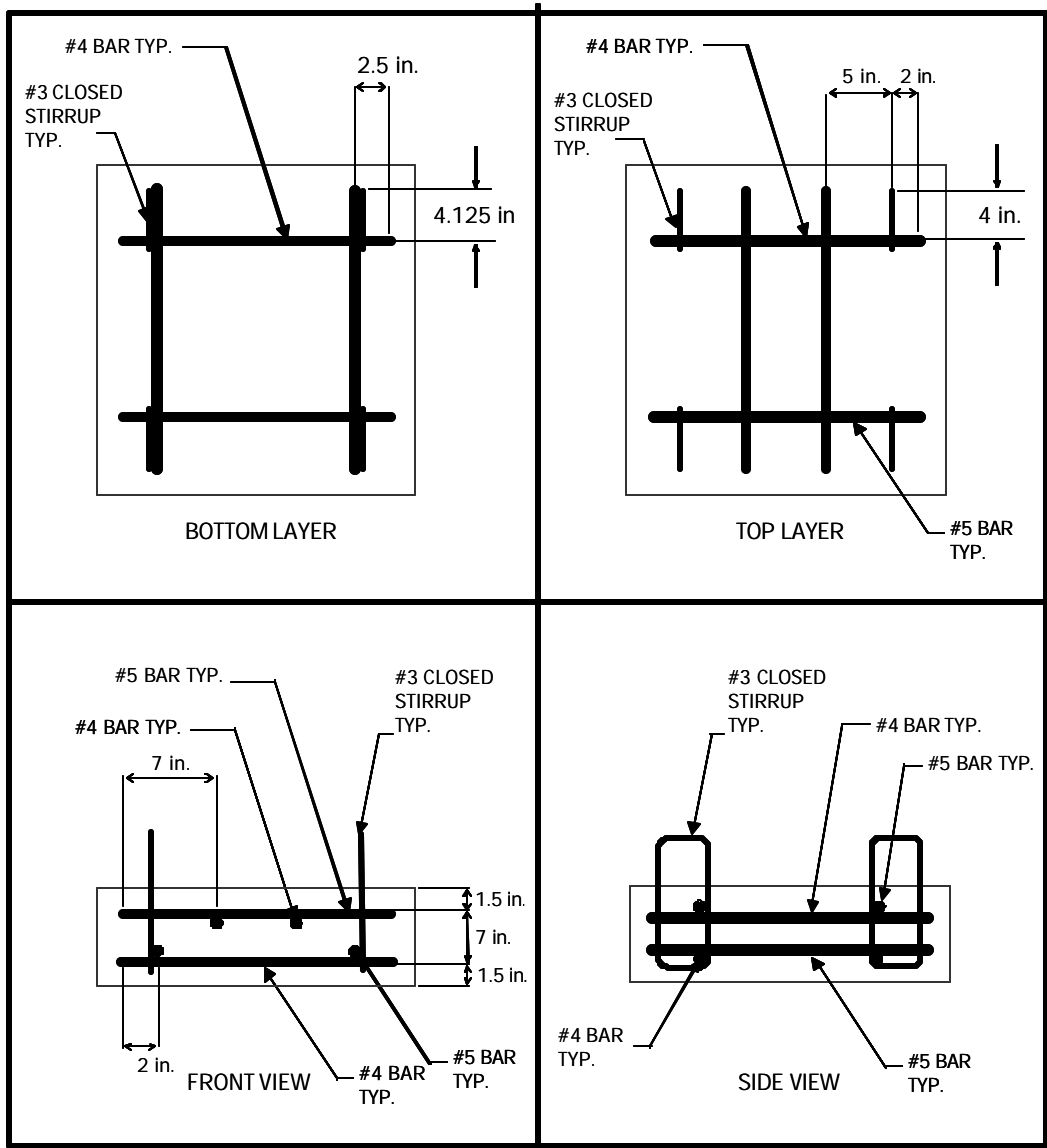
Figure 4.18: Reinforcing steel layout and dimensions

4.4.2   Form Preparation

Fiberglass waffle-slab forms were used as molds for the test specimens. The interior dimensions of the forms were 22-1/2 in. square at the bottom, 23-1/2 in. square at the top, and 12 in. deep. To model the prototype bridge a specimen depth of 7 in. was needed. To achieve this, 22-1/4 x 22-1/4 x 5/8 in. plywood sheets were placed on 4-3/8 in. plastic reinforcing chairs inside the forms, giving usable interior dimensions of 22-1/4 in. x 22-1/4 in. at the bottom, 23-1/2 in. x 23-1/2 in. at the top, and a depth of 7 in.

The perimeter of the plywood sheets was first sealed to prevent concrete from seeping through the gaps, and also to hold the sheets in place. To make lifting and handling of the concrete blocks easier, 1/2-in. diameter Ferrule Loop Inserts were attached to the forms, to be cast within the concrete blocks. These inserts were short enough to not interfere with the reinforcing steel but strong enough to carry the weight of the concrete blocks. The waffle forms were drilled on two sides with a hand-held drill and a 3/4-in. diameter bit. Threaded bolts, 3/4-in. in diameter by 1-1/2 in. long, were used to hold the Ferrule Loop Inserts in place. Once the plywood sheets and the threaded bolts were placed, the forms were vacuumed and coated with form oil to prevent the concrete from sticking to the forms and bolts. Finally, the Ferrule Loop Inserts were screwed onto the threaded bolts and the forms were ready for the placement of reinforcement. A waffle form at each step of the preparation process is shown in Figure 4.19.

For POSST and DBLNB methods, 3.5-in. and 2-in. diameter PVC pipes were glued to the center of the plywood sheets respectively. This was an easy way to precast the holes required to install the connectors.
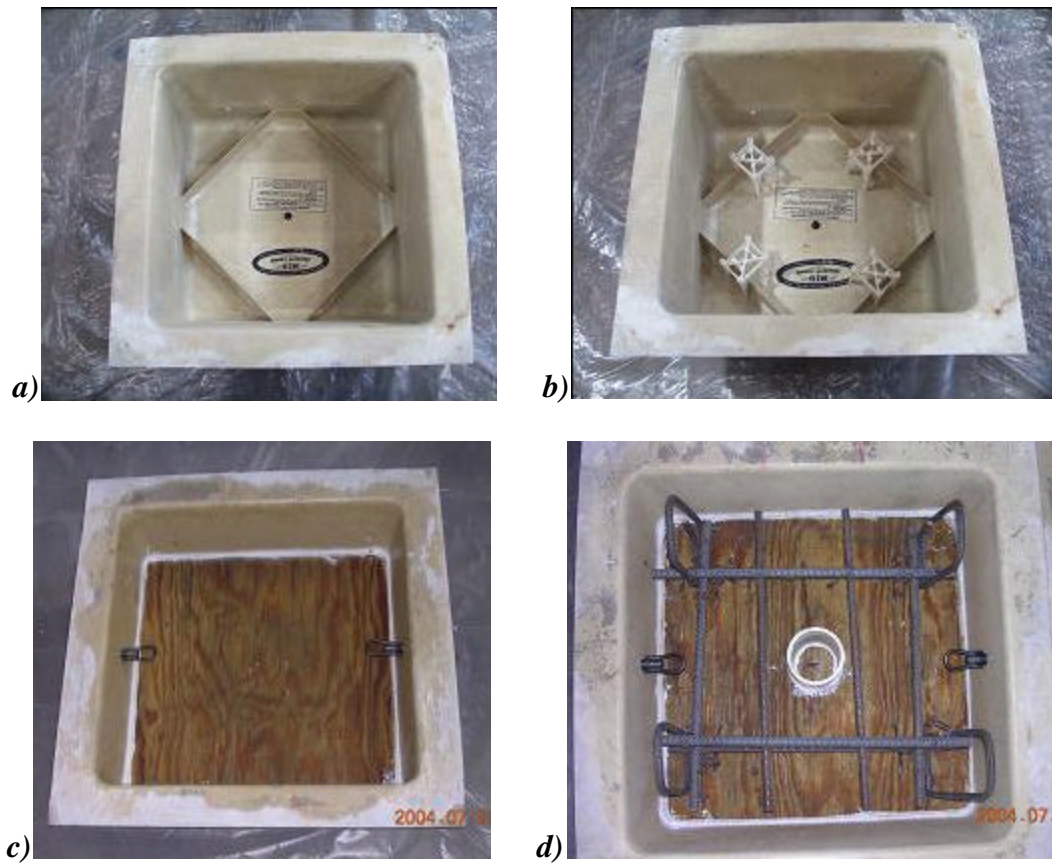
Figure 4.19: Waffle forms: a) Inside of waffle form b) with plastic chairs c) with plywood sheet and inserts d) with reinforcing cage and PVC pipe

4.4.3 Casting

The concrete was delivered to the laboratory in a ready-mix truck. Using a 1-cubic yard bucket, each form was filled with concrete in a single lift. The concrete was then vibrated, avoiding the reinforcing cages. The surface of each specimen was finally screeded and finished, and thirty-five 6- x 12-in. cylinders were cast for concrete strength tests.

Once the concrete was cast and finished, the blocks and cylinders were covered with plastic sheets, and splashed with water twice a day for the next five days.

4.5   MATERIAL PROPERTIES

The basic materials used in the construction of the test specimens include: concrete, steel, grout, and shear connectors. This section provides detailed information about these materials.

4.5.1   Concrete

The concrete used for the test specimens was ordered from Capitol Aggregates in Austin, Texas (Mixture Design #261). The concrete consisted of Type I Portland cement, 3/4-in. river aggregate, fine aggregate, and retarder; it had a water-cementitious ratio of 0.37. Even though the concrete mixture was specified to have a 28-day compressive strength of 3000 psi with a 4-in. slump, a concrete mixture with 7-in. slump was received from the manufacturer. Components of the concrete mixture and proportions are shown in Table 4.2.

Table 4.2: Mixture proportions of concrete

Mix Component	Quantity (per cubic yard)	Description
Cement	376 lb	Type I Portland Cement
Course Aggregate	1927 lb	¾ in. river aggregate
Fine Aggregate	1541 lb	-
Retarder	5.6 oz	Pozzolith® 100 XR
Water	151.2 lb	-

Concrete strength was evaluated by cylinder tests at 7, 14, 21, and 28 days using the 6- x 12-in. cylinders. Average concrete strength was determined as 2961 psi at 28 days, lower than the specified strength of 3000 psi. Additional cylinder tests were performed regularly throughout the testing program. The increase in average concrete strength within the first 28 days is shown in Figure 4.20.
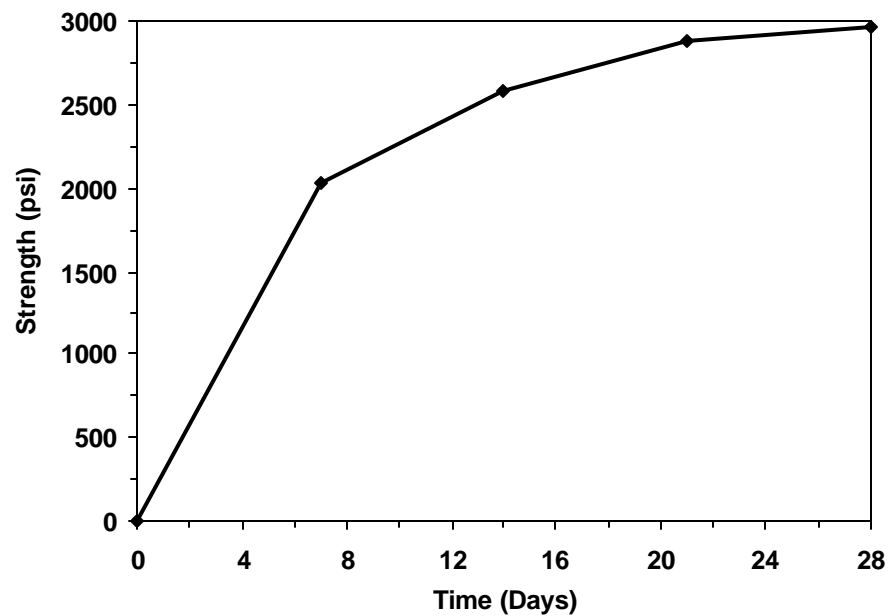
Figure 4.20: Average concrete compressive strength up to 28 days

4.5.2   Steel

Steel plates were provided by Namasco Inc., Austin, Texas. The steel plates were specified as A36 steel, representative of the grade of steel used in bridges surveyed by Schaap (2004) and Hungerford (2004). The same heat number was requested from the manufacturer for all steel plates. Based on the mill report provided, the steel had an average tensile yield strength of 48.1 ksi and an average ultimate tensile strength of 71.9 ksi. The plates were delivered in 6- x

1- x 40-in. sections. To prevent bending of the steel plates during testing, 32-1/2 x 3- x 1/4-in. steel plates were welded on as stiffeners. The stiffeners were 7-1/2 in. shorter than the plate length to leave enough room for the clevis to be bolted onto the steel plate. The resulting cross-section of the steel plates resembles a channel section as shown in Figure 4.21. A 1-5/16 in. diameter hole for the clevis bolt and a hole for each connector type had to be drilled through the steel plates. A rectangular section was also cut out of the end of the steel plate enough for the clamping bolt to travel during loading. The dimension and location of these holes are shown in Figure 4.22.

FRONT VIEW   SIDE VIEW

32-1/2 in. x 3 in. x ¼ in. STIFFENERS

32-1/2 in.   7-1/2 in.

6 in. x 1 in. x 40 in. A36 STEEL PLATE
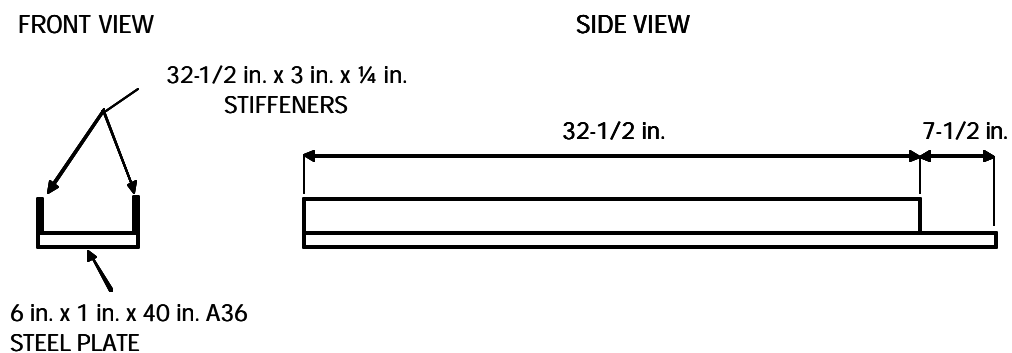
Figure 4.21: Dimensions of the steel test plate
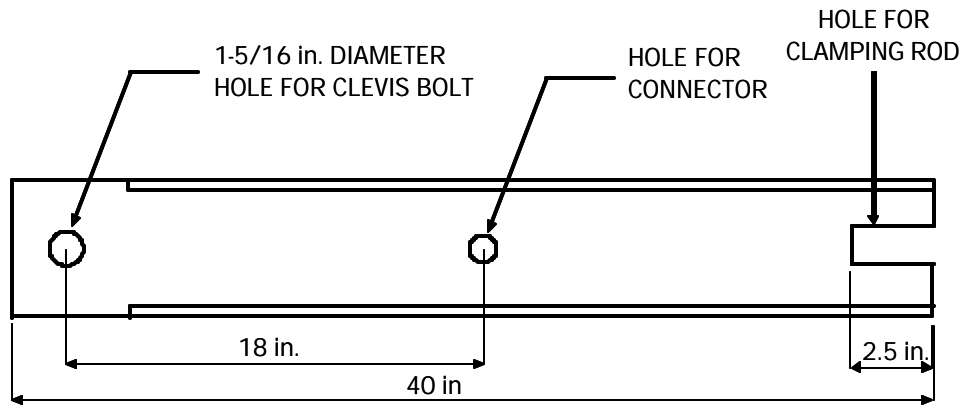
Figure 4.22: Hole locations on the steel test plate

4.5.3 Grout

For the selection of the grout material, the following qualities were necessary:

- suitable for traffic applications
- fast setting
- high early compressive strength
- low shrinkage
- simple application

Five Star® Highway Patch met all of the above requirements and was selected for use in the POSST and DBLNB specimens of this study. This is a fast-setting hydraulic grout typically used in traffic areas, including bridges. It is a one-component material with a specified compressive strength of 2000 psi at 2 hours, 5100 psi at 24 hours, 7000 psi at 7 days. Due to its high early strength, roads can be opened to traffic 2 hours after application (Five Star Products 2006).

The manufacturer specifies a minimum water amount of 2.5 quarts and a maximum water amount of 3 quarts to be used for a 50 lb bag. The strength of the grout used in each specimen is presented in Chapter 5.

4.5.4 Shear and Tensile Tests of Shear Connectors

Individual shear and tensile tests were performed on shear connection methods involving steel bolts or rods. Their main purpose was to compare the probable strengths of those connectors with the specified values.

4.5.4.1 Shear Connectors Investigated in Strength Tests

Shear connectors tested for shear and tension include the welded headed shear stud used for CIPST specimens, the ASTM A193 B7 threaded rod used for DBLNB specimens, the Wedge-Bolt® concrete screw used for WEDGB specimens, the standard ASTM A325 bolt used for HTFGB specimens, the and Hilti HAS-E threaded rod used for HASAA specimens.

4.5.4.2 Test Setup and Equipment for Strength Tests

Individual anchors were tested in single shear using a customized bolt testing apparatus consisting of two shearing plates and a top and bottom block. The connector was placed through the holes in the shearing plates. While one shearing plate was placed to rest on the bottom block the second shearing plate was held up by the connector (Figure 4.23a). The top block was then placed to rest on the second shearing plate (Figure 4.23b). Using a universal testing machine, load was applied to the top block; shearing plates sliced through the connector; and the corresponding load was displayed on the machine.
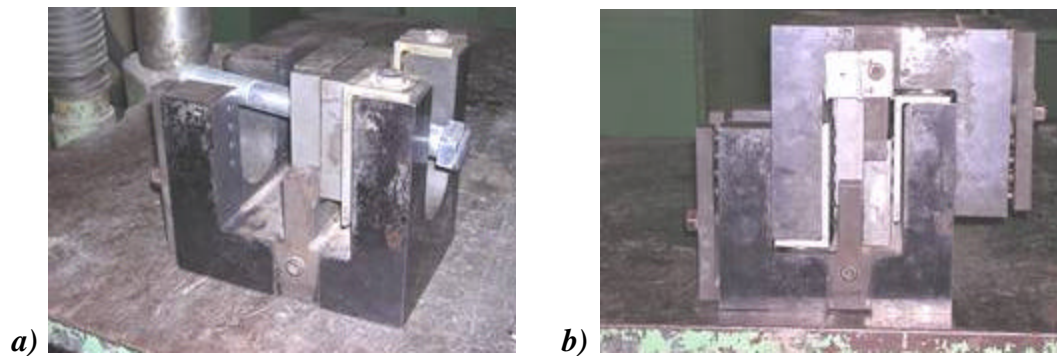
Figure 4.23: Apparatus used for shear tests on single connectors: a) bottom block with bolt and shearing plates; b) complete test apparatus

4.5.4.3   Results of Strength Tests on Single Connectors

In Table 4.3 are presented the measured mean ultimate shear strength of each connector type, along with corresponding theoretical values. A strength ratio, which is the quotient of the experimental value divided by the theoretical value is given for each connector type. The theoretical ultimate shear strength for each connector type was calculated as 60 percent of the specified ultimate tensile strength except for HTFBG (ASTM A325 bolt), where the shear strength value was taken from the American Institute of Steel Construction Manual 13th Edition (AISC) Section J3 Table J3.2. As expected, the observed shear strengths were greater than the theoretical ones.

Table 4.3: Experimental and theoretical ultimate shear strength of connectors

Connector Type	Experimental Average Shear Strength (ksi)	Theoretical Ultimate Shear Strength (ksi)	Strength Ratio
CIPST & POSST	48.7	36	0.81
DBLNB	91.7	72	1.27
HASAA	74.2	43.5	1.70
HTFGB	82.7	72	1.15
WEDGB	100.6	87	1.16

4.6   SHEAR CONNECTOR INSTALLATION PROCEDURES

Listed in this section are the installation procedures for each connection method. CIPST specimens were the only specimens with shear connectors that were cast inside the concrete blocks and required no post installation. The remaining connection methods all required shear connectors to be installed after the concrete blocks cured.

4.6.1   Installation of CIPST Specimens

Cast-in-Place Welded Shear Stud specimens were the only method where the shear stud was cast within the concrete block. Before casting of concrete, seven steel plates with welded shear studs were placed on the molds and were centered (Figure 4.24). Concrete was then poured in the molds and was vibrated, avoiding the shear studs. The specimens were ready for testing after 28 days.

Figure 4.24: CIPST specimens before casting

4.6.2   Installation of POSST Specimens

The same shear studs used for CIPST specimens were also used for POSST specimens. The shear studs for both connection methods were welded at the same time.

The Post-Installed Welded Shear Studs were installed in seven steps:

1. The concrete blocks were removed from the waffle forms and the 3.5 in. diameter PVC pipes that were cast within the blocks were taken out.

2. The precast holes were saturated for 24 hours with water-soaked paper towels or cloths. For two specimens, Five Star® Bonding Adhesive was applied inside the precast hole instead of saturating the holes with water. The bonding adhesive enabled the immediate casting of the grout after application.

3. The steel plates were placed on the floor with the welded studs pointing upwards.

4. To seal the gap between the concrete block and the steel plate, caulk was applied around the perimeter of the precast holes. This was intended to

contain the grout within the hole.

5. The bottom formed faces of the concrete blocks were placed on the steel plates with the studs centered in the precast holes (Figure 4.25).

6. Grout was mixed using the mixture proportions specified by the manufacturer, using a mixing paddle and hand-held drill. Enough grout was prepared to fill the holes in the specimens, as well as 4 in. x 8 in. test cylinders (ideally 3 cylinders per test specimen). The grout was poured into the holes and was rodded with a piece of wire to eliminate voids.

7. The grouted surface of the specimens and test cylinders were splashed with water and covered with plastic, and the grout was cured for at least one day.

Grout cylinders were tested at 24 hours and after testing each POSST specimen. Results of grout cylinder tests are presented in Chapter 5.

Figure 4.25: Precast hole with welded stud before grouting

4.6.3   Installation of STWPL Specimens

Stud Welded to Plate specimens were not actually constructed for this study. If these specimens were to be constructed, the same installation procedures specified for POSST specimens would have been followed. The only additional installation steps would be the preparation and welding of the smaller steel plates as discussed in Chapter 3.

4.6.4   Installation of DBLNB Specimens

The same installation procedures followed for POSST specimens also held for DBLNB specimens. The additional steps are listed below.

1. 13/16-in. diameter holes were drilled through the steel plates using a Jancy magnetic Slugger®.
2. The rod was placed to a 5-in. embedment.
3. The connectors were tightened to a pretension of 28 kips. At first, a torque wrench was used, but this required one person to hold the nuts on one side of the plate and another person to tighten the nut from the other side. To simplify the tightening procedure, an impact wrench was later used, with "Squirter" Direct Tension Indicating (SDTI) washers to verify the specified bolt pretension (Figure 4.26).

The Skidmore-Wilhelm Bolt-Tension Calibrator was used to determine the precision and reliability of SDTI washers. The pretension applied to a bolt was determined by inserting the bolt into the Skidmore and tightening it on to the plate of the calibrator, with a torque wrench. The pressure created from tightening the bolt is transmitted through the hydraulic fluid present in the calibrator to the gage of the calibrator. Meanwhile, the tension in the bolt is displayed in pounds. This helps determine the exact torque that needs to be applied to tighten a bolt to its recommended minimum pretension (Skidmore-Wilhelm 2006).
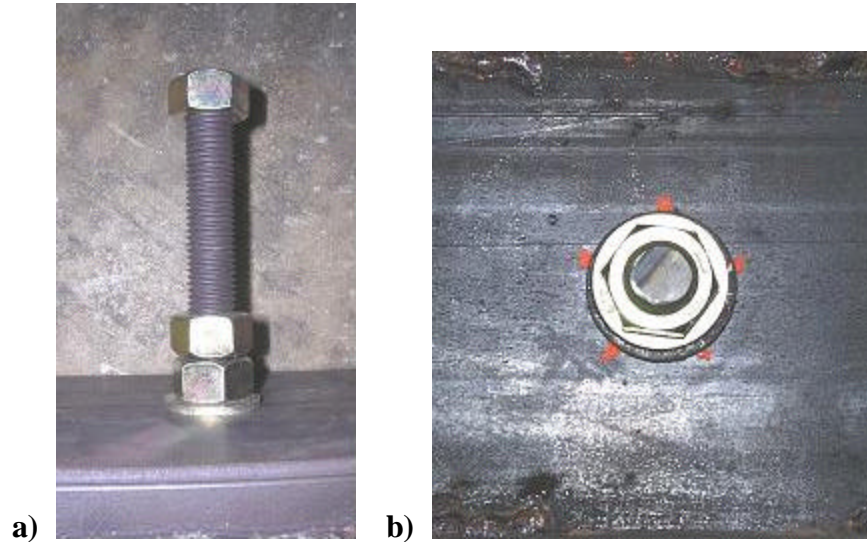
Figure 4.26: Double-Nut bolt attached to the steel plate: a) side of bolt to be embedded in concrete b) tightened side of bolt with SDTI washers

4.6.5   Installation of HTFGB Specimens

HTFBG specimens were installed in six steps:

1. A 3/4-in. diameter hole was drilled through the steel plates using a Jancy magnetic Slugger® bit.

2. A 2-in. diameter hole with a Hilti-TE 92 rotary hammer drill was drilled 2.7 in. deep, starting from the finished side of the concrete blocks (the depth of the hole provided adequate clear cover for the bolt head).

3. The blocks were flipped onto their opposite side and a 3/4 in. diameter hole was match-drilled through the previously drilled 2-in. diameter hole. Because the larger diameter hole was drilled first, concrete did not break out when the smaller hole was drilled. While care was taken to drill the two holes concentrically, this was difficult. The uneven edges on the finished side of the concrete blocks made it difficult to locate the true

center point of the block. The smaller holes in some specimens were drilled off-center, as shown in Figure 4.27.

4. The ASTM A325 bolt and a washer were placed with the bolt head resting on the bottom of the 2-in. diameter hole, which was chiseled flat to provide an even surface for the washer and bolt head.

5. The concrete blocks were flipped onto their opposite side and the steel plates were placed on top of them.

6. The bolt was tightened to clamp the steel plate and concrete block together until a bolt pretension of 28 ksi was reached as verified by SDTI washers.

In an actual bridge application the 2-in. diameter holes corresponding to the surface of the bridge deck would be grouted for both structural and aesthetic purposes. HTFGB specimens were not grouted as it was deemed unnecessary for this research.

a)

b)
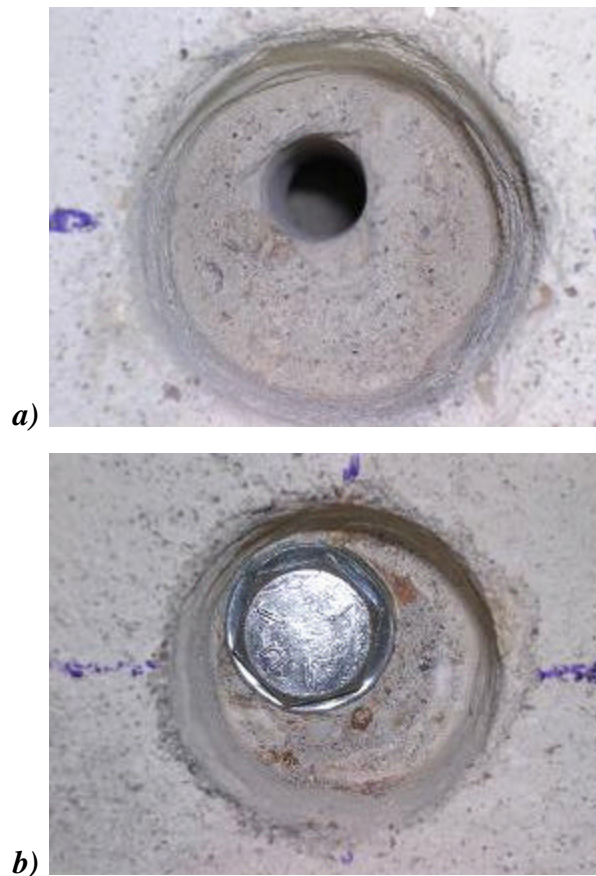
Figure 4.27: Offset holes a) after drilling b) after bolt is tightened

4.6.6   Installation of HASAA Specimens

HASAA specimens were installed in 8 steps:

1. A 13/16 in. diameter hole was drilled through the steel plates using a Jancy magnetic Slugger®.

2. A 13/16 in. diameter hole was drilled 5-1/2 in. deep through each concrete block using a Hilti TE-52 rotary hammer drill.

3. A wire brush, compressed air, and vacuum were used to clean the debris from the hole.

4. The Hilti HY 150 adhesive was injected to fill up 2/3 of the pre-drilled

hole.

5. Connectors were twisted clockwise as they were being inserted through the steel plates into the adhesive filled holes.

6. Excess adhesive that surfaced through the holes of the steel plates was wiped off.

7. The adhesive was allowed to cure for 50 minutes.

8. The connectors were tightened until a specified torque of 150 ft-lb. was reached (Figure 4.28), using a torque wrench.

Figure 4.28: HAS-E anchor after installation

4.6.7 Installation of WEDGB Specimens

WEDGB specimens were installed in five steps:

1. 13/16 in. diameter holes were drilled through the steel plates using a Jancy magnetic Slugger®.

2. 3/4-in. diameter holes were drilled 5-3/4 in. deep into the concrete blocks using a special carbide drill bit by Power Fasteners.

3. The debris was cleaned from the holes using compressed air and a vacuum.

84

4. The steel plates were aligned on the concrete blocks and the bolts were inserted.

5. Using a torque wrench, the screws were inserted through the plate into the concrete and tightened until the bolt heads were flush with the plates until achieving a torque of 200 ft-lb (the manufacturer's specified value for 3000-psi concrete). A torque wrench was used to screw the bolts into the concrete blocks through holes in the steel plates.

4.6.8   Installation of 3MEPX Specimens

3MEPX specimens (Figure 4.29) were installed in five steps:

1. 7-in. wide strips down the center of the formed face of the concrete blocks were sand blasted until the course aggregate in the concrete was visible.

2. The adhering surface of the steel plates were scoured with a scouring pad and then wiped clean with 70% Isopropyl Alcohol.

3. Eight cartridges of epoxy were applied onto the sandblasted strip of each block.

4. The plate was then placed on the epoxy and another test block was placed on top to apply the manufacturer's minimum specified pressure of 1-2 psi.

5. The epoxy was allowed to cure for 7 days.

85
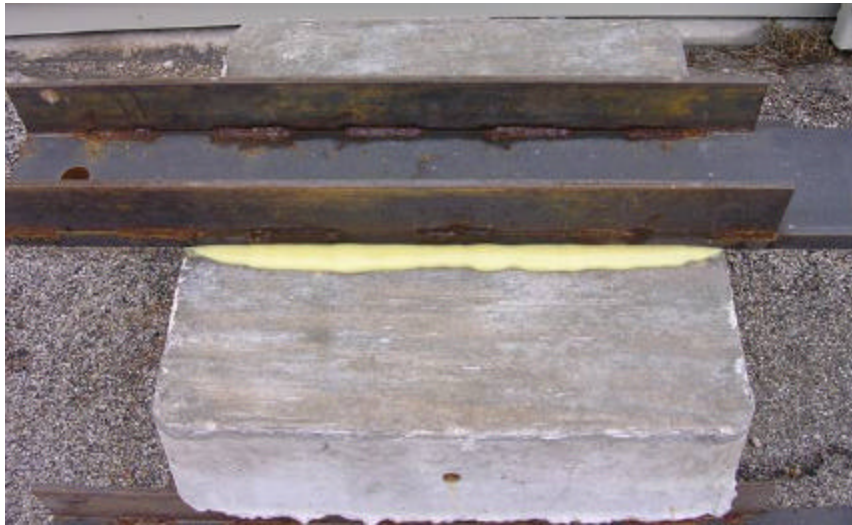
Figure 4.29: Epoxy Plate after installation

4.7   TEST PROGRAM

This section describes the three types of tests that were performed in this study: static tests, high-cycle fatigue tests, and low-cycle fatigue tests. Below is a brief description of each type of test, the steps taken to perform each one, and the test matrix followed to conduct this research.

4.7.1   Static Tests

Static tests were performed to obtain the load-slip behavior of each type of connector. They provided information on connection stiffness, ultimate strength and ductility. Data gathered were compared to those of Schaap (2004) and Hungerford (2004), and were also used to plan the fatigue tests.

One static test per connection method was deemed adequate. Replicate tests were performed for the POSST and WEDGB connection methods. As a result, a total of eight tests were performed.

Several steps were followed to conduct the static tests:

1. The specimens were placed on neoprene pads on the base plate of the frame.

2. The gaps between the specimen and the restraining angles were filled with hydrostone poured in plastic bags. The gap between the underside of the specimens and the test frame were filled with hydrostone at the corners. Neoprene pads were placed between the concrete block and the clamping angles. For cyclic tests, neoprene pads were replaced with hydrostone.

3. Once hydrostone in all locations had hardened, clamping angles were tightened down to restrain the movement of the concrete block.

4. The locations of the brackets were marked and were then glued to the sides of the steel plate with fast setting epoxy.

5. Once the epoxy had hardened, the LVDT's were clamped to the concrete block using carpenter's clamps.

6. The LVDT's were offset on the PDAQ to read zero initial displacement.

7. The 407 Controller was programmed to stop the test in the case of connector failure.

8. The load was manually increased at a slow rate.

9. Time, displacement, and load values were recorded by the PDAQ at a frequency of 1-2 Hz.

10. The controller stopped the test once the connector failed and zero load was read. If the concrete block cracked severely, the test was stopped manually.

4.7.2 High-Cycle Fatigue Tests

Tests in high-cycle fatigue were performed to assess the fatigue performance of shear connectors under repeated service loads. For these tests, stress range was used as the independent variable and the corresponding fatigue

life of each connector was measured in the number of cycles to failure, permitting construction of S-N curves as discussed in Chapter 2.

The stress ranges used in this research were selected as follows:

1. Stress ranges used by earlier researchers for the fatigue assessment of welded studs were also used for CIPST specimens. This enabled a direct comparison of results and gave additional information on the reliability of the direct shear test setup.

2. For all other connection methods, a single test was performed for each type of connector at a stress range already used for CIPST specimens. Depending on the response of each connector, the subsequent stress ranges were adjusted as needed.

3. It was essential that the selected stress ranges lie below the yield stress of the connector material. This was ensured by using the load-deflection response obtained from static tests for each connector type.

For cyclic tests, the 407 Controller required specified load ranges rather than stress ranges. Stress ranges were multiplied by the effective tensile stress area of each connector to obtain the corresponding load ranges.

To prevent inadvertent reversal of load, which could damage the specimen and the loading apparatus, a minimum load of 0.9 kips was specified for each load range. For most tests, a constant mean value was used, eliminating mean load as a variable. For tests with high stress ranges, however, the mean load was adjusted to keep the maximum load below the specified yield strength of the connector.

4.7.2.1 Test Matrix for High-cycle Fatigue Tests

Due to the unknown fatigue lives of the majority of connectors investigated and time constraints, only three tests per connection method were initially scheduled. The CIPST method was the only exception with seven tests

and four different stress ranges, intended to create more reliable benchmark data for comparison with retrofit alternatives. Table 4.4 is the test matrix of stress ranges for each connection method. The number of additional specimens tested for a give stress range is shown in parentheses adjacent to the stress ranges. A total of 20 high-cycle fatigue tests were performed on shear connectors. Each test generated a point on the S-N curves presented in Chapter 5.

Table 4.4: Test matrix for high-cycle fatigue tests

Shear Connection Methods with Tested Stress Ranges					
CIPST	**POSST**	**DBLNB**	**HTFGB**	**WEDGB**	**HASAA**
25 ksi	25 ksi	60 ksi	45 ksi	40 ksi	40 ksi
20 ksi	20 ksi (1)	40 ksi	35 ksi	30 ksi	35 ksi
15 ksi	15 ksi	33 ksi		25 ksi	30 ksi
10 ksi (1)					

4.7.2.2 *Testing Procedure for High-cycle Fatigue Tests*

The procedure for high-cycle fatigue tests followed the same first eight steps as for the static tests. The tests were started with an initial static loading before the application of cyclic loads, permitting comparison of the load-displacement data between high-cycle fatigue and static tests. The static load was applied by first manually increasing the load up to the upper limit of the load range (maximum load). Next, the load was reduced down to the lower limit (minimum load). Finally, the load was increased up to the mean load which corresponds to the "set point" in the 407 Controller.

Once the "set point" was reached, half of the loading amplitude (span) and the loading frequency were specified in the controller. Cyclic loading was then

applied until connector failure. A fatigue test was typically stopped if a connector showed no signs of failure after 5 million loading cycles. The number of load cycles applied to each specimen was displayed on the controller monitor. Several specimens that did not fail were loaded statically up to failure.

4.7.3 Low-Cycle Fatigue Tests

Shear connectors that showed adequate performance under high-cycle fatigue were also tested in low-cycle fatigue. The purpose of these tests was to assess the behavior of a shear connector subjected to overloads.

As is typical for tests in low-cycle fatigue, the connectors were tested under displacement control. This required the selection of a displacement range that forced the connector beyond its yield strength. In light of static test results, a displacement range between 0.1 in. and 0.2 in. was selected for each specimen. The specimens were tested until failure or 4000 displacement cycles were reached. At least 2 tests were performed per connector type (1 test for the CIPST method), for a total of 10 tests.

The procedure low-cycle fatigue tests followed the same steps as for high-cycle fatigue tests, with the only difference being that displacement control was used instead of load control. This required modifications only in the data acquisition process as explained in Section 4.2.3. Because instantaneous load values were not tracked by the controller, the tests could not be automatically stopped after connector failure. These tests were stopped manually and the number of load cycles was displayed on the controller monitor. Specimens that remained intact up to 4000 cycles were tested statically to determine their ultimate strength.

CHAPTER 5
Test Results

5.1   INTRODUCTION

This chapter presents the results from static, high-cycle fatigue, and low-cycle fatigue tests conducted on the cast-in-place welded stud and retrofit shear connectors. The reported results include the load-slip behavior of connections under static loading, high-cycle and low-cycle fatigue, and the failure modes of each specimen.

Results for 38 individual tests are reported in the following sections by their corresponding specimen identification (ID). The specimen ID's for static tests consist of the abbreviation of the connection method (Table 4.1) followed by "-ST" to indicate a static test. For example the static test conducted for the Cast-in-Place Welded Stud is referred to as CIPST-ST. Specimens for high-cycle tests are referred to as the abbreviation of the connection method followed by the stress range at which the specimen was tested. For example, a Cast-in-Place Welded Stud specimen tested at 25 ksi stress range is referred to as CIPST25. Specimens for low-cycle fatigue tests use the abbreviation for the connection method followed by a number indicating the order in which the specimen was tested. For example, the second low-cycle fatigue test specimen for the Double-Nut Bolt is referred to as DBLNB2.

5.2   STATIC TEST RESULTS

In this study, one of each of the investigated shear-connection methods was tested under static loading. Test results are summarized in Table 5.1. The

compressive strength of concrete on the day each specimen was tested is presented in Table A.1.

The ultimate shear load of connectors ranged between 21.1 kips for the Specimen POSST and 63.8 kips for Specimen 3MEPX. Connector slip at ultimate load from 0.001 in. for Specimen 3MEPX-ST to 0.70 in. for Specimen WEDGB-ST were obtained. Most failures occurred as a result of shearing of the connector at the steel-concrete interface, except Specimens WEDGB-ST and HTFGB, for which failure occurred through the connector below the steel-concrete interface, and Specimen 3MEPX-ST, which failed below the adhered surface of the concrete. Throughout this chapter, the failure mode of each specimen is described. In these descriptions "in front of the connector" refers to the side of the connector towards the loading ram, and "behind the connector" refers to the side of the connector away from the loading ram. Several images of failed specimens are also presented in this chapter, and the rest are provided in Appendix B.

Table 5.1: Summary of static test results

Specimen	Ultimate Load (kips)	Slip at Ultimate Load (in)	Load at 0.2 in. (kips)	Failed Component	Failure Location
CIPST-ST	29.4	0.69	20.5	Weld	Weld pool
POSST-ST	21.1	0.03	-	Weld	Steel-concrete interface
POSST-ST(F)*	28.8	0.27	28.4	Connector	Stem of stud
DBLNB-ST	28.9	0.32	27.1	Connector	Steel-concrete interface
HTFGB-ST	38.8	0.61	29.6	Connector	Below steel-concrete interface
HASAA-ST	22.9	0.33	22.0	Connector	Steel-concrete interface
WEDGB-ST	27.5	0.70	14.5	Connector	Below steel-concrete interface
3MEPX-ST	63.8	0.001	-	Concrete surface	Below adhered surface

*(F) denotes fillet-welded stud.

The relative slip between the steel plate and the concrete block was measured at the connector level by two LVDT's on each side of the steel plate. Slip values reported in this chapter are the average of the two LVDT readings in the direction of loading. Twisting of the steel plate was observed in some specimens, either by visual observation or from slip values measured by each

LVDT. Such twisting was removed by averaging each set of two LVDT readings, and that average is the relative slip reported in each test.

Grout was used for POSST and DBLNB specimens. The compressive strength of grout was determined by cylinder tests as previously mentioned in Chapter 4 at ages of 24 hours, 7 days, and after each test. Three separate sets of grouted specimens were constructed for static and fatigue tests. In Table 5.2 are reported the 24-hour and 7-day grout compressive strengths in those test specimens. Strength values were below the manufacturer-specified strengths of 5100 psi at 24 hours and 7000 psi at 7 days. This may be due to differences in actual mixture proportions used. The compressive strength of grout on the day of testing is reported in the following sections for each specimen.

Table 5.2: Tested average compressive grout strength for POSST and DBLNB specimens at 24 hours and 7 days

Time	Compressive Strength of Grout		
	POSST-ST POSST 25, 20, 20a DBLNB-ST, DBLNB 33, 40, 60	POSST-ST(F), POSST 15(F)	DBLNB1, DBLNB2
24 hours	4881 psi	4788 psi	4511 psi
7 days	6234 psi	5650 psi	5172 psi

5.2.1   Results for Cast-In-Place Welded Shear Stud (CIPST)

The load-slip curve of Specimen CIPST-ST is shown in Figure 5.1. The ultimate load of the connector reached 29.4 kips with a corresponding slip of 0.69 in.
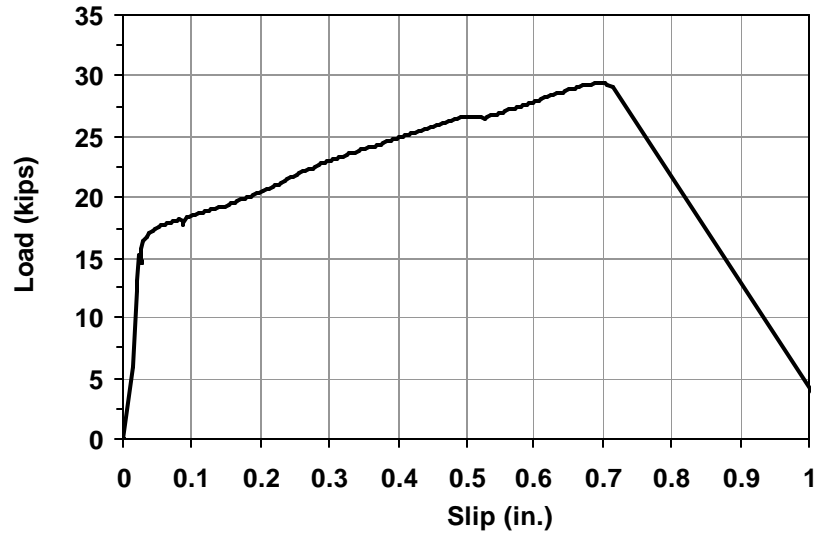
Figure 5.1: Load-slip curve for Specimen CIPST-ST

The stud failed through the weld collar as shown in Figure 5.2 (b). In Figure 5.2 (a) the local crushing of concrete in front of the stud is shown. Longitudinal cracks were observed in the line of loading, both behind and in front of the connector as shown in Figure 5.3. Air voids in the concrete were also apparent at the surface underneath the steel plate. The voids at this location can be attributed to the rising of air bubbles to the surface of the concrete during casting of concrete. These air bubbles most likely were trapped underneath the steel plate, causing air pockets to form.

a)   *b)*
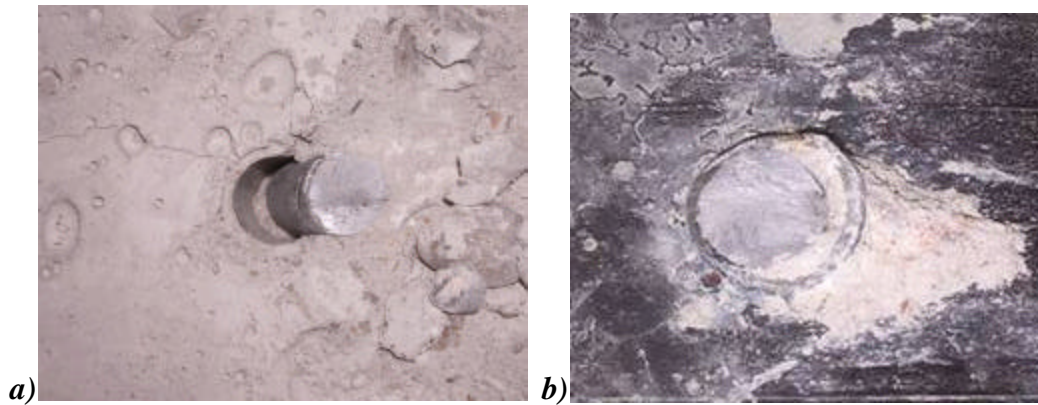
Figure 5.2: Failed Specimen CIPST-ST: a) concrete block, b) steel plate

Figure 5.3: Voids and longitudinal crack behind stud (Specimen CIPST-ST)

During the testing of Specimen CIPST-ST, linear potentiometers (LP) were used at both ends of the steel plate (in the line of loading) to check for the lifting of the plate. Small acrylic pieces were taped on each end of the steel plate for the LP's to rest on. This was done to reduce the friction between the LP and the steel surface. The LP data did not indicate any vertical movement of the steel plate. The clamping rod was also checked to determine whether it resisted any

96

applied load, by pulling the steel plate monotonically after connector failure and monitoring any increase in load. No resistance was observed due to clamping.

5.2.2   Results for Post-Installed Welded Shear Stud (POSST)

The load-slip curve for Specimen POSST-ST is shown in Figure 5.4. The ultimate load of the connector reached 21.1 kips with a corresponding slip of 0.03 in. Specimen POSST-ST had a bent steel plate which left a gap relative to the concrete block at the connector level. A maximum gap size of approximately 1/8 in. was measured (Figure 5.5).
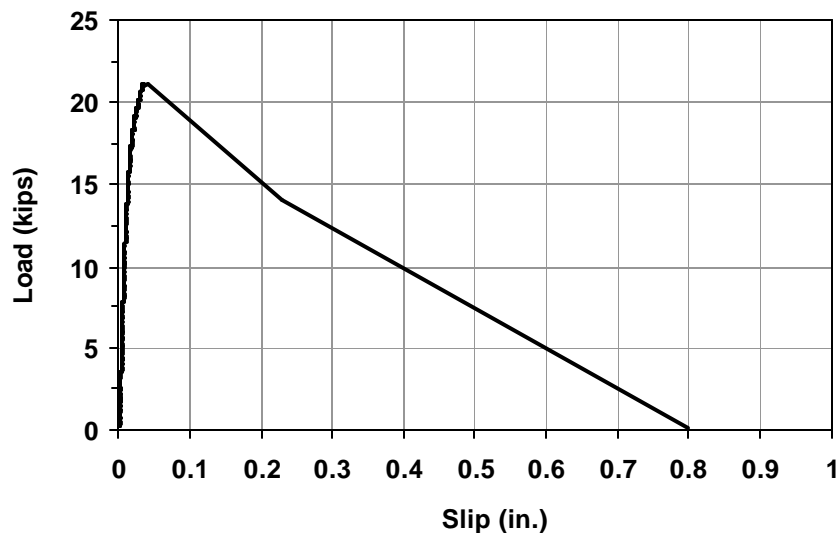
Figure 5.4: Load-slip curve for Specimen POSST-ST

Specimen POSST-ST failed in a brittle manner at an overall slip of less than 0.1 in. The stud failed through the weld, removing some of the plate material behind the shear stud as shown in Figure 5.6. Local crushing and cracking of the grout was also observed in front of the stud (Figure 5.7).

97

Cylinder tests were conducted to determine the strength of grout on the day of testing. An average compressive grout strength of 7281 psi was obtained at an age of 27 days.

Figure 5.5: Gap between steel plate and concrete block (Specimen POSST-ST)

Figure 5.6: Failure of weld in shear (Specimen POSST-ST)

Figure 5.7: Crushing of grout in front of stud (Specimen POSST-ST)

To determine the cause of the brittle failure of Specimen POSST-ST, a supplementary test specimen was built using a fillet-welded stud. For this specimen, a bent plate was used, similar to the one observed for Specimen POSST-ST. The load-slip curve for Specimen POSST-ST(F), shown in Figure 5.8, indicates increased strength and ductility due to the use of a fillet-weld. Based on this curve, it was concluded that the weld for Specimen POSST-ST was defective and caused the brittle failure of the specimen. The bent plate did not affect the failure mode.
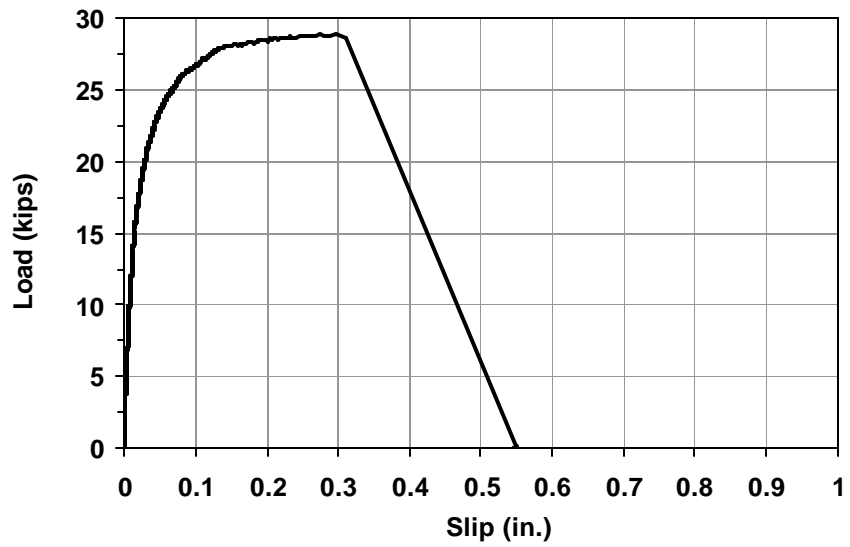
Figure 5.8: Load-slip curve for Specimen POSST-ST(F)

The fillet-welded stud failed through the stem of the stud as shown in Figure 5.9. Figure 5.10 shows local crushing of grout in front of the stud. The average compressive strength of the grout in the specimen was 7852 psi at an age of 27 days.

100
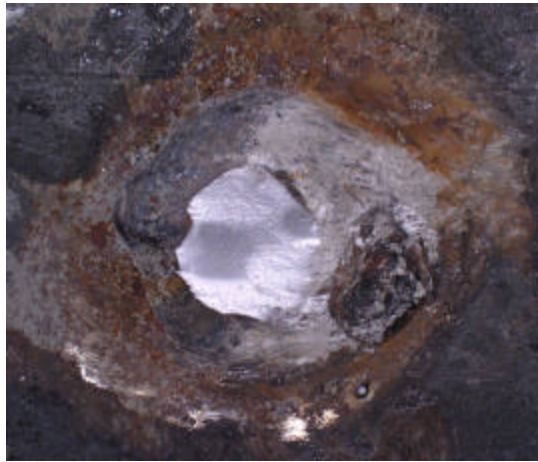
Figure 5.9: Failure of stud through stem (Specimen POSST-ST(F))

Figure 5.10: Crushing of grout in front of stud (Specimen POSST-ST(F))

5.2.3 Results for Double-Nut Bolt (DBLNB)

Specimen DBLNB-ST reached an ultimate load of 28.9 kips with a corresponding slip of 0.32 in. Due to the pretension applied to this type of connector, the load-slip curve in Figure 5.11 shows an initial increase in load without any related slip. The pretension was eventually overcome after an applied load of about 5 kips, after which load and slip increased, accompanied by bearing of the connector against the steel plate.
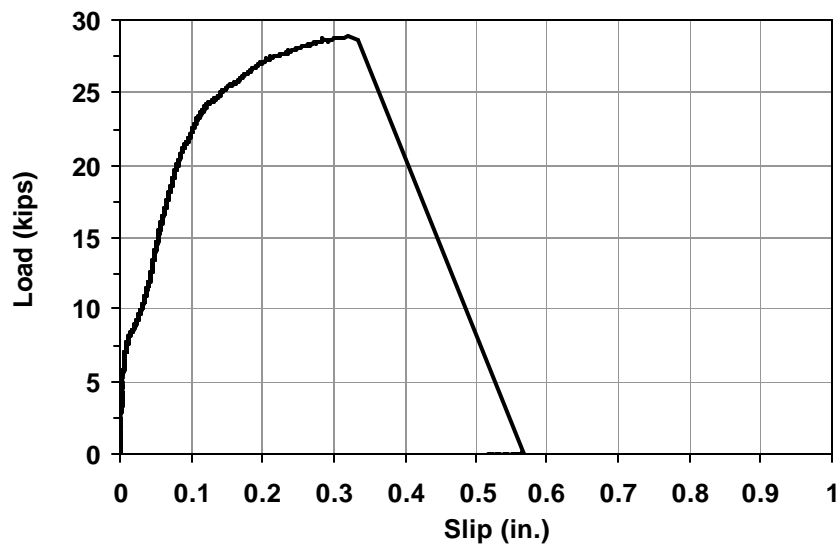
Figure 5.11: Load-slip curve for Specimen DBLNB-ST

The connector failed in shear at the steel-concrete interface (Figure 5.12), accompanied by local crushing of grout in front of the connector. In Figure 5.13 the section of the failed connector above the steel-concrete interface is shown. The bearing deformation in the steel plate is shown in Figure 5.14.

Figure 5.12: Failed connector at steel-concrete interface (Specimen DBLNB-ST)

Figure 5.13: Side and top view of the failed connector (Specimen DBLNB-ST)

Figure 5.14: Bearing deformation in steel plate (Specimen DBLNB-ST)

The compressive strength of grout was obtained immediately after the connection specimen was tested, and the average compressive strength was 9788 psi at 40 days.

5.2.4 Results for High-Tension, Friction Grip Bolt (HTFGB)

Similar to Specimen DBLNB-ST, pretension was applied to the connector during installation. During testing, this resulted in an initial increase in load without slip until approximately 5 kips (Figure 5.15), followed by an increase in load due to bearing of the connector against the steel plate. Specimen HTFGB-ST reached an ultimate load of 38.8 kips with a corresponding slip of 0.61 in. The slip values were based on the readings from one LVDT only, because at the end of the test the second LVDT was found to not be in contact with the bracket adhered to the steel plate. During the initial stages of the test, the disregarded LVDT readings displayed slightly smaller slip values compared to the other LVDT. Therefore, the actual slip at ultimate in the line of the connector may be slightly less than the reported value.
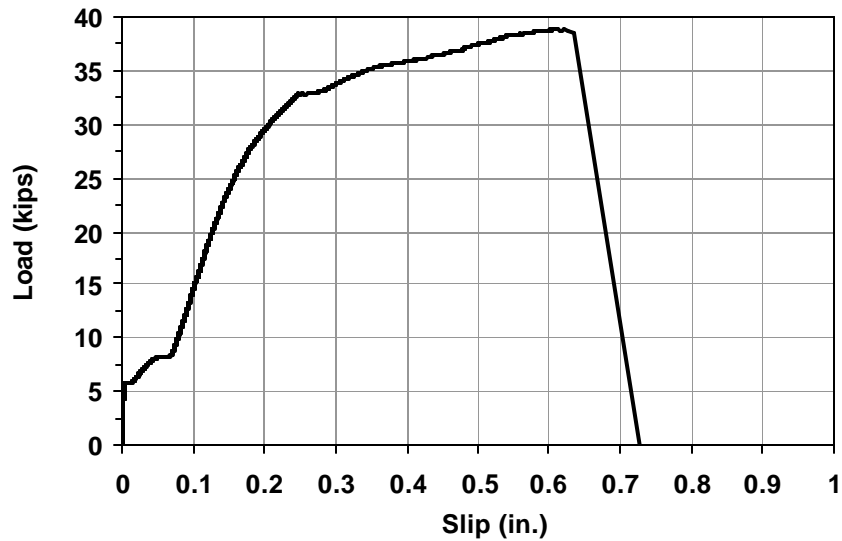
Figure 5.15: Load-slip curve for Specimen HTFGB-ST

The connector failed in shear slightly below the steel-concrete interface (Figure 5.16). In Figure 5.17 the section of the failed connector above the failure plane is shown. Connector failure was accompanied by cracking of the concrete block (Figure 5.18), local crushing of concrete in front of the connector, and bearing deformation of the steel plate.
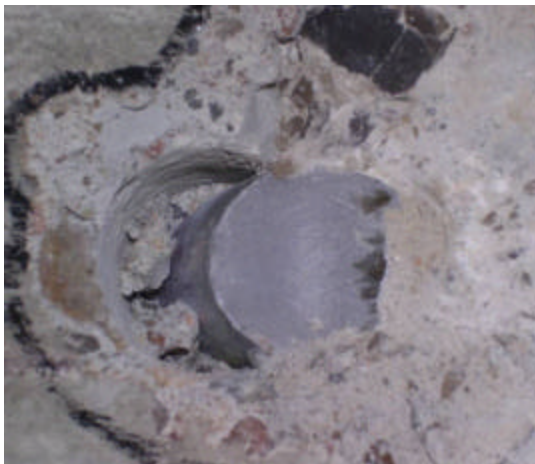
Figure 5.16: Shear failure of the Specimen HTFGB-ST below the steel - concrete interface

Figure 5.17: Failed connector (Specimen HTFGB-ST)

Figure 5.18: Shear failure of connector accompanied by cracking of the concrete block (Specimen HTFGB-ST)

5.2.5 Results for Adhesive Anchor (HASAA)

Specimen HASAA-ST reached an ultimate load of 22.9 kips at a slip of 0.33 in. The load–slip curve for this specimen, shown in Figure 5.19, indicates an initial loading without slip of up to approximately 5 kips. This is due to the pretensioning of the connector during installation. Once the friction force due to pretension was overcome, load and slip increased, and the connector slipped into bear against the steel plate.
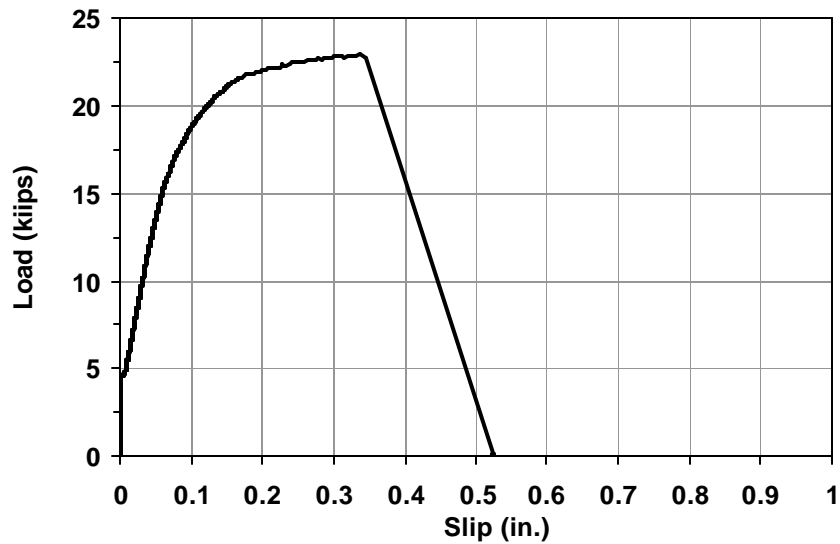
Figure 5.19: Load-slip curve for Specimen HASAA-ST

The connector failed in shear at the steel-concrete interface. During installation, excess adhesive spread around the connector at the steel-concrete interface and in the hole in the steel plate. The local crushing of concrete and adhesive in front of the connector is shown in Figure 5.20. After failure, the section of the failed connector inside the steel plate could not be removed (Figure 5.21).

Figure 5.20: Shear failure of Specimen HASAA-ST at steel-concrete interface

Figure 5.21: Failed HAS-E Anchor in steel plate (Specimen HASAA-ST)

5.2.6   Results for Concrete Screw (WEDGB)

The load-slip curve, as a result of the static testing of Specimen WEDGB-ST, is shown in Figure 5.22. This specimen showed the largest slip among all

connections tested. Specimen WEDGB-ST reached an ultimate load of 27.5 kips at a slip of 0.70 in. An initial increase in load without any slip is observed up to about 2.5 kips. This can be attributed to the fact that the locking teeth underneath the bolt head locked against the steel plate as the connector was tightened. Once friction forces between the bolt head and steel plate were overcome, the connector slipped into bearing with the steel plate, resulting in an increase in load and slip.
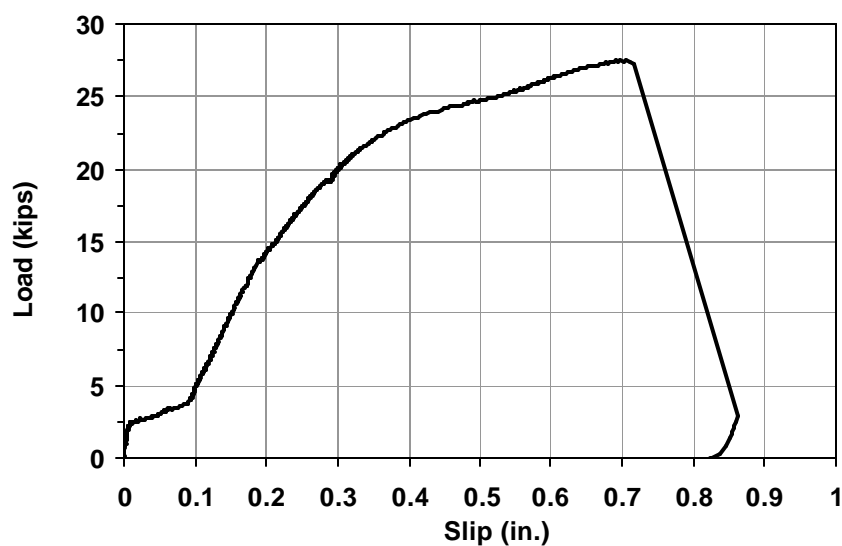
Figure 5.22: Load-slip curve for Specimen WEDGB-ST

Specimen WEDGB-ST failed in a combination of shear and tension below the steel-concrete interface (Figure 5.23), accompanied by local crushing of concrete behind and in front of the connector (Figure 5.24), suggesting a possible pryout failure. In Figure 5.25, of the side and front view of the failed connector, the bearing location of the connector on the steel plate is shown, as well as cracks opposite the bearing side of the connector. The connector caused significant bearing deformation in the steel plate (Figure 5.26).

Figure 5.23 Failed Specimen WEDGB-ST

Figure 5.24 Local crushing of concrete (Specimen WEDGB-ST)

Figure 5.25 Side and front view of failed connector (Specimen WEDGB-ST)

Figure 5.26 Bearing deformation of steel plate (Specimen WEDGB-ST)

5.2.7 Results for Epoxy Plate (3MEPX)

Specimen 3MEPX-ST showed the highest ultimate shear strength and the least amount of slip among all connectors tested. The load-slip curve of the specimen is shown in Figure 5.27. Specimen 3MEPX-ST reached an ultimate load of 63.8 kips without slip until failure.
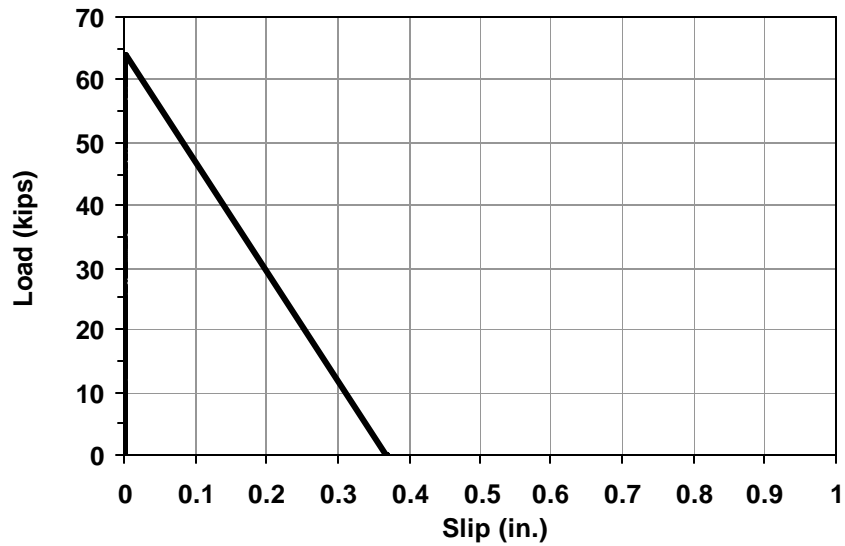
Figure 5.27: Load-slip curve for Specimen 3MEPX-ST

Figure 5.28 shows Specimen 3MEPX-ST after failure. Shear failure occurred primarily below the adhered surface of the concrete. Less than one-quarter of the adhered surface failed at the steel-concrete interface, possibly due to insufficient bond between the epoxy and steel at those locations.

Figure 5.28: Failed Specimen 3MEPX-ST

5.3 RESULTS FOR HIGH-CYCLE FATIGUE TESTS

This section presents results from 20 high-cycle fatigue tests conducted at predetermined stress ranges for each shear connection method. Due to the brittle behavior exhibited by Specimen 3MEPX-ST, 3MEPX specimens were not tested in high-cycle fatigue.

Each high-cycle fatigue test started with an initial application of monotonic load followed by the application of load cycles until failure, as previously described in Chapter 4. Each specimen was tested either until failure occurred or until 5 million loading cycles was reached. Test results are summarized in Table 5.3, and test parameters for each specimen are provided in Table A.2.

Stress range was the primary variable for investigations in high-cycle fatigue. S-N plots, which are typically used to present the fatigue life of a

material (number of cycles to failure) at different stress ranges, are used in the following subsections to present results for each shear connection method. The stress range applied to each connector is plotted on the vertical axis and the number of cycles to failure is plotted on the horizontal axis in logarithmic scale. Stress ranges were calculated based on the effective tensile stress area of each connector at the steel-concrete interface.

Table 5.3: Summary of results for high-cycle fatigue tests

Specimen	Stress Range (ksi)	Load Range (kips)	Cycles to Failure
CIPST25	25	11.0	5815
CIPST20	20	8.8	31690
CIPST15	15	6.6	49234
CIPST10	10	4.4	312094
CIPST10a[+]	10	4.4	>14700000
POSST25	25	11.0	124731
POSST20	20	8.8	94180
POSST20a[+]	20	8.8	112829
POSST15(F)*	15	6.6	>5000000
DBLNB60	60	20.0	72961
DBLNB40	40	13.4	>5500000
DBLNB33	33	11.0	>5000000
HTFGB45	45	19.9	191819
HTFGB35	35	15.5	>5600000
WEDGB40	40	15.4	1172
WEDGB30	30	11.5	297500
WEDGB25	25	9.6	543133
HASAA40	40	13.4	92400
HASAA35	35	11.7	424789
HASAA30	30	10.0	694633

* (F) denotes fillet-welded stud
+ "a" denotes replica test

Table 5.4: Summary of failure modes in high-cycle fatigue

Specimen	Failed Component	Failure Location
CIPST25	Weld	Steel-concrete interface
CIPST20	Weld	Steel-concrete interface
CIPST15	Weld	Steel-concrete interface
CIPST10	Weld	Steel-concrete interface
CIPST10a[+]	No Failure	-
POSST25	Weld	Steel-concrete interface
POSST20	Weld	Steel-concrete interface
POSST20a[+]	Weld	Steel-concrete interface
POSST15(F)*	Connector	Stem of stud above weld pool
DBLNB60	Connector	Below steel-concrete interface
DBLNB40	No Failure	-
DBLNB33	No Failure	-
HTFGB45	Connector	Above steel-concrete interface
HTFGB35	No Failure	-
WEDGB40	Connector	Below steel-concrete interface
WEDGB30	Connector	Below steel-concrete interface
WEDGB25	Connector	Below steel-concrete interface
HASAA40	Connector	Above and below steel-concrete interface
HASAA35	Connector	Above and below steel-concrete interface
HASAA30	Connector	Above steel-concrete interface

* (F) denotes fillet-welded stud
+ "a" denotes replica test

Load-slip readings for connectors were recorded during the initial application of monotonic load and intermittently throughout cyclic testing, to

assess degradation in stiffness under high-cycle fatigue loading. The resulting load-slip curves showed increasing slip and decreasing stiffness with cycling for all connectors, with quantitative changes varying with stress range and connection type. In Figure 5.29 are shown the static and cyclic load-slip curves for Specimen CIPST25, representative of the general trend observed in the load-slip behavior of all investigated connectors. The load-slip curves of individual test specimens are presented in Appendix C, with the exception of Specimen CIPST20, for which the data acquisition system malfunctioned at the time of testing.
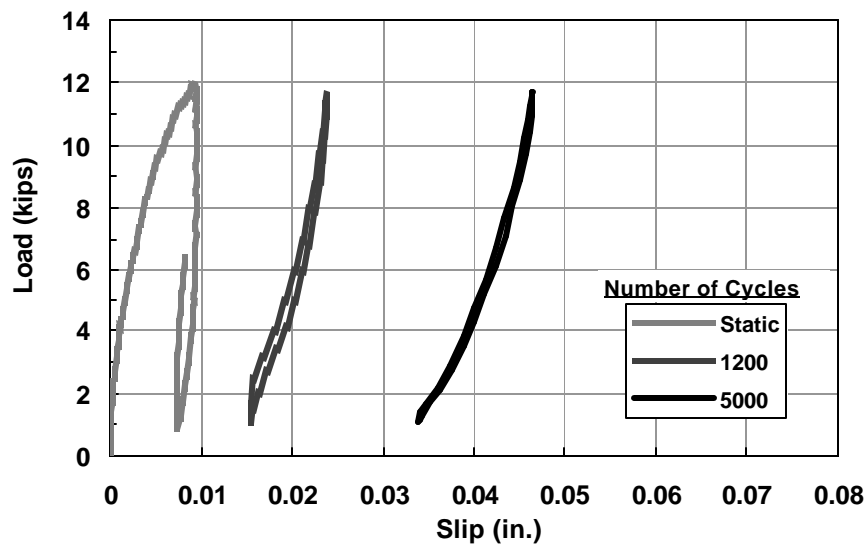
Figure 5.29: Static and cyclic load-slip curves for Specimen CIPST25

The failure mode of each specimen is described in this section along with figures representative of general failure modes. Images of failed specimens not presented here are provided in Appendix D.

5.3.1 Results for Cast-in-Place Welded Stud (CIPST)

Five CIPST specimens were tested under high-cycle fatigue at four different stress ranges: 25 ksi, 20 ksi, 15 ksi, and two tests at 10 ksi. The resulting S-N plot is shown in Figure 5.30. The number of cycles to failure ranged between 5815 cycles for Specimen CIPST25 and 312094 cycles for Specimen CIPST10. Specimen CIPST10a did not fail before 14.7 million load cycles and is shown as a runout specimen with an arrow adjacent to the corresponding data point.
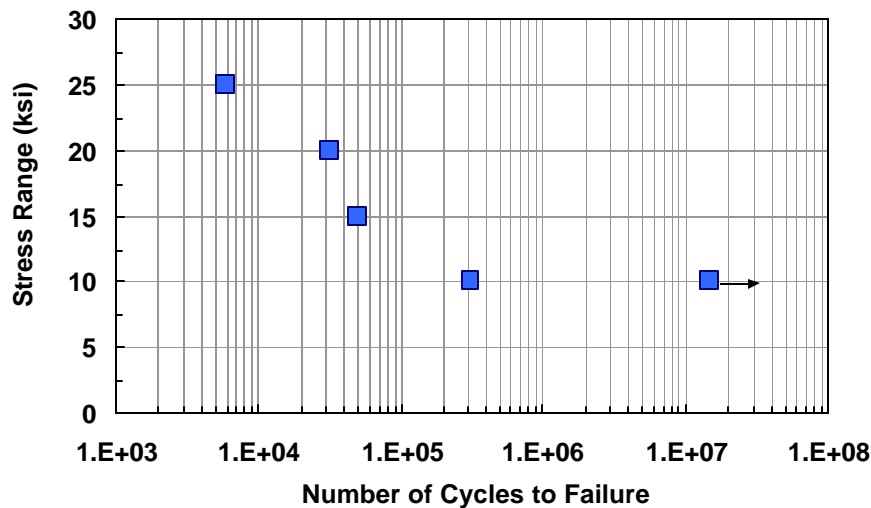
Figure 5.30: S-N curve for CIPST specimens

At a stress range of 10 ksi, one CIPST specimen failed while the other did not fail within 5 million cycles. It is probable that 10 ksi is very close to the endurance limit for that type of specimen.

All CIPST specimens except Specimen CIPST10a failed in shear at the steel-concrete interface. Failure initiated at the stud weld and penetrated through the steel plate; removing some of the plate material. In Figure 5.31 the failed

120

Specimen CIPST15 is shown, and is representative of the typical failure mode observed for all CIPST specimens. Failure of shear studs was accompanied by local crushing of concrete in front of the stud. Voids on the concrete surface under the steel plate were also observed (Figure 5.31).

a)

b)
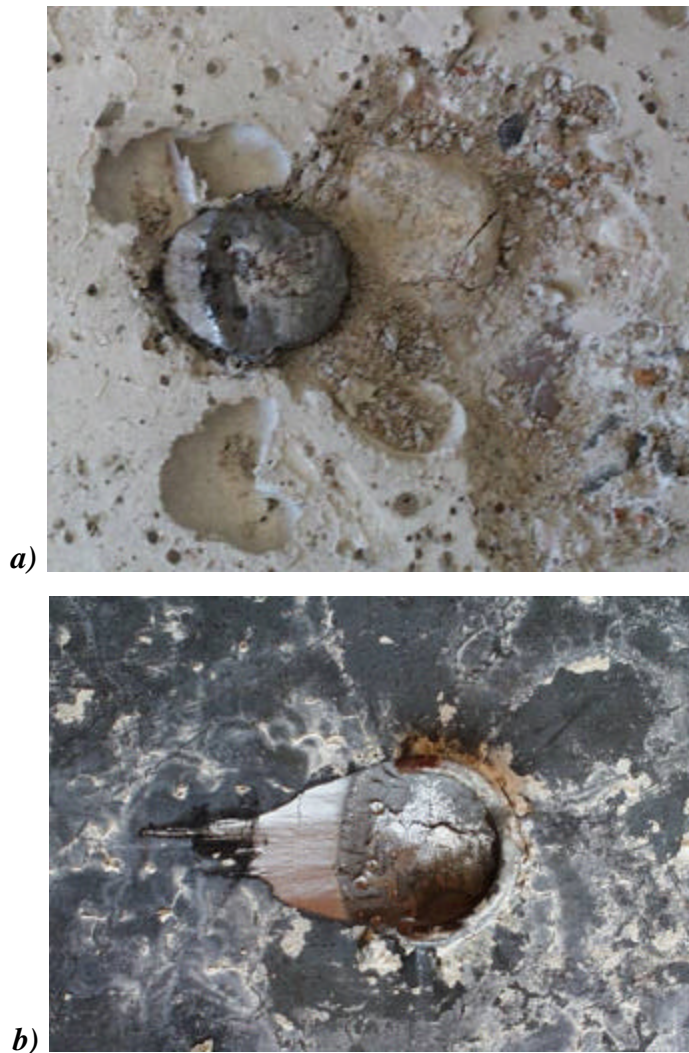
Figure 5.31: Failed Specimen CIPST15: a) concrete block, b) steel plate

During the testing of Specimen CIPST20, a defective servovalve caused several applications of reversed loading (slightly below zero kips) on the connector. The servovalve was replaced after 400 loading cycles.

Slight rocking of the concrete block was observed during the testing of Specimens CIPST15 and CIPST10a. This was due to the insufficient application of hydrostone around the concrete blocks.

5.3.2 Results for Post-Installed Welded Stud (POSST)

Four POSST specimens were tested under high-cycle fatigue at three different stress ranges: 25 ksi, two specimens at 20 ksi, and 15 ksi. The resulting S-N plot is shown in Figure 5.32. The number of cycles to failure ranged between 124731 cycles for Specimen POSST25 and 94180 cycles for Specimen POSST20. Specimen POSST15(F) did not fail at 5 million cycles, and is shown with an arrow next to its data point. An additional test was conducted at a 20 ksi stress range, since Specimen POSST20 had a shorter fatigue life than Specimen POSST25 specimen. The similar fatigue lives of Specimens POSST20a and POSST20 confirms the reliability of the result for those specimens. The data point for POSST25 may also be reliable, even though it shows the scatter typically associated with fatigue data.
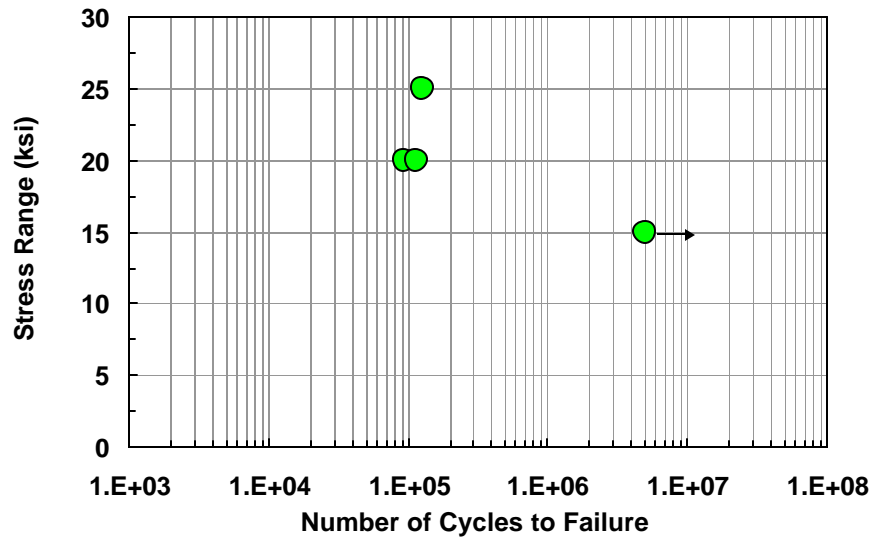
Figure 5.32: S-N plot for POSST specimens

The 24-hour and 7-day grout strengths for POSST specimens are presented in Table 5.2. The compressive grout strength of each POSST specimen on the day of testing is presented in Table 5.5.

Table 5.5: Tested average compressive grout strength for POSST specimens on the day of testing

Specimen	Compressive Strength (psi)
POSST25	9178
POSST20	8051
POSST20a	8462
POSST15(F)	7852

All POSST specimens except Specimen POSST15(F) failed in shear at the steel-concrete interface. Failure was typically marked by local crushing of grout in front of the stud. Specimens POSST25 and POSST20a showed the same failure mode where fracture occurred at the weld. The failed Specimen POSST25 is shown in Figure 5.33, in which bending of the stud is apparent at the steel-concrete interface. Specimen POSST20 failed through the heat-affected zone of the steel plate as shown in Figure 5.34. For this specimen, misalignment of the steel plate with the loading ram was observed prior to testing. This resulted in a torsional movement of the steel plate under load.

a)

b)

Figure 5.33: Failed Specimen POSST25: a) concrete block, b) steel plate

a)

b)
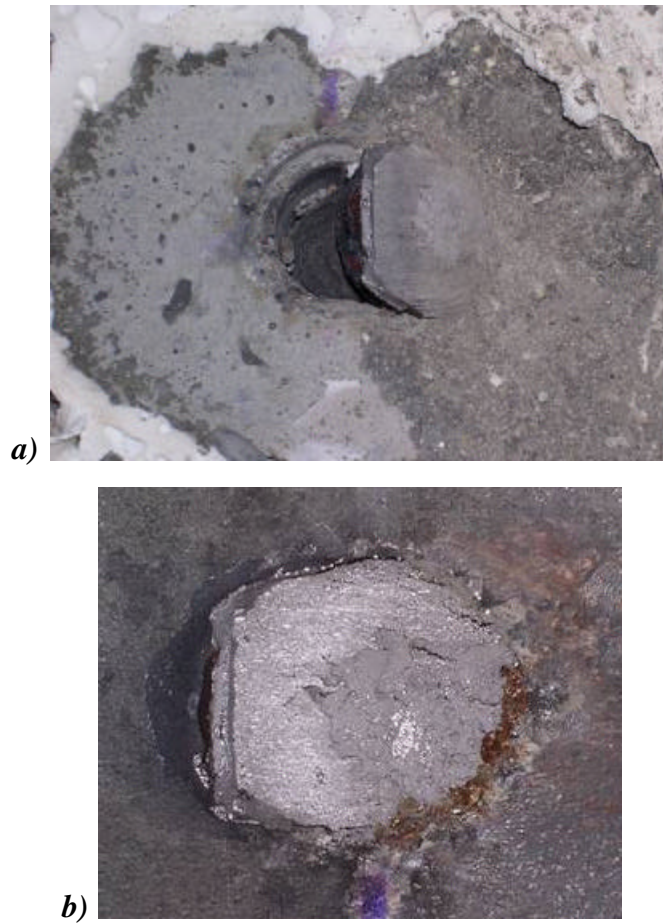
Figure 5.34: Failed Specimen POSST20: a) concrete block, b) steel plate

Specimen POSST15(F) was constructed at the same time as Specimen POSST-ST(F) and had a fillet-welded stud. After 5 million fatigue cycles, the connector was tested statically to determine its ultimate load, and a value of 29.0 kips was obtained. Specimen POSST15(F) failed, like Specimen POSST-ST(F), through the stem of the stud above the weld pool (Figure 5.35).
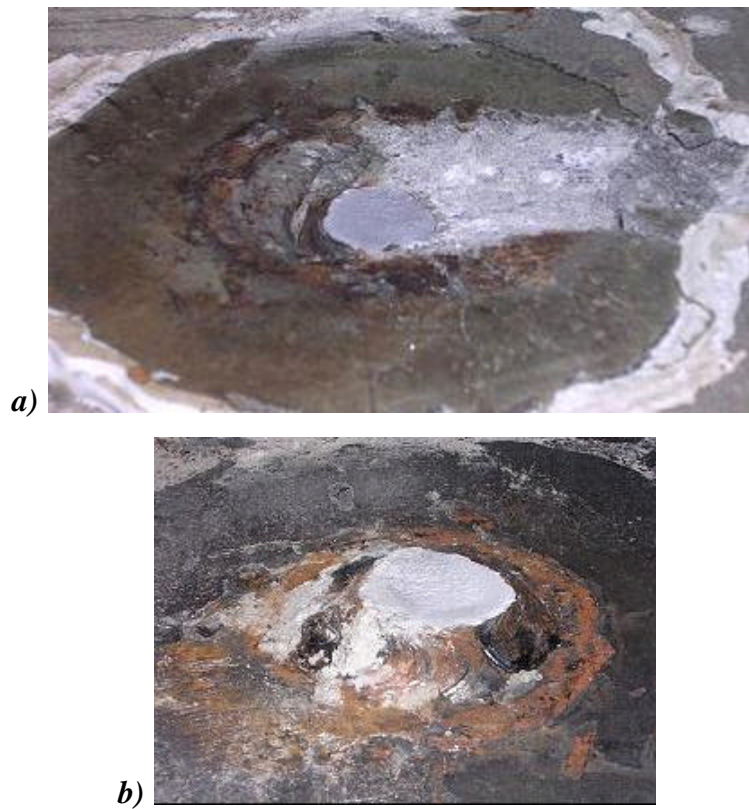
Figure 5.35: Failed Specimen POSST15(F): a) concrete block, b) steel plate

5.3.3 Results for Double-Nut Bolt (DBLNB)

Three DBLNB specimens were tested under high-cycle fatigue at three different stress ranges: 60 ksi, 40 ksi, and 33 ksi. The resulting S-N plot is shown in Figure 5.36. Fatigue failure was obtained only for Specimen DBLNB60. Specimens DBLNB40 and DBLNB33 remained intact up to 5 million loading cycles. The fatigue testing of these specimens was stopped and both specimens were loaded statically to obtain the ultimate load of the connectors.
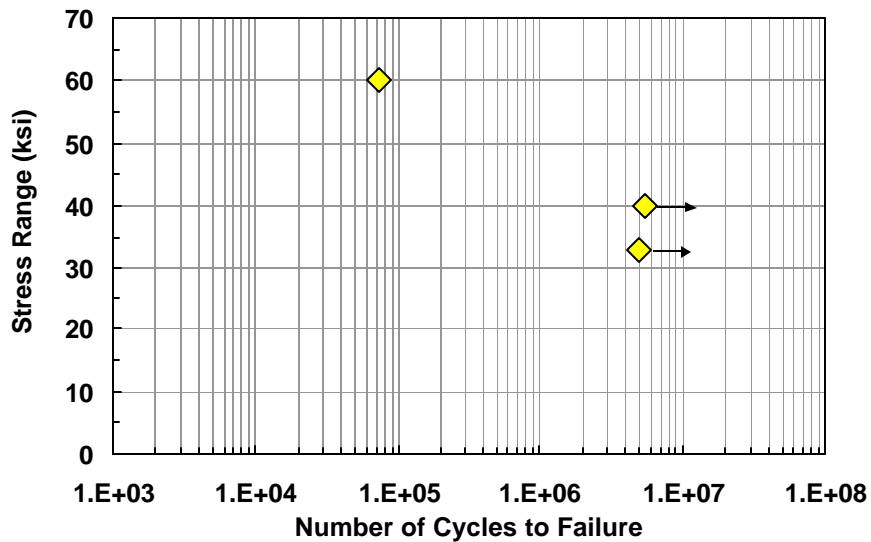
Figure 5.36: S-N curve for DBLNB specimens

The 24-hour and 7-day grout strength for DBLNB specimens were presented earlier in Table 5.2. The compressive grout strength of each DBLNB specimen on the day of testing is presented in Table 5.6.

Table 5.6: Tested average compressive grout strength for DBLNB specimens on the day of testing

Specimen	Compressive Strength of Grout (psi)
DBLNB60	9648
DBLNB40	10226
DBLNB33	10557

The only fatigue failure occurred for Specimen DBLNB60, through the connector below the steel-concrete interface. The failure plane corresponded to

128

the level at which the second nut on the threaded rod ended (Figure 5.37). Significant crushing of both the grout and concrete was observed in front of the connector. This may be attributed to the layer of sealant between the grout and concrete at the steel-concrete interface. The sealant may have decreased the confinement around the grout, causing it to crush locally at early stages of loading. This may have shifted the reaction on the connector below the steel-concrete interface resulting in the observed failure mode.

Figure 5.37: Failed Specimen DBLNB60

Specimens DBLNB40 and DBLNB33 failed in shear at the steel-concrete interface. Specimen DBLNB40 reached an ultimate load of 29.0 kips, while Specimen DBLNB33 reached 29.4 kips. In Figure 5.38, the failed Specimen DBLNB40 is shown and is representative of the failure mode of Specimen DBLNB33.

129

The concrete block of Specimen DBLNB40 had an uneven surface which left a gap relative to the steel plate of approximately 1/2 in. at the back and 1/8 in. in the front of the specimen. Specimen DBLNB33, on the other hand, had a bent steel plate which left a gap relative to the concrete block of approximately 1/8 in. at each end of the specimen. During testing, the steel plate lifted and twisted slightly. Slip readings from only one LVDT were used, because one of the brackets broke during testing.

a)

b)
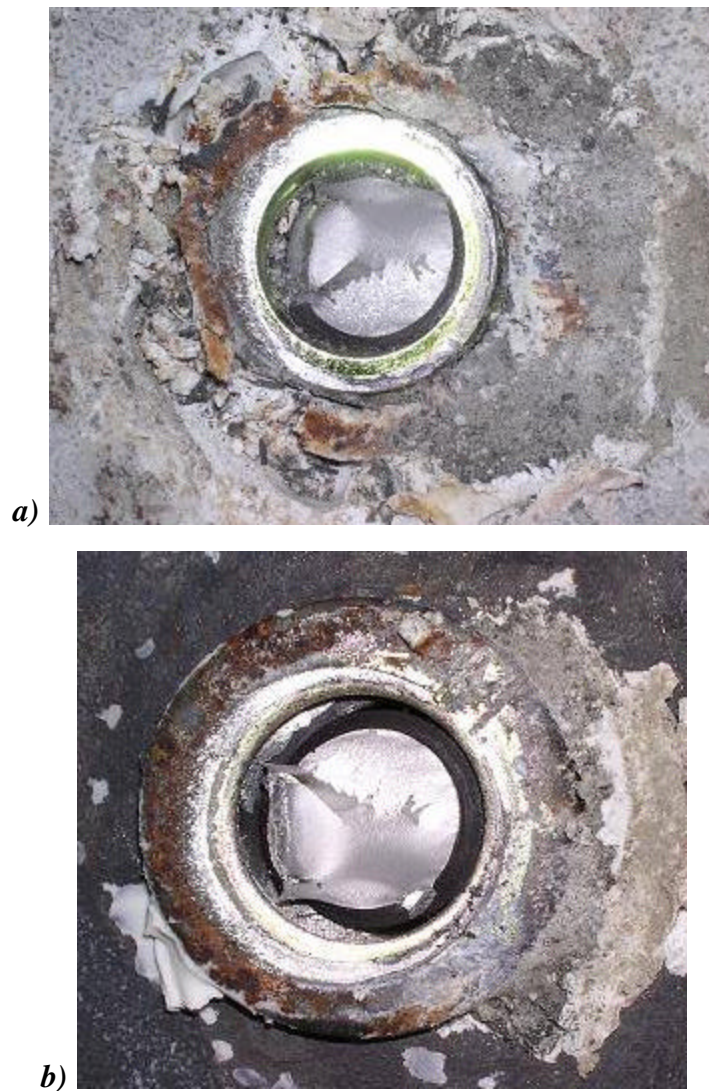
Figure 5.38: Failed Specimen DBLNB40: a) concrete block, b) steel plate

5.3.4 Results for High-Tension, Friction Grip Bolt (HTFGB)

Two HTFGB specimens were tested under high-cycle fatigue at two different stress ranges: 45 ksi and 35 ksi. The resulting S-N plot is shown in Figure 5.39. Only Specimen HTFGB45 failed in fatigue. Specimen HTFGB35

withstood 5.6 million loading cycles and was later tested under low-cycle fatigue; results for that test are discussed in Section 5.4.
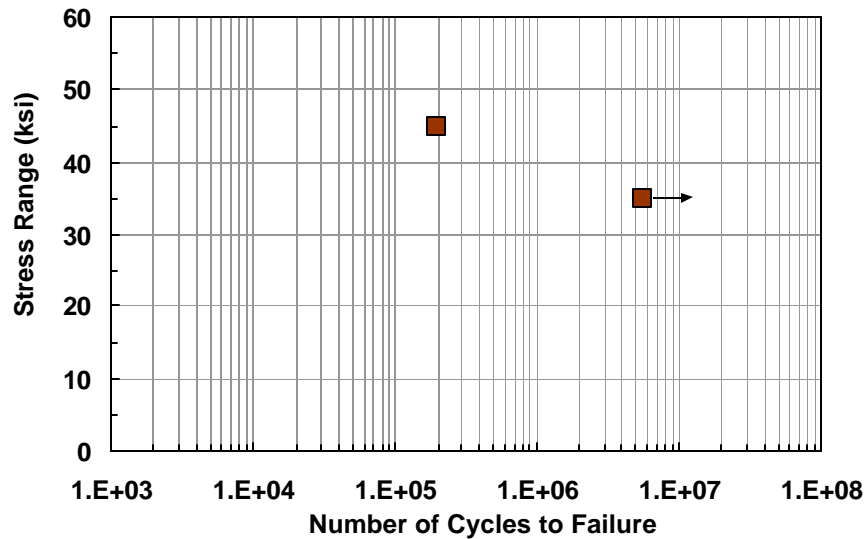
Figure 5.39: S-N curve for HTFGB specimens

Specimen HTFGB45 failed above the steel-concrete interface, within the steel plate. Local crushing of concrete around the connector and significant bearing deformation in the steel plate were observed.

5.3.5   Results for Adhesive Anchor (HASAA)

Three HASAA specimens were tested under high-cycle fatigue at three different stress ranges: 40 ksi, 35 ksi, and 30 ksi. The resulting S-N plot is shown in Figure 5.40. Fatigue failure was obtained for all three specimens.
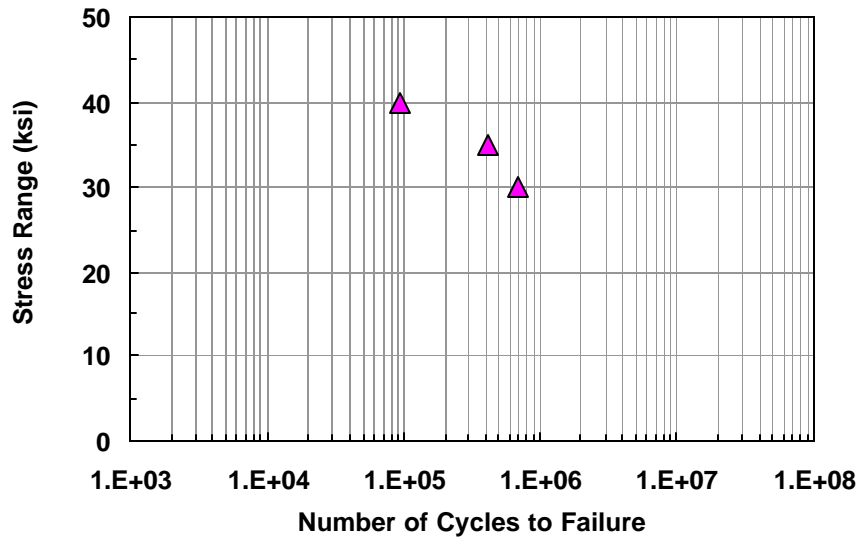
Figure 5.40: S-N curve for HASAA specimens

Fatigue failure of Specimens HASAA40 and HASAA35 occurred at two locations through the connectors, above and below the steel-concrete interface. The failed Specimen HASAA40 is shown in Figure 5.41 and the failed connector is shown in Figure 5.42.   This type of failure may be due to the presence of HY 150 adhesive in the hole in the steel plate. It is likely that the adhesive provided a restraint for part of the connector (adhesive was not spread through the entire depth of the hole) in the steel plate, preventing the slip of the connector within the hole. This possibly resulted in two reactions on the connector: below the steel-concrete interface (inside the concrete block) and above the steel-concrete interface (inside the steel plate). This may have caused stress concentrations at the reaction points, causing the connector to fail in double shear. Local crushing of concrete was also observed in front of the connector.

133

a)

b)

Figure 5.41: Failed Specimen HASAA40: a) concrete block, b) steel plate

Figure 5.42: HAS-E anchor failed at two locations (Specimen HASAA40)

Specimen HASAA30 failed only at one location through the connector, above the steel-concrete interface. The part of the connector inside the concrete block was not checked for fracture. It is possible that the connector also failed below the steel-concrete interface like Specimens HASAA40 and HASAA30. In Figure 5.43, failed Specimen HASAA30 is shown with excess HY 150 adhesive spread around the connector at the steel-concrete interface as well as in the hole in the steel plate. Local crushing of concrete and the adhesive is also shown.

a)

b)
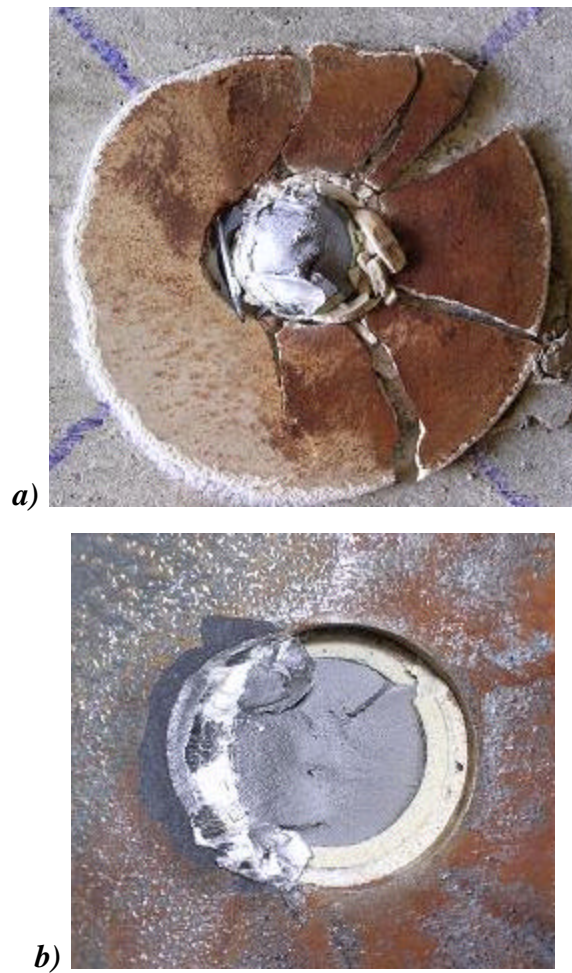
Figure 5.43: Failed Specimen HASAA30: a) concrete block, b) steel plate

Specimen HASAA30 had a bent steel plate which created a gap relative to the concrete block of about 1/8 in., in line with the connector. For Specimen HASAA40 a gap between the steel plate and concrete block of less than 1/8 in. was noticed along the steel-concrete interface.

5.3.6 Results for Concrete Screw (WEDGB)

Three WEDGB specimens were tested under high-cycle fatigue at three different stress ranges: 40 ksi, 30 ksi, and 25 ksi. The resulting S-N plot is shown in Figure 5.47. All three specimens failed in fatigue after 1172, 297500, and 543133 cycles respectively.
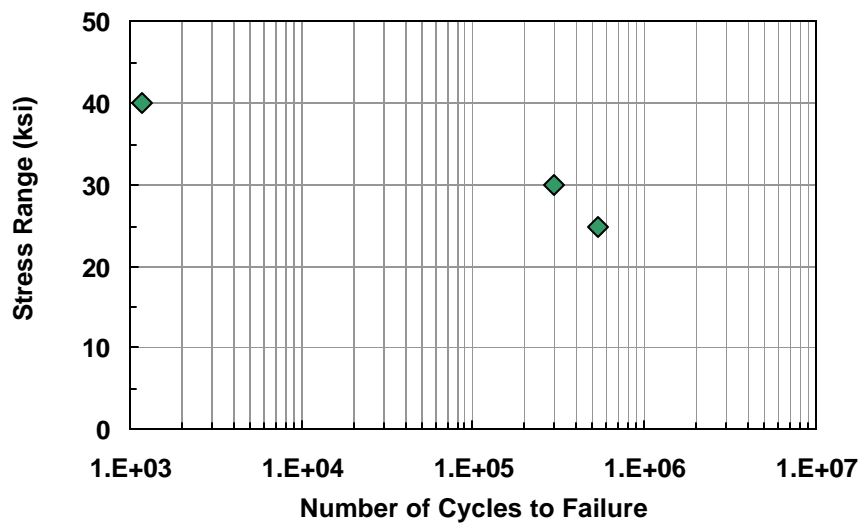
Figure 5.44: S-N curve for WEDGB specimens

WEDGB specimens failed below the steel-concrete interface. This indicates that a combination of shear and tension forces acted on each connector. Significant crushing and spalling of concrete around the connectors and bearing deformation in the steel plates were observed. The severity of the crushing in concrete and bearing deformation in the steel plates decreased with decreasing stress range.

The failed Specimen WEDGB40 is shown in Figure 5.45. Failure of the connector began at the root of a thread below the steel-concrete interface.

137

Figure 5.45: Failed Specimen WEDGB40

Specimens WEDGB30 and WEDGB25 failed like Specimen WEDGB40. Failed Specimen WEDGB25 is shown in Figure 5.46 and is representative of the failure mode of Specimen WEDGB30. Failure occurred at the beginning of threaded section of the connector. The location of failure for these two connectors was closer to the steel-concrete interface than for Specimen WEDGB40. Less crushing of concrete was observed in front of the connector than for Specimen WEDGB40.

Figure 5.46: Failed Specimen WEDGB25

5.4   RESULTS OF LOW-CYCLE FATIGUE TESTS

Shear connection methods that performed well under high-cycle fatigue were tested under low-cycle fatigue. Specimens were tested cyclically under displacement control until either failure or 4000 cycles was reached. As described previously in Chapter 4, a maximum displacement of 0.2 in. and a minimum displacement of 0.1 in. were applied to each specimen. Parameters used for the testing of each connector are provided in Table A.3.

Table 5.6 summarizes the results obtained from low-cycle fatigue tests. All specimens for candidate shear connection methods performed better than Specimen CIPST1, which failed immediately upon the application of fatigue cycles. Failure occurred only in Specimen HTFGB1, which had previously been subjected to 5.6 million cycles of fatigue loading under a 35 ksi stress range. Specimens that remained intact up to 4000 cycles (5000 cycles for HTFGB2)

139

were finally tested statically to failure. Results of these static tests are also given for each specimen in the following sections.

Table 5.7: Summary of results for low-cycle fatigue tests

Specimen	Number of Cycles to Failure	Failed Component & Location
CIPST1	-	Shear at weld
DBLNB1	>4000	No Failure
DBLNB2	>4000	No Failure
HTFGB1	1250	Shear of connector above steel-concrete interface
HTFGB2	>5000	No Failure
HTFGB3	>4000	No Failure
HASAA1	>4000	No Failure
HASAA2	>4000	No Failure
WEDGB1	>4000	No Failure
WEDGB2	>4000	No Failure

The load sustained by the connector at each displacement cycle was recorded during each test, permitting the development of a load-time graph for each specimen. The load-time graph for Specimen DBLNB1 is shown in Figure 5.47 and is representative of the trend observed for each specimen. The graph indicates a considerable reduction in the load applied to the connector with each cycle to constant displacement amplitude.   This load reduction is due to decreasing lateral stiffness of the connector as the concrete around the connector crushes. The decrease in applied load continues until a somewhat constant load is reached. Load reversal starts with the monotonic application of the displacement range and continues throughout the 4000 displacement cycles. This suggests that

the connector behaves inelastically and endures loading in the opposite direction to achieve the required minimum displacement. Load reversal was not observed for the WEDGB specimens, which suggests that the connectors behaved elastically throughout the displacement cycles.
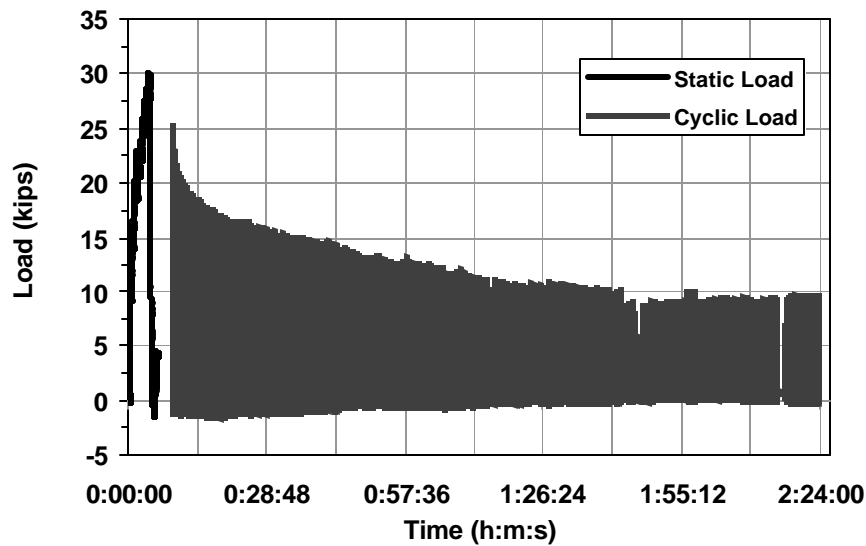
Figure 5.47: Change in load sustained by connector over time (Specimen DBLNB1)

5.4.1 Results for Cast-in-Place Welded Stud (CIPST)

Specimen CIPST1 failed immediately after the application of the monotonic displacement cycle, before any fatigue cycles could be applied. Failure occurred at the steel-concrete interface by the shearing of the clearly defective stud weld. Since, Specimen CIPST1 was the last cast-in-place specimen, no replica tests were performed.

5.4.2 Results for Double-Nut Bolt (DBLNB)

Specimens DBLNB1 and DBLNB2 remained intact under low-cycle fatigue up to 4000 displacement cycles, after which fatigue testing was stopped and static loading was applied. Under that static load, both connectors failed in shear at the steel-concrete interface, like Specimen DBLNB-ST. Specimen DBLNB1 reached an ultimate strength of 32.5 kips, while Specimen DBLNB2 reached 34.6 kips. The load-slip curves of these specimens under static loading is shown in Figure 5.48.
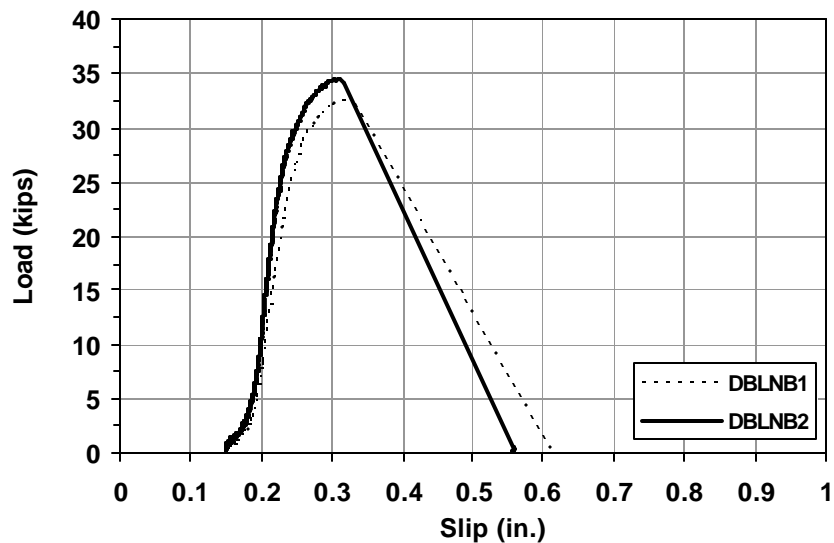
Figure 5.48: Load-slip curves for static strength tests of Specimens DBLNB1 and DBLNB2

A grout compressive strength of 9405 psi was measured for Specimen DBLNB1. No grout cylinders were tested for Specimen DBLNB2.

5.4.3 Results for High Tension, Friction Grip Bolt (HTFGB)

The first low-cycle fatigue test on the High Tension, Friction Grip Bolt was performed on Specimen HTFGB35. This specimen had previously been subjected to 5.6 million fatigue cycles at 35 ksi before any low-cycle fatigue cycles were applied. It was used as a pilot test to confirm the reliability of the displacement control system, and to gain insight on the effect of overloads on the fatigue life of shear connectors which have previously been subjected to large number of cyclic service loads. Since Specimen HTFGB35 was tested under low-cycle fatigue, from this point on it will be referred to as Specimen HTFGB1. This specimen endured 1250 cycles of low-cycle fatigue before failure occurred through the connector above the steel-concrete interface.

Specimens HTFGB2 and HTFGB3 did not fail in low-cycle fatigue. Specimen HTFGB was tested to 5000 cycles, and Specimen HTFGB2, to 4000 cycles. Both specimens were later subjected to static loading. The load-slip behavior of each specimen is shown in Figure 5.49. Ultimate static loads of 18 kips and 37.5 kips were obtained for Specimens HTFGB2 and HTFGB3 respectively.
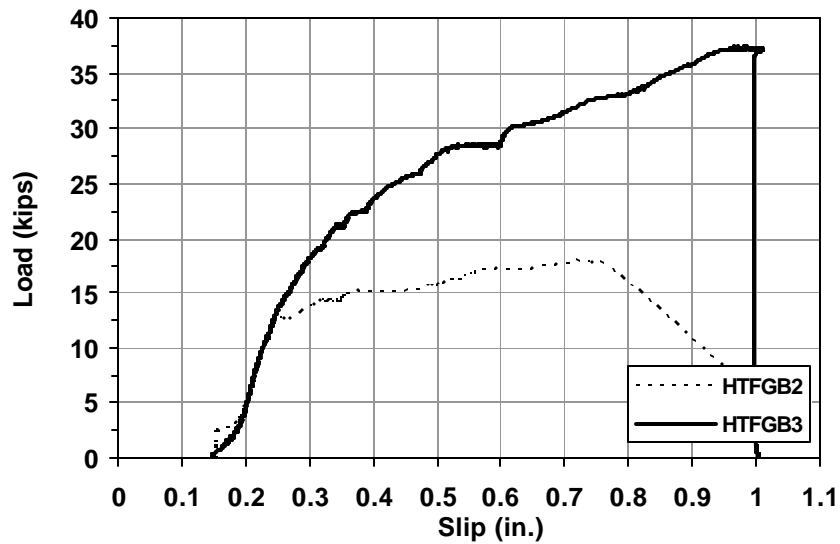
Figure 5.49: Load-slip curves for strength tests of Specimens HTFGB2 and HTFGB3

Specimens HTFGB2 and HTFGB3 failed in two different modes. As shown in Figure 5.50, Specimen HTFGB2 failed by shearing of the connector above the steel-concrete interface, inside the steel plate; Specimen HTFGB3 failed by splitting of the concrete block. The test was stopped immediately after the failure of the concrete. Failure of these specimens was marked by local crushing of concrete around the connectors, and by significant bearing deformation in the steel plates (Figure 5.51).

144

Figure 5.50: Failed Specimen HTFGB2

Figure 5.51: Bearing deformation of steel plate (Specimen HTFGB2)

5.4.4   Results for Adhesive Anchor (HASAA)

Adhesive anchor Specimens HASAA1 and HASAA2 each endured 4000 displacement cycles without failure. Both specimens were then tested under static

loading, giving the static load-slip curves of Figure 5.52, and ultimate loads of 23.6 kips and 21.8 kips for Specimens HASAA1 and HASAA2 respectively. Both specimens failed in connector shear at the steel-concrete interface, accompanied by local crushing of concrete around the connectors. The failed Specimen HASAA2, shown in Figure 5.53, is representative of the failure mode of Specimen HASAA1.
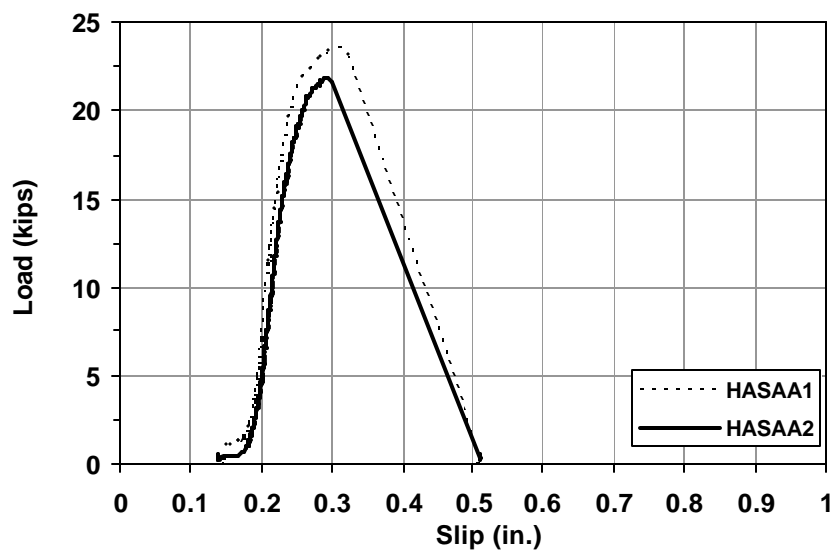
Figure 5.52: Static load-slip curves of Specimens HASAA1 and HASAA2

A gap of approximately 1/8 in. was observed between the steel plate and concrete block at the connector level and in front of the block, prior to testing Specimen HASAA1. The steel plate for Specimen HASAA2 twisted significantly during the first few displacement cycles, due to a misalignment of the plate with the loading ram. The clevis was manually prevented from rotating during testing, which prevented the steel plate from twisting further and enabled the load to be applied in a straight line.

Figure 5.53: Failed Specimen HASAA2

5.4.5 Results for Concrete Screw (WEDGB)

No fatigue failure was observed for Specimens WEDGB1 and WEDGB2 under low-cycle fatigue. Fatigue testing continued until 4000 cycles, after which each specimen was loaded statically to failure. The resulting load-slip curves from these static tests are shown in Figure 5.54. The ultimate loads obtained for Specimens WEDGB1 and WEDGB2 were 28.4 kips and 27.8 kips respectively.
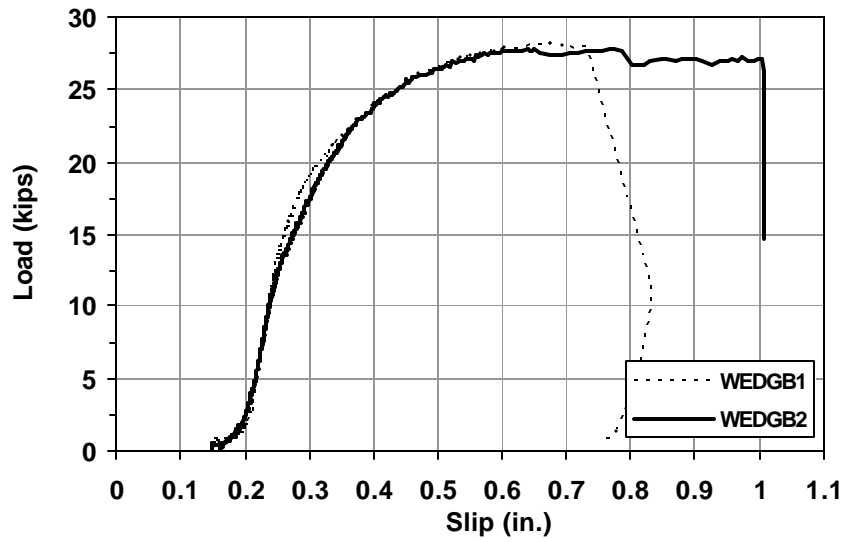
Figure 5.54: Static load-slip curves for Specimens WEDGB1 and WEDGB2

Both specimens failed by shearing of the connectors below the steel-concrete interface, indicating combined tension and shear forces. The failed Specimen WEDGB2, shown in Figure 5.55, is representative of the failure mode of Specimen WEDGB1.

148

Figure 5.55: Failed Specimen WEDGB2

Prior to testing, a consistent gap of approximately 1/8 in. between the steel plate and concrete block was observed for Specimen WEDGB1. During the testing of Specimen WEDGB2, the steel plate lifted slightly at the back of the specimen opposite the loading ram due to the significant bending of the connector.

CHAPTER 6

Discussion of Test Results

6.1 INTRODUCTION

In this chapter the static and fatigue test results presented in Chapter 5 are discussed, and the constructability of each alternative retrofit shear connector is evaluated. Finally, based on an evaluation of static and fatigue performance of the connectors, as well as on an evaluation of cost and constructability, recommendations are provided for retrofit shear connectors that should be considered for further evaluation in full-scale beam tests.

6.2 DISCUSSION OF STATIC TEST RESULTS

As discussed in Chapter 4, static tests were performed to obtain the load-slip behavior and ultimate load of post-installed shear connectors. Using the results for the Cast-in-Place Welded Stud as a reference, the following sections include a comparison of retrofit shear connectors based on their load-carrying capacity at 0.2 in. slip and at ultimate displacement; their stiffness; their slip capacity; and their failure mode. Further comparisons are made to results of Schaap (2004) and Hungerford (2004). Finally, an analysis and discussion is provided regarding the reliability of existing design equations for predicting the ultimate load of shear connectors.

6.2.1 Load-Slip Behavior of Investigated Shear Connectors

In Figure 6.1 the load-slip curves of investigated shear connection connectors are shown. This figure does not include the load-slip curve for the

Epoxy Plate, because the specimen failed in a brittle manner without experiencing any significant slip.
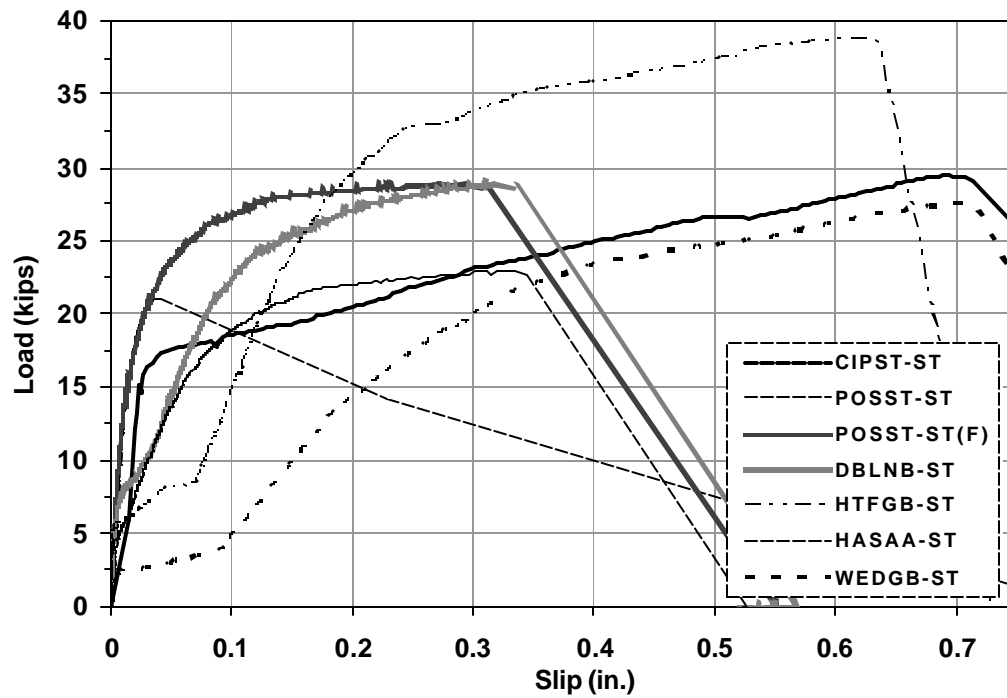
Figure 6.1: Load-slip curves of investigated shear connection methods

The different shapes of load-slip curves can be observed in Figure 6.1 for each specimen. Factors that contribute to the different load-slip behaviors include differences in the amount of pretension in each connector, the ductility of the connectors, and the stiffness, overall slip capacity, and ultimate shear strength of the connection.

Specimens for DBLNB, HTFGB, HASAA, and WEDGB methods showed an initial increase in load with little or no slip, due to the pretension in the connectors. In this range of loading, friction between the steel plate and concrete block is the primary load-transfer mechanism. Specimens with the welded shear

stud (CIPST and POSST specimens) do not provide an initial pretension and therefore experienced slip at the onset of loading.

Once the friction forces due to pretension were overcome, the DBLNB, HTFGB, and WEDGB specimens experienced slip into bearing with the surrounding steel and concrete with little increase in load. The HTFGB and WEDGB experienced the largest early slip due to large gaps between the connectors and the surrounding steel and concrete.

A decrease in the amount of slip prior to yielding is evident with increasing connection stiffness. Only the POSST specimens had an initial stiffness higher than that of the CIPST specimen, and experienced the least amount of slip before yielding.

The WEDGB and HTFGB specimens experienced at least twice as much overall slip as the other post-installed shear connectors. This may imply that connectors confined by either grout (POSST and DBLNB) or adhesive (HASAA), experience less overall slip than connectors that are less confined (WEDGB and HTFGB). This is a reasonable observation, since a more confined connector will not deform as much as a connector with less confinement. Also, a higher strength grout, adhesive, or concrete may limit the amount of deformation a connector experiences prior to failure. Thus, while providing high-strength concrete, grout or adhesive around the anchor may increase the connector's strength, it may also decrease its ductility.

As shown in Figure 6.1, the ultimate strength of the various connectors is sometimes developed at significantly different levels of slip. In some cases, strength values developed at very large slip levels may not be appropriate for design, since very large beam deflections may be needed to develop the strength of the composite beam. Consequently, to provide an alternative method to compare shear connector performance, it is useful to compare shear resistance at a

constant level of slip. Schaap (2004) and Hungerford (2004) provide a review of past research on the question of what level of slip should be used to characterize shear connector strength. They conclude there is no consensus on this question, but also conclude that the shear connector resistance measured at a slip of approximately 0.2 in. has been cited by a number of past researchers as a reasonable basis for assessing shear connector strength. Consequently, Schaap (2004) and Hungerford (2004) report the resistance of shear connectors at a slip value of 0.2 in., as well as the ultimate shear resistance of the connector. For consistency, a similar approach is used for the test results reported here.

Table 6.1 reports the ultimate strength of each shear connector, the load at 0.2 in. of slip, and the slip when the ultimate strength is achieved. All values are shown as a percentage of the corresponding values obtained for Specimen CIPST-ST. A plot of the values presented in this table is depicted as a bar chart in Figure 6.2.

Table 6.1: Load sustained at 0.2 in. of slip and at ultimate, and slip at ultimate load, as a percentage of the corresponding values for Specimen CIPST-ST

Specimen	Ultimate Load (%)	Slip at Ultimate (%)	Load at 0.2 in. (%)
CIPST-ST	100	100	100
POSST-ST	72	4	0
POSST(F)-ST	98	39	139
DBLNB-ST	98	46	132
HTFGB-ST	132	88	144
HASAA-ST	78	48	107
WEDGB-ST	94	101	71
3MEPX-ST	217	0	0
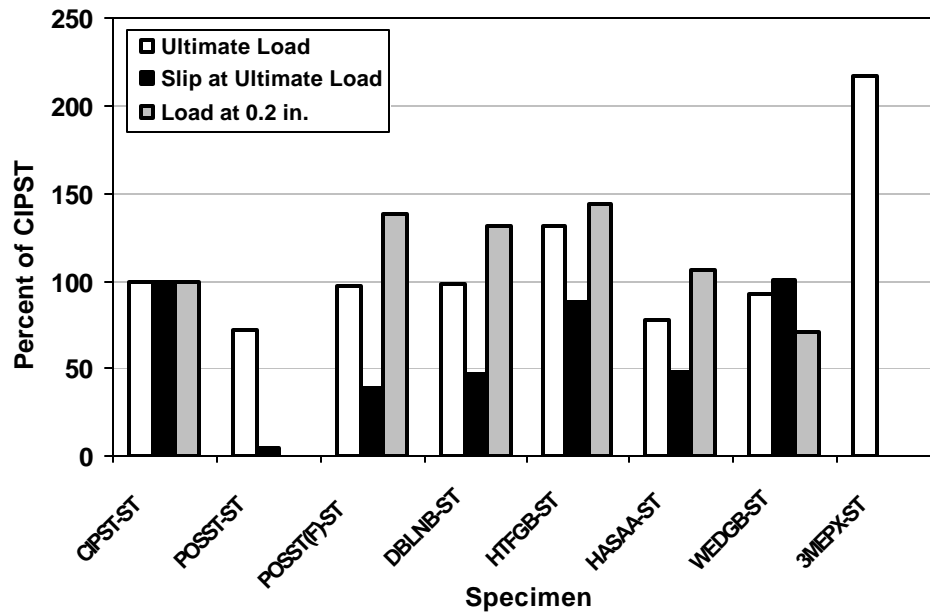
Figure 6.2: Comparison of load at 0.2 in. of slip and ultimate, and slip at ultimate load as a percentage of corresponding values for Specimen CIPST-ST

All but three specimens (Specimens POSST-ST, WEDGB-ST, and 3MEPX-ST) exhibited higher strength at 0.2 in. of slip than Specimen CIPST-ST. At ultimate, however, only two specimens (Specimens HTFGB-ST and 3MEPX-ST) had higher values than that of Specimen CIPST-ST. Specimens DBLNB-ST and WEDGB-ST failed at loads very close to but not higher than that of Specimen CIPST-ST. Due to the low initial stiffness of Specimen WEDGB-ST and the significant amount of localized crushing of concrete, the load-slip curve of this specimen was consistently below the load-slip curve of Specimen CIPST-ST until failure. Although Specimen HASAA-ST resisted a higher load than Specimen CIPST-ST at a slip level of 0.2 in, it sustained less load after 0.3 in. of slip up to failure.

6.2.2 Comparison of Test Results with those of Schaap (2004) and Hungerford (2004)

The results of static tests conducted by Schaap (2004) and Hungerford (2004) are presented here for comparison. Comparison was possible because the test setup and testing procedures used by those researchers were very similar to those used in this study. The only differences between this study and those are the presence of stiffeners on the steel test plates and a clamping rod, possible variation in material properties of connectors, and the strength of the concrete and grout used in this study.

Throughout this section, the specimens tested by Schaap (2004) and Hungerford (2004) are referred to using the abbreviation of the connection type followed a number indicating the order in which the specimen was tested. For example, the first and second Cast-in-Place Welded Stud specimens tested by these researchers are referred to as CIPST01 and CIPST02 respectively. For tests conducted as part of this current study, the specimen designation is followed by an "ST."

In Table 6.2 the averaged results obtained by Schaap (2004) and Hungerford (2004) are presented for each type of shear connection. Load and slip ratios are also provided, which are the quotient of the values obtained by Schaap (2004) and Hungerford (2004) divided by values obtained in the current study. A difference in ultimate load carrying capacities ranged between -28% and 8%. The average ultimate load of the CIPST specimens tested by Schaap and Hungerford is lower than that of Specimen CIPST-ST. The overall slip experienced by specimens in the two studies showed significantly different values. HTFGB and WEDGB specimens tested by Schaap (2004) and Hungerford (2004) experienced higher loads on average at 0.2 in. of slip compared to those tested in the current study.

156

Table 6.2: Comparison of test results obtained by Schaap (2004) and Hungerford (2004) with those of the current study

Type of Connection	Ultimate Load		Slip at Ultimate Load		Load at 0.2 in.	
	Previous Exp. Load (kips)	Load Ratio	Previous Exp. Slip (in)	Load Ratio	Previous Exp. Load (kips)	Slip Ratio
CIPST	21.3	0.72	0.53	0.77	17.4	0.85
POSST	22.8	1.08	0.32	-	22.2	-
DBLNB	30.0**	1.04	0.576*	-	24.2	0.89
HTFGB	32.8	0.85	0.649*	-	32.8	1.11
HASAA	22.5	0.98	0.21	0.64	22.1	1.00
WEDGB	24.8	0.90	0.51	0.73	17.8	1.23
3MEPX	55.4	0.87	-	-	-	-

*LVDT's removed prior to failure of specimen.
** Failure of the concrete block without failure of the connector.

A more detailed comparison of load-slip curves is provided in the following pages for individual test specimens from both studies. Possible reasons for different test results are discussed, aside from differences associated with variations in testing procedures, testing assembly, and equipment. A comparison of 3MEPX specimens is not given due the brittle failure mode of this connection.
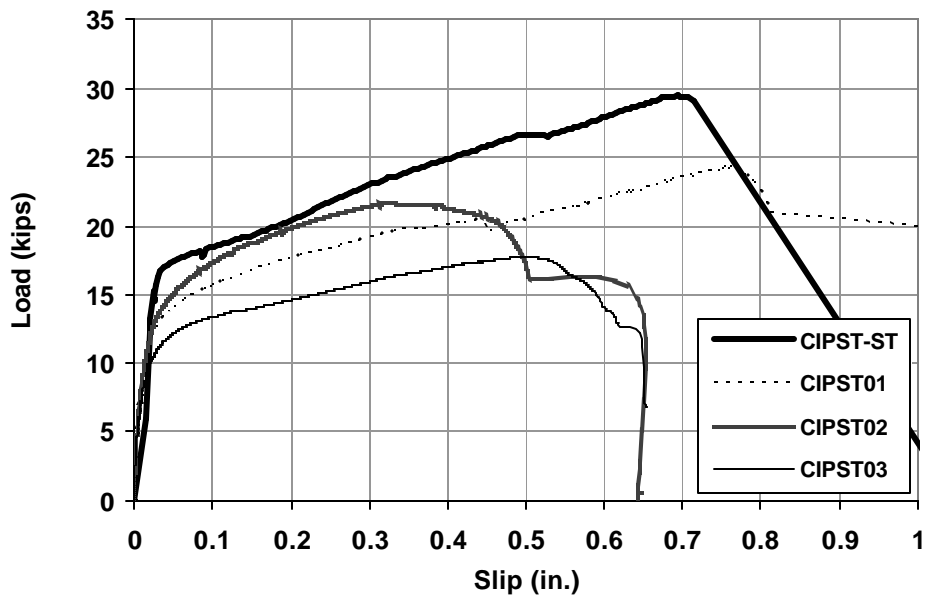
Figure 6.3: Comparison of load-slip curves for CIPST specimens

Load-slip curves for CIPST specimens are compared in Figure 6.3. At both 0.2 in. of slip and at ultimate, Specimen CIPST-ST had a higher bad than those tested by Schaap (2004) and Hungerford (2004). The higher strength of Specimen CIPST-ST may be due to the presence of a stronger weld. Also, the presence of a clamping rod and stiffeners may have reduced the amount of tension applied to the connector by minimizing the lifting and bending of the steel plate. A slightly lower initial stiffness can be observed for Specimen CIPST-ST. It is possible that the voids around the stud reduced the confinement around the stud, thereby increasing the slip values at low levels of load. Specimen CIPST-ST shows more ductility than Specimens CIPST02 and CIPST03. Specimens CIPST-ST and CIPST01 have similar shaped load-slip curves that run parallel to each other beyond the elastic limit of the connectors. Specimen CIPST01 shows more ductility than Specimen CIPST-ST. Overall, the load-slip curve for Specimen

158

CIPST-ST appears to be a conservative benchmark against which to compare alternative retrofit connectors.
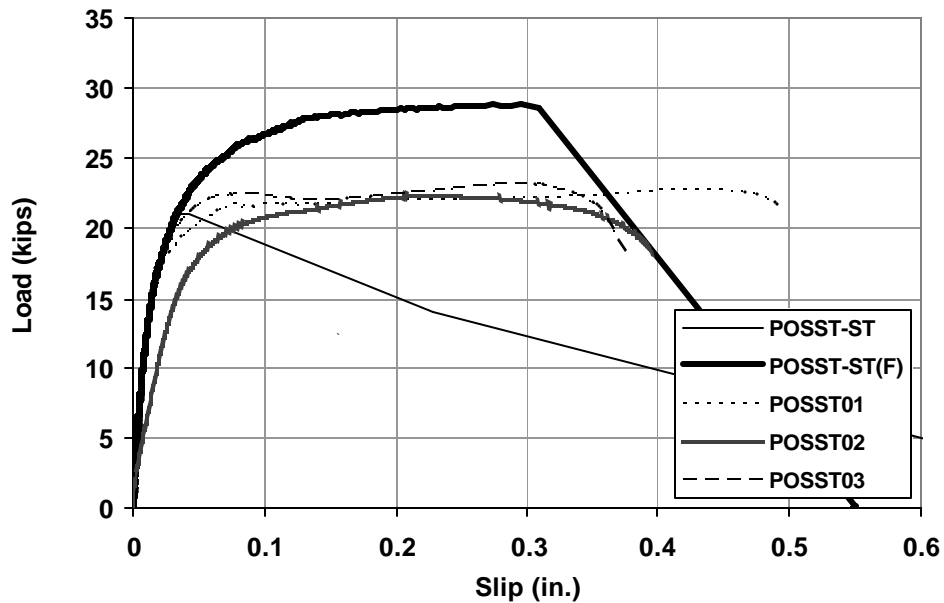
Figure 6.4: Comparison of load-slip curves for POSST specimens

Load-slip curves of different POSST specimens are compared in Figure 6.4, along with the load-slip curve for the fillet-welded Specimen POSST-ST(F). Due the brittleness of Specimen POSST-ST an evaluation of this connector cannot be made. All specimens except Specimen POSST03 had similar initial stiffnesses. Specimen POSST-ST(F) achieved a higher strength both at 0.2 in. and at ultimate, perhaps due to the presence of a stronger fillet weld.
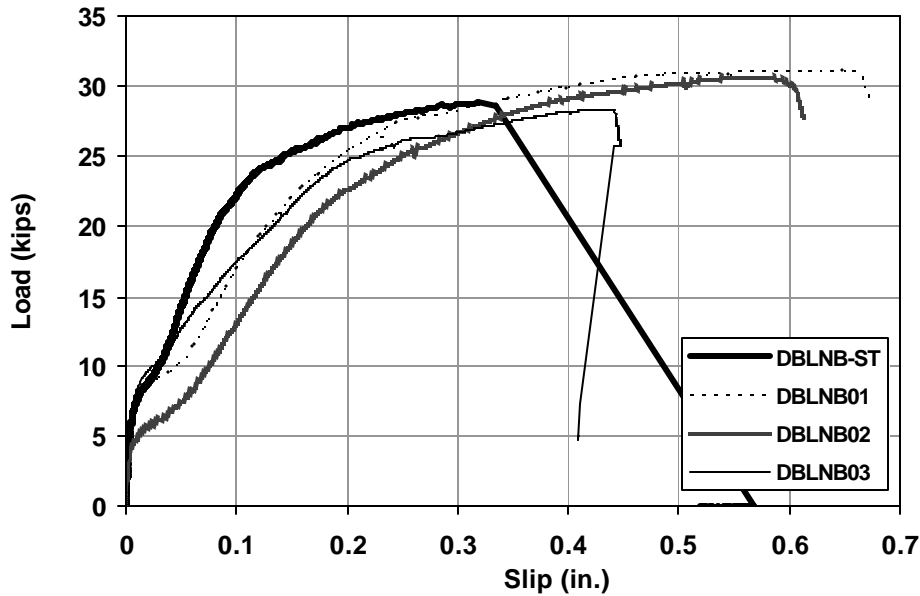
Figure 6.5: Comparison of load-slip curves for DBLNB specimens

An ASTM A193 B7 threaded rod was used for the DBLNB specimens in this study, while the specimens tested by Schaap (2004) and Hungerford (2004) used an A490 bolt. The load-slip curves of their specimens are shown in Figure 6.5, along with that of Specimen DBLNB-ST. Schaap (2004) reports that for each specimen the concrete block split before the connectors failed. Testing was reportedly stopped once the concrete failure was noticed. The use of a high-strength A490 bolt may have caused this type of failure. According to Schaap (2004) the load-slip data for Specimen DBLNB03 is not accurate beyond 0.35 in. of slip due to twisting of the steel plate. Although an accurate comparison between ultimate loads and ultimate slip values cannot be made, Specimen DBLNB-ST may well have had a lower ultimate strength and smaller slip even if connector failure had been obtained for all other specimens. The lower ultimate strength would be due to the use of a lower strength A193 B7 bolt, and the

160

smaller slip would be due to the higher compressive grout strength (possibly also concrete strength) measured for Specimen DBLNB-ST. Schaap (2004) reports an average grout strength of 3175 psi on the day of testing, only one-third of the 9788 psi obtained for Specimen CIPST-ST. The effect of a higher strength grout (and possibly concrete) is also reflected in the initial connection stiffness, where Specimen DBLNB-ST had higher connection stiffness prior to yielding.
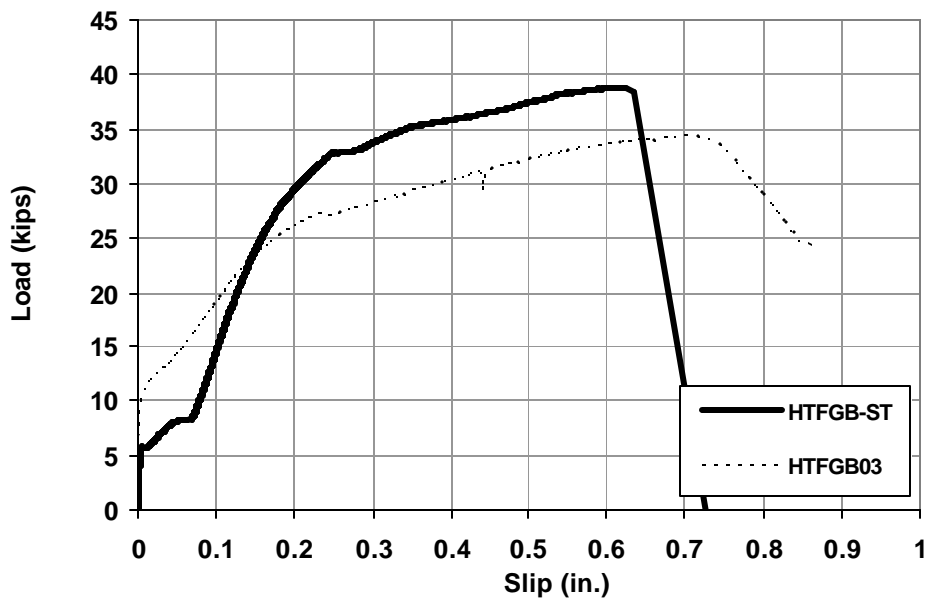
Figure 6.6: Comparison of load-slip curves for HTFGB specimens

Schaap (2004) and Hungerford (2004) observed failure of only one HTFGB specimen, whose load-slip curve is shown in Figure 6.6. Connector pretension in Specimen HTFGB-ST was overcome at a lower load than for Specimen HTFGB03. Despite the early loss of frictional resistance, Specimen HTFGB-ST experienced higher load at both 0.2 in. of slip and at ultimate. Relatively smaller overall slip can also be observed for this specimen than for

161

Specimen HTFGB03. Schaap (2004) reports that failure of the connector was associated with transverse cracking in the concrete block. A similar failure mode was observed for Specimen HTFGB-ST as well.
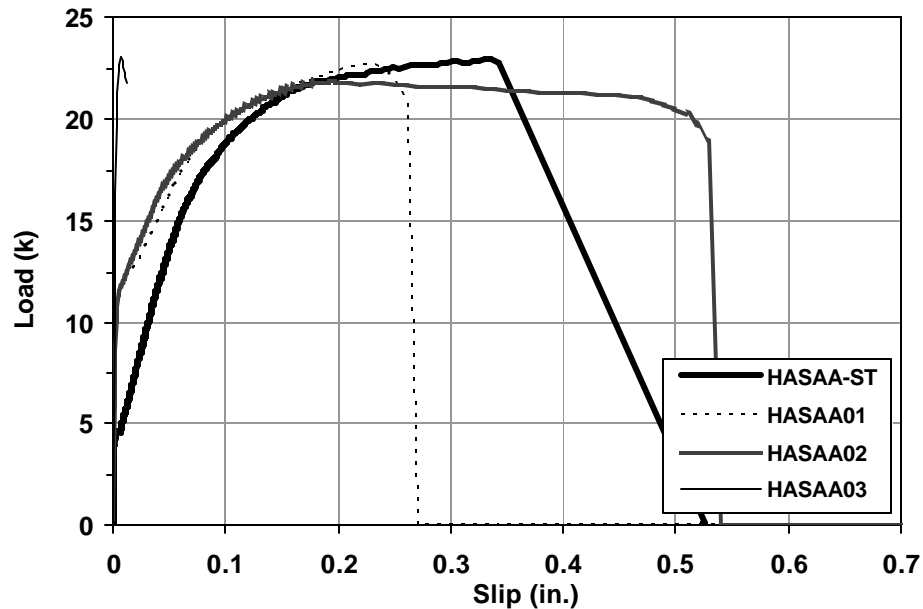
Figure 6.7: Comparison of load-slip curves for HASAA specimens

Load-slip curves for HASAA specimens are compared in Figure 6.7. The specimens of Schaap (2004) and Hungerford (2004) experienced an increase in load without slip up to approximately 10 kips, while Specimen HASAA-ST showed initial significant slip at approximately 5 kips. At 0.2 in. of slip all specimens but Specimen HASAA03 sustained approximately the same amount of load. At ultimate, Specimen HASAA-ST failed at a slightly higher load compared to other specimens except Specimen HASAA03. Hungerford (2004) reported that Specimen HASAA03 had excess adhesive surrounding the connector at the steel-concrete interface, which may have caused the concrete and

162

steel plate to bond. The same situation was experienced with Specimen HASAA-ST, however, did not result in the same type of load-slip behavior. Finally, none of the connectors exhibited a plateau in the load-slip curve as the connector came into bearing, possibly due to the presence of excess adhesive inside the hole in the steel plate.
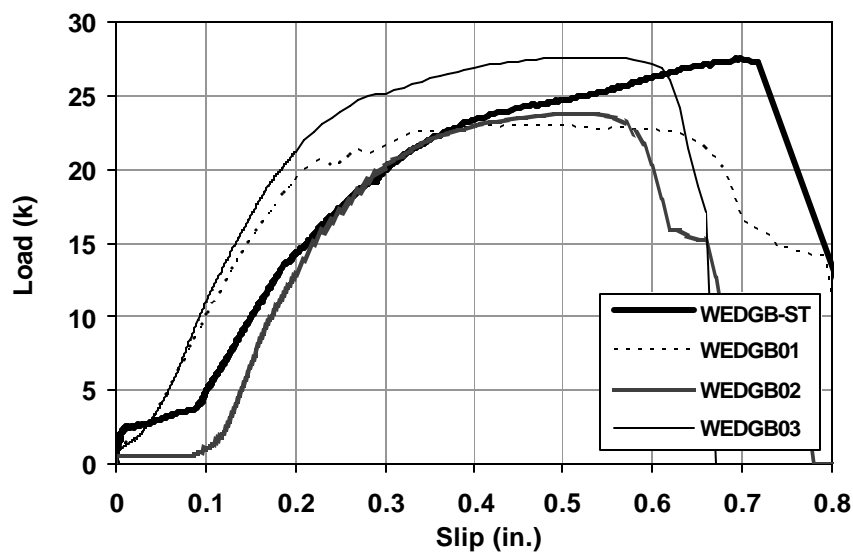
Figure 6.8: Comparison of load-slip curves for WEDGB specimens

Load-slip curves for WEDGB specimens are compared in Figure 6.8. Specimens WEDGB02 and WEDGB03 experienced less slip into bearing than Specimens WEDGB-ST and WEDGB01, and also show higher connection stiffness prior to yielding. Specimen WEDGB-ST sustained a higher load without slip compared to other specimens. Although Specimen WEDGB-ST showed lower stiffness, this specimen developed an ultimate load similar to that of Specimen WEDGB03, which had the highest initial stiffness. The connectors for all WEDGB specimens failed below the steel-concrete interface at the root of a

163

thread. Failure was typically accompanied by significant crushing and spalling of concrete. For specimens tested by Schaap (2004) and Hungerford (2004), cracking was also observed in the concrete block.

6.2.3 Predicting the Ultimate Strength of Shear Connectors

Design equations for predicting the ultimate shear strength of cast-in-place and post-installed connectors are available in design codes and specifications as well as in the literature. As previously discussed in Chapter 2, AASHTO LRFD specifications include a design equation for the ultimate load of welded studs embedded in concrete. This equation, presented as Equation 2.11, is based on the work by Ollgaard et al. (1971). This equation is also used in the AISC Specification for the design of composite beams in buildings and is presented here as Equation 6.1.

$$Q_n = 0.5 A_{sc} \sqrt{f'_c\, E_c} \leq A_{sc} f_u \qquad \textbf{(6.1)}$$

Where: A_{sc} = cross sectional area of stud connector (in^2);

f_u = specified minimum tensile strength of stud connector (ksi);

f_c' = compressive strength of concrete (ksi)

E_c = modulus of elasticity of concrete (ksi)

This equation implies that the strength of a shear stud is governed either by the strength of the concrete or by the strength of the connector steel, whichever is less.

Design equations for the nominal shear strength of cast-in-place studs and post-installed anchors are also provided in Appendix D of ACI 318-05. The commentary to ACI 318-05 states that the shear strength of cast-in-place and post-installed anchors far from the edge of concrete are usually governed by either the pryout strength of concrete or the shear strength of the anchor. Since no pryout failure was observed during static tests in this study failure should therefore be

governed by the strength of the anchor steel. ACI 318-05 provides two separate equations for the shear strength of cast-in-place studs and post-installed anchors. The equation for cast-in-place studs is the same equation given in AISC for the ultimate tensile strength of steel, and is repeated here as Equation 6.2. The specified ultimate tensile strength is used instead of ultimate shear strength because the area of the weld pool is greater than the nominal cross-sectional area of the connector.

$$V_{sa} = A_{se} f_{uta} \qquad \textbf{(6.2)}$$

Where: A_{se} = effective cross sectional area of anchor (in^2)

f_{uta} = specified tensile strength of anchor steel (ksi)

An equation predicting the ultimate shear strength of post-installed connectors exists only in ACI 318-05, and is based on the ultimate shear strength of steel. This equation is shown here as Equation 6.3.

$$V_{sa} = 0.6 A_{se} f_{uta} \qquad \textbf{(6.3)}$$

For adhesive anchors, manufacturer specified strengths reference AISC for the shear strength of steel and is the same as Equation 6.3.

An ultimate shear strength equation accounting for the compressive strength of concrete and grout, and also for the strength of steel has been proposed by Oehlers and Johnson (1987). This equation includes terms that also account for the size, strength, and stiffness of the connector and is presented here as Equation 6.4.

$$Q_u = 5.0 A_s f_u \left(\frac{E_c}{E_s}\right)^{0.4} \left(\frac{f'_{cu}}{f_u}\right)^{0.35} \qquad \textbf{(6.4)}$$

Where: E_s = modulus of elasticity of connector material (ksi)

f'_{cu} = specified compressive cube strength of concrete (ksi).

E_c = modulus of elasticity of concrete (ksi)

In the following pages experimentally measured ultimate loads are compared to the capacities predicted by the above equations. The experimental values used in these comparisons include those obtained in this study and those obtained by Schaap (2004) and Hungerford (2004). Each experimental value is compared to a predicted value calculated based on several different assumptions, described later.

Table 6.3 through Table 6.10, show comparisons for 8 different cases belonging to 3 different categories:

1. Equations governed by the strength of the connector steel (Equations 6.1, 6.2, and 6.3)

   Case 1a: using specified values for f_u

   Case 1b: using measured values for f_u (values reported in Chapter 4)

2. Equations governed by the strength of concrete (Equation 6.1)

   Case 2a: for POSST and DBLNB specimens, using a weighted average (f'_{avg}) of the measured compressive strength of concrete (f'_c) and grout (f'_g) depending on the area of crushed grout and concrete

   Case 2b: for POSST and DBLNB specimens, using only the compressive strength of grout (f'_g)

3. Equations governed by a combination of the strength of concrete and connector steel (Equation 6.4)

   Case 3a: using specified values for f_u and f'_{avg}

   Case 3b: using measured values for f_u and f'_{avg}

   Case 3c: using specified values for f_u and f'_g

   Case 3d: using measured values for f_u and f'_g

When f_u is used as a variable, "specified values" are the minimum values specified by the corresponding ASTM material specification, and "measured

values" are those reported in Chapter 4. The actual shear strength of connectors was not measured by Schaap (2004) and Hungerford (2004) and is not considered here.

The variable f_{avg} was computed using a weighted average of measured values for f_c and f_g based on the crushed zone in front of the connector. For example, for Specimen DBLNB-ST a crushing zone was observed with a 2-1/4-in. diameter. This resulted in a calculated f_{avg} based 70.9% on f'_g and 29.1% on f'_c. This approach was also used by Schaap (2004). The values reported by Schaap (2004) were used in this analysis. For the equation used in Category 3, f'_{avg} and f'_g were used to calculate the compressive cube strength of concrete (f'_{cu}). The cube strength of concrete is typically 15-20% higher than its cylinder compressive strength. To obtain f'_{cu}, f'_{avg} or f'_g was multiplied by 1.20 to conservatively estimate the compressive cube strength of concrete (or grout) in this study. Variables and corresponding values used in each equation are presented in Appendix F for each case.

Table 6.3 presents a comparison of experimental and predicted values for the ultimate load of each specimen for Case 1a. Predicted values were calculated using equations that are governed by the ultimate strength of the connector steel. These equations are the ultimate tensile strength of steel ($A_s f_u$), which is used in Equations 6.1 and 6.2, and the ultimate shear strength of steel ($0.6 A_s f_u$), which is used in Equation 6.3. Load ratios representing the quotient of the experimental load divided by the predicted load also are given for each specimen. Load ratios less than 1.0 indicate that the predicted strength was higher than the experimentally measured ultimate strength (in other words, the predicted strength was unconservative). Load ratios for both equations are compared in Figure 6.9. The ultimate tensile strength equation gives an unconservative estimate of the ultimate load for all specimens except Specimen CIPST-ST. The ultimate shear

strength equation more conservatively estimates the ultimate load. Most specimens except WEDGB specimens and two HTFGB specimens (no connector failure for HTFGB01) reached higher ultimate loads than predicted by this equation.

Table 6.4 presents the same comparison as in Table 6.3, but using measured values for f_u. The load ratios are plotted in a bar chart in Figure 6.10. Using measured values for f_u increases the predicted ultimate load and decreases the load ratio. As a result, ultimate loads are significantly overestimated by the tensile strength equation for each specimen. Some specimens whose ultimate load was previously underestimated by the ultimate shear strength equation are overestimated when measured values are used for f_u.

Table 6.5 and Table 6.6 present a comparison of experimental and predicted values for ultimate load predicted based on concrete strength using the first part of Equation 6.1 (Case 2). The equation used in Table 6.5 uses f'_{avg} for calculating ultimate load, while that of Table 6.6 uses f'_g. The corresponding bar chart is shown for load ratios in Figure 6.11. The equation governed by the compressive strength of concrete conservatively underestimates the ultimate shear strength of almost all post-installed shear connectors except that of POSST specimens and Specimen DBLNB-ST. Except for Specimen CIPST-ST, the ultimate load of all welded connectors is overestimated. For POSST and DBLNB specimens, using either f'_{avg} or f'_g in calculations of ultimate load does not cause a significant difference in the predicted strength.

Table 6.7 through Table 6.10 give a comparison of experimental and predicted ultimate strength values for Cases 3a through 3d for the equation proposed by Oehlers and Johnson (1987). In Figure 6.12 through Figure 6.15, load ratios are compared in bar chart form. Predicted ultimate load values are generally unconservative even for the cast-in-place welded stud, the connector for

168

which this equation was derived. Using measured values for f_u makes the predicted values even more unconservative. No significant differences can be observed in predicted strengths based on f'_{avg} and f'_g.

Based on the above comparisons it appears that none of the existing equations conservatively predicts the experimentally observed ultimate load for all shear connectors tested in this current research or those tested by Schaap (2004) and Hungerford (2004). Variability in experimental data is also clearly apparent. As an alternative to the existing shear connector strength design equations discussed above, the following equation is proposed for estimating the shear strength of connectors for design purposes:

$$Q_u = 0.5\, A_s\, f_u \qquad\qquad\qquad \textbf{(6.5)}$$

This equation corresponds to one-half the ultimate tensile strength of the connector steel. Based on specified values of f_u, predicted ultimate load values and corresponding load ratios for this formula are presented in Table 6.11. Load ratios are compared in Figure 6.16, and it can be observed that the proposed equation provides a conservative estimate of ultimate shear strength for cast-in-place and post-installed shear connectors, except the Concrete Screw. Results using measured values for f_u are compared in Table 6.12 and Figure 6.17. In this case, the equation still provides a conservative estimate for ultimate shear strength, except for the Concrete Screw. For the POSST, DBLNB, HTFGB and HASAA specimens, the predicted strength is 10 to 25 percent lower than the experimentally measured ultimate strength. This suggests that the proposed Equation 6.5 is not excessively conservative.

Table 6.3: Comparison of experimental and predicted values for ultimate load

(Case1a – Predicted strength governed by connector steel

using specified values for f_u)

Specimen	Exp. Load (kips)	$A_s f_u$		$0.6 A_s f_u$	
		Predicted Load (kips)	Load Ratio	Predicted Load (kips)	Load Ratio
CIPST-ST	29.4	26.5	1.11	15.9	1.85
CIPST01	24.3	26.5	0.92	15.9	1.53
CIPST02	21.7	26.5	0.82	15.9	1.36
CIPST03	17.8	26.5	0.67	15.9	1.12
POSST-ST	21.1	26.5	0.80	15.9	1.33
POSST01	22.8	26.5	0.86	15.9	1.43
POSST02	22.4	26.5	0.84	15.9	1.41
POSST03	23.3	26.5	0.88	15.9	1.46
DBLNB-ST	28.9	40.1	0.72	24.0	1.20
DBLNB01*	31.1	40.1	0.78	24.0	1.29
DBLNB02*	30.6	40.1	0.76	24.0	1.27
DBLNB03*	28.4	53.2	0.53	31.9	0.89
HTFGB-ST	38.8	53.0	0.73	31.8	1.22
HTFGB01*	30.7	53.0	0.58	31.8	0.96
HTFGB02*	34.3	53.0	0.65	31.8	1.08
HTFGB03	33.5	53.0	0.63	31.8	1.05
WEDGB-ST	27.5	55.8	0.49	33.5	0.82
WEDGB01	23.0	55.8	0.41	33.5	0.69
WEDGB02	23.8	55.8	0.43	33.5	0.71
WEDGB03	27.6	55.8	0.49	33.5	0.82
HASAA-ST	22.9	24.2	0.95	14.5	1.58
HASAA01	22.7	24.2	0.94	14.5	1.56
HASAA02	21.8	24.2	0.90	14.5	1.50
HASAA03	23.1	24.2	0.95	14.5	1.59

* Failure of the concrete block without failure of the connector.

Table 6.4: Comparison of experimental and predicted values for ultimate load
(Case1b – Predicted strength governed by connector steel
using measured values for f_u)

Specimen	Exp. Load (kips)	$A_s f_u$		$0.6 A_s f_u$	
		Predicted Load (kips)	Load Ratio	Predicted Load (kips)	Load Ratio
CIPST-ST	29.4	35.9	0.82	21.5	1.37
POSST-ST	21.1	35.9	0.59	21.5	0.98
DBLNB-ST	28.9	51.0	0.57	30.6	0.94
HTFGB-ST	38.8	60.9	0.64	36.5	1.06
WEDGB-ST	27.5	64.5	0.43	38.7	0.71
HASAA-ST	22.9	41.3	0.55	24.8	0.92

Table 6.5: Comparison of experimental and predicted values for ultimate load (Case2a – Predicted strength governed by concrete – weighted average of concrete and grout strength used for POSST and DBLNB specimens)

| Specimen | Exp. Load (kips) | $0.5 \, A_s \, \sqrt{f'_c \, E_c}$ | |
		Predicted Load (kips)	Load Ratio
CIPST-ST	29.4	22.5	1.31
CIPST01	24.3	22.7	1.07
CIPST02	21.7	22.7	0.96
CIPST03	17.8	22.7	0.79
POSST-ST	21.1	38.9	0.54
POSST01	22.8	27.8	0.82
POSST02	22.4	30.6	0.73
POSST03	23.3	31.1	0.75
DBLNB-ST	28.9	33.9	0.85
DBLNB01*	31.1	17.8	1.75
DBLNB02*	30.6	17.8	1.71
DBLNB03*	28.4	23.7	1.20
HTFGB-ST	38.8	24.9	1.56
HTFGB01*	30.7	23.3	1.32
HTFGB02*	34.3	23.3	1.47
HTFGB03	33.5	23.3	1.44
WEDGB-ST	27.5	22.0	1.25
WEDGB01	23.0	21.0	1.09
WEDGB02	23.8	21.0	1.13
WEDGB03	27.6	21.0	1.31
HASAA-ST	22.9	18.6	1.23
HASAA01	22.7	17.5	1.29
HASAA02	21.8	17.5	1.24
HASAA03	23.1	17.5	1.32

* Failure of the concrete block without failure of the connector.

Table 6.6: Comparison of experimental and predicted values for ultimate load (Case2b – Predicted strength governed by concrete – grout strength used for POSST and DBLNB specimens)

Specimen	Exp. Load (kips)	0.5 A_s sqrt(f¢ E_c)	
		Predicted Load (kips)	Load Ratio
POSST-ST	21.1	40.9	0.52
POSST01	22.8	28.8	0.79
POSST02	22.4	32.1	0.70
POSST03	23.3	32.6	0.71
DBLNB-ST	28.9	37.6	0.77
DBLNB01*	31.1	17.3	1.80
DBLNB02*	30.6	17.3	1.77
DBLNB03*	28.4	23.0	1.24

* Failure of the concrete block without failure of the connector.

Table 6.7: Comparison of experimental and predicted values for ultimate load (Case3a – Predicted strength based on Eq. 6.4 using f$'_{avg}$ and specified f$_u$)

Specimen	Exp. Load (kips)	$5\ A_s\ f_u\ (E_c/E_s)^{0.4}\ (f'_{cu}/f_u)^{0.35}$	
		Predicted Load (kips)	Load Ratio
CIPST-ST	29.4	20.9	1.40
CIPST01	24.3	21.0	1.16
CIPST02	21.7	21.0	1.03
CIPST03	17.8	21.0	0.85
POSST-ST	21.1	31.3	0.67
POSST01	22.8	24.4	0.93
POSST02	22.4	26.2	0.85
POSST03	23.3	26.5	0.88
DBLNB-ST	28.9	41.2	0.70
DBLNB01*	31.1	25.7	1.21
DBLNB02*	30.6	25.7	1.19
DBLNB03*	28.4	34.1	0.83
HTFGB-ST	38.8	35.3	1.10
HTFGB01*	30.7	33.7	0.91
HTFGB02*	34.3	33.7	1.02
HTFGB03	33.5	33.7	0.99
WEDGB-ST	27.5	35.2	0.78
WEDGB01	23.0	34.1	0.68
WEDGB02	23.8	34.1	0.70
WEDGB03	27.6	34.1	0.81
HASAA-ST	22.9	19.1	1.20
HASAA01	22.7	18.3	1.24
HASAA02	21.8	18.3	1.19
HASAA03	23.1	18.3	1.26

* Failure of the concrete block without failure of the connector.

Table 6.8: Comparison of experimental and predicted values for ultimate load (Case3b – Predicted strength based on Eq. 6.4 using $f'c_{avg}$ and measured f_u)

Specimen	Exp. Load (kips)	$5\ A_s\ f_u\ (E_c/E_s)^{0.4}\ (f'_{cu}/f_u)^{0.35}$	
		Predicted Load (kips)	Load Ratio
CIPST-ST	29.4	25.5	1.15
POSST-ST	21.1	38.1	0.55
DBLNB-ST	28.9	48.2	0.60
HTFGB-ST	38.8	38.7	1.00
WEDGB-ST	27.5	38.7	0.71
HASAA-ST	22.9	27.1	0.85

Table 6.9: Comparison of experimental and predicted values for ultimate load (Case3c – Predicted strength based on Eq. 6.4 using $f'c$ and specified f_u)

Specimen	Exp. Load (kips)	$5\ A_s\ f_u\ (E_c/E_s)^{0.4}\ (f'_{cu}/f_u)^{0.35}$	
		Predicted Load (kips)	Load Ratio
POSST-ST	21.1	32.4	0.65
POSST01	22.8	25.0	0.91
POSST02	22.4	27.1	0.83
POSST03	23.3	27.4	0.85
DBLNB-ST	28.9	44.3	0.65
DBLNB01*	31.1	25.1	1.24
DBLNB02*	30.6	25.2	1.22
DBLNB03*	28.4	33.4	0.85

* Failure of the concrete block without failure of the connector.

Table 6.10: Comparison of experimental and predicted values for ultimate load

(Case3d – Predicted strength based on Eq. 6.4 using f'$_c$ and measured f$_u$)

Specimen	Exp. Load (kips)	$5 A_s f_u (E_c/E_s)^{0.4} (f'_{cu}/f_u)^{0.35}$	
		Predicted Load (kips)	Load Ratio
POSST-ST	21.1	39.5	0.53
DBLNB-ST	28.9	51.8	0.56

Table 6.11: Comparison of experimental and predicted values for ultimate load using Eq. 6.5 with specified values for f_u

Specimen	Exp. Load (kips)	0.5 A_s f_u Predicted Load (kips)	0.5 A_s f_u Load Ratio
CIPST-ST	29.4	13.3	2.22
CIPST01	24.3	13.3	1.83
CIPST02	21.7	13.3	1.64
CIPST03	17.8	13.3	1.34
POSST-ST	21.1	13.3	1.59
POSST01	22.8	13.3	1.72
POSST02	22.4	13.3	1.69
POSST03	23.3	13.3	1.76
DBLNB-ST	28.9	20.0	1.44
DBLNB01	31.1	20.0	1.55
DBLNB02	30.6	20.0	1.53
DBLNB03	28.4	26.6	1.07
HTFGB-ST	38.8	26.5	1.46
HTFGB01	30.7	26.5	1.16
HTFGB02	34.3	26.5	1.29
HTFGB03	33.5	26.5	1.26
WEDGB-ST	27.5	27.9	0.99
WEDGB01	23.0	27.9	0.82
WEDGB02	23.8	27.9	0.85
WEDGB03	27.6	27.9	0.99
HASAA-ST	22.9	12.1	1.89
HASAA01	22.7	12.1	1.87
HASAA02	21.8	12.1	1.80
HASAA03	23.1	12.1	1.91

Table 6.12: Comparison of experimental and predicted values for ultimate load using Eq. 6.5 with measured values for f_u

Specimen	Exp. Load (kips)	0.5 A_s f_u Predicted Load (kips)	Load Ratio
CIPST-ST	29.4	17.9	1.64
POSST-ST	21.1	17.9	1.18
DBLNB-ST	28.9	25.5	1.13
HTFGB-ST	38.8	30.5	1.27
WEDGB-ST	27.5	32.3	0.85
HASAA-ST	22.9	20.7	1.11
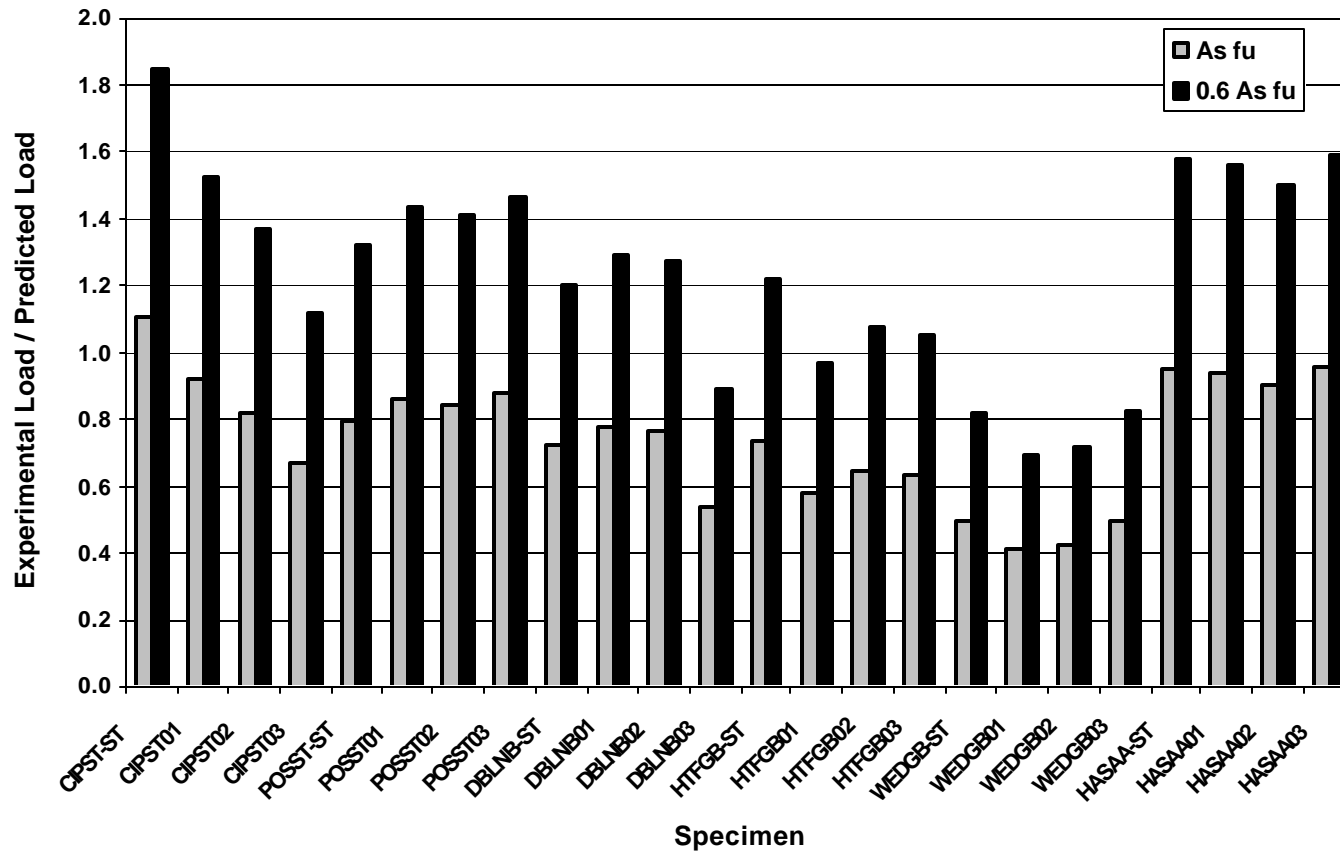
Figure 6.9: Comparison of load ratios for all specimens

(Case 1a – Predicted strength governed by connector steel using specified values for f_u)
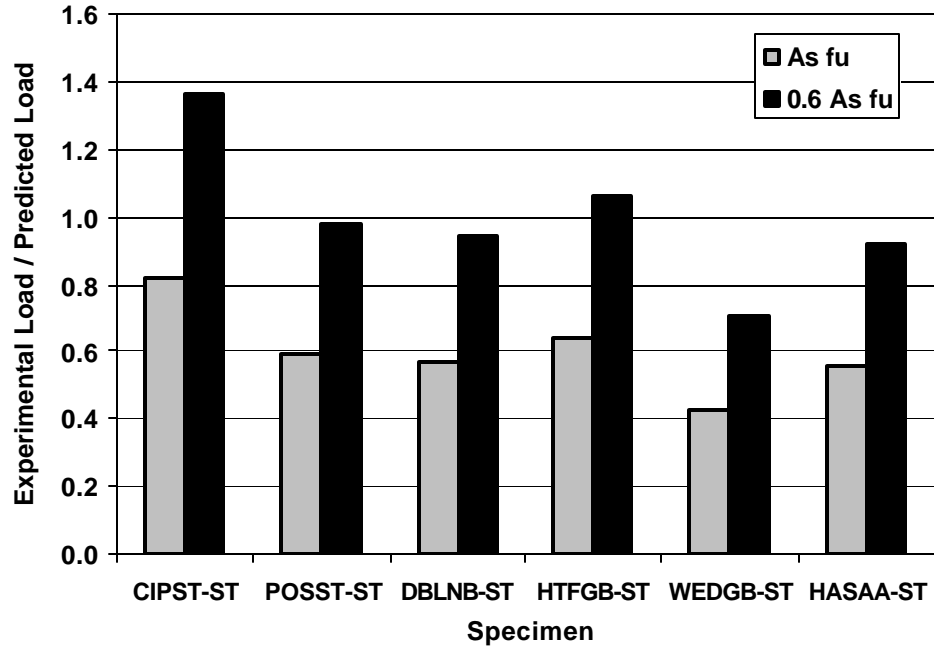
Figure 6.10: Comparison of load ratios for specimens tested in current study

(Case 1b– Predicted strength governed by connector steel

using measured values for f_u)
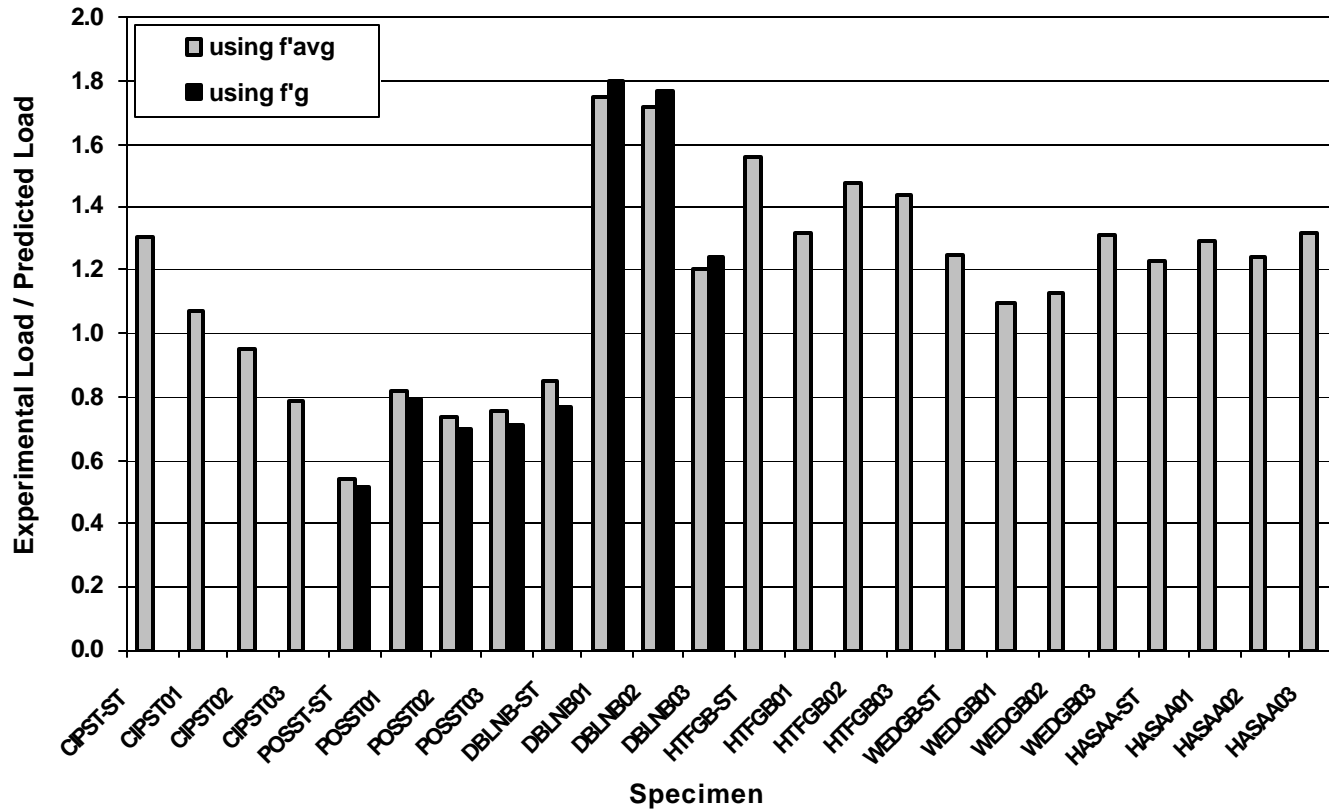
Figure 6.11: Comparison of load ratios for all specimens (Case 2 – Predicted strength governed by concrete: Case

2a - weighted average of concrete and grout strength used for POSST and DBLNB specimens;

Case2b - grout strength used for POSST and DBLNB specimens)
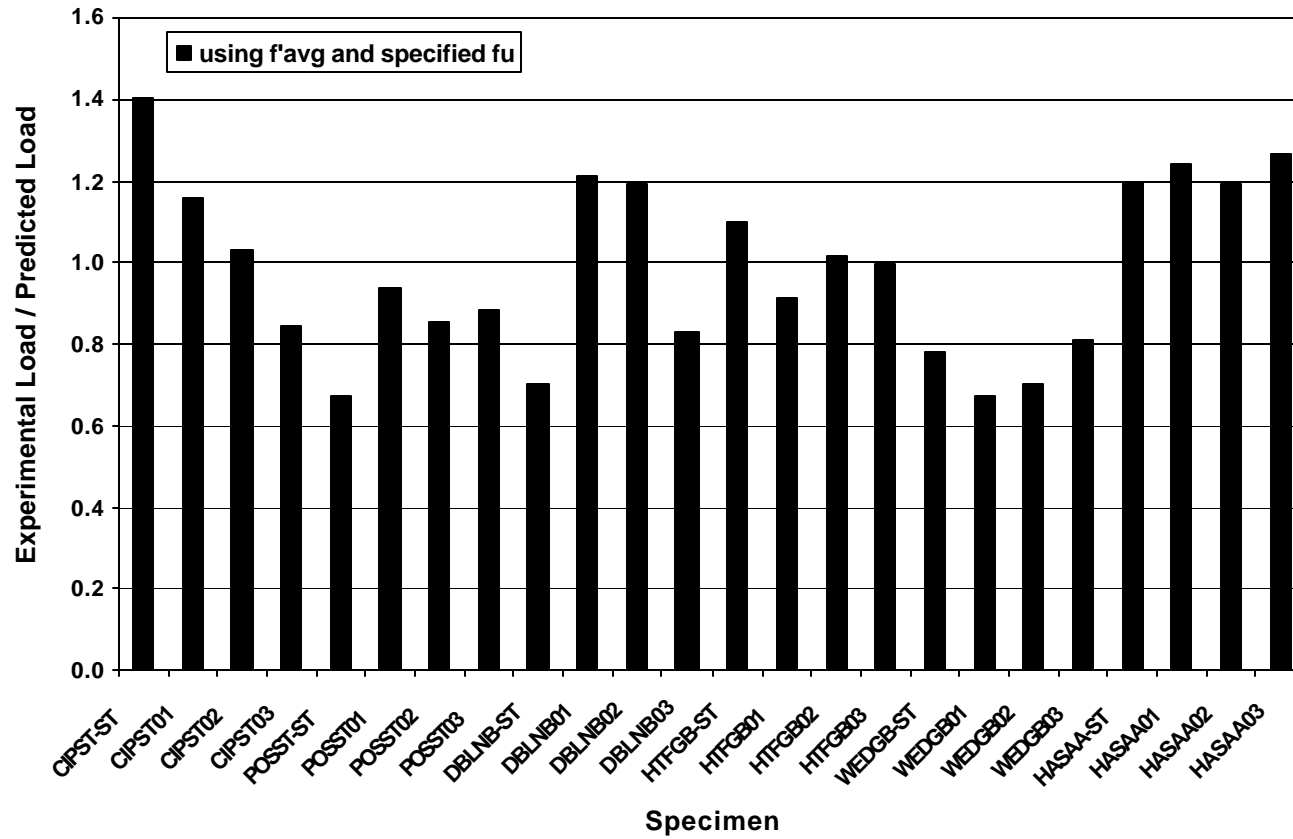
Figure 6.12: Comparison of load ratios for all specimens

(Case 3a - Predicted strength based on Eq. 6.4 using f$'_{avg}$ and specified f$_u$)

Figure 6.13: Comparison of load ratios for specimens tested in current study (Case 3b – Predicted strength based on Eq. 6.4 using f'$_{avg}$ and measured f$_u$)

Figure 6.14: Comparison of load ratios for grouted specimens

(Case 3c – Predicted strength based on Eq. 6.4 using f′g and specified fu)

184

Figure 6.15: Comparison of grouted specimens tested in current study
(Case 3d – Predicted strength based on Eq. 6.4 using f'ç and measured fᵤ)

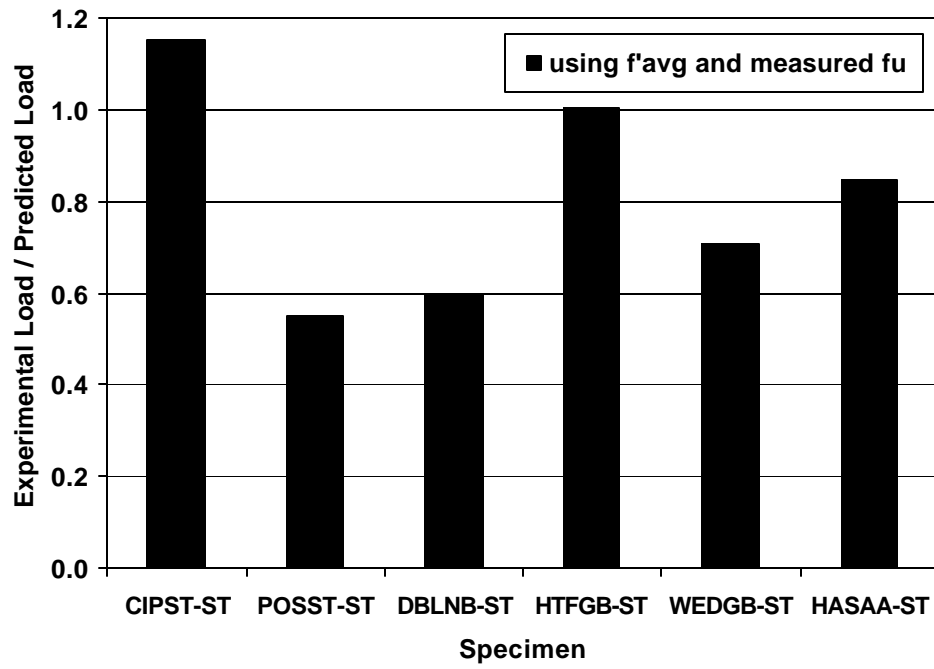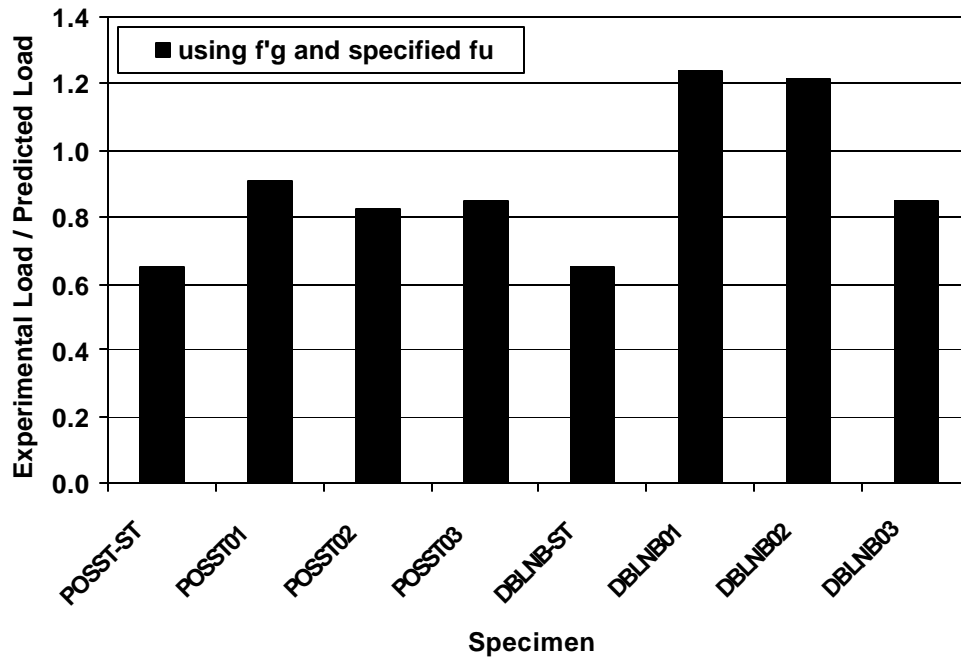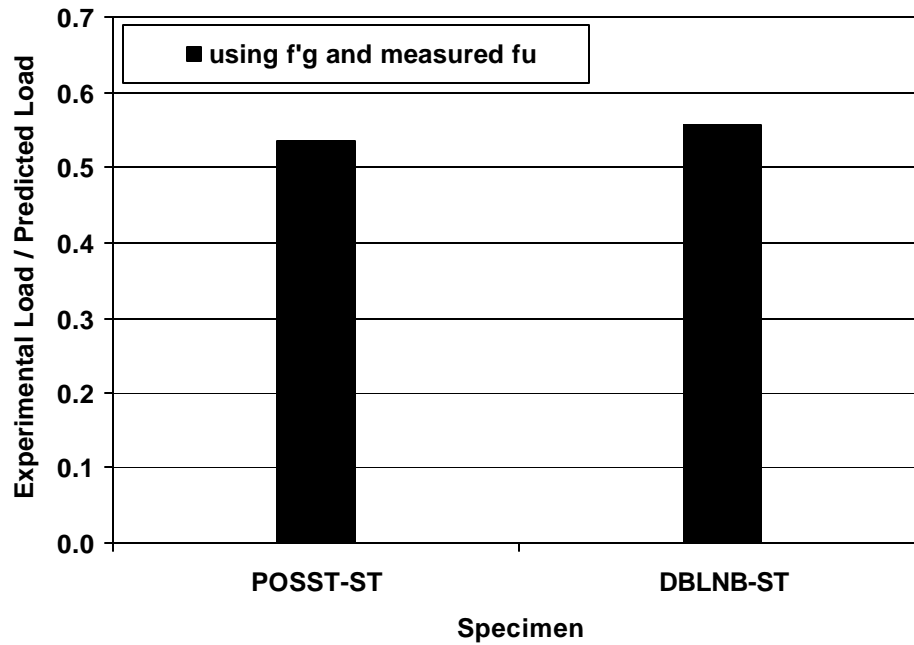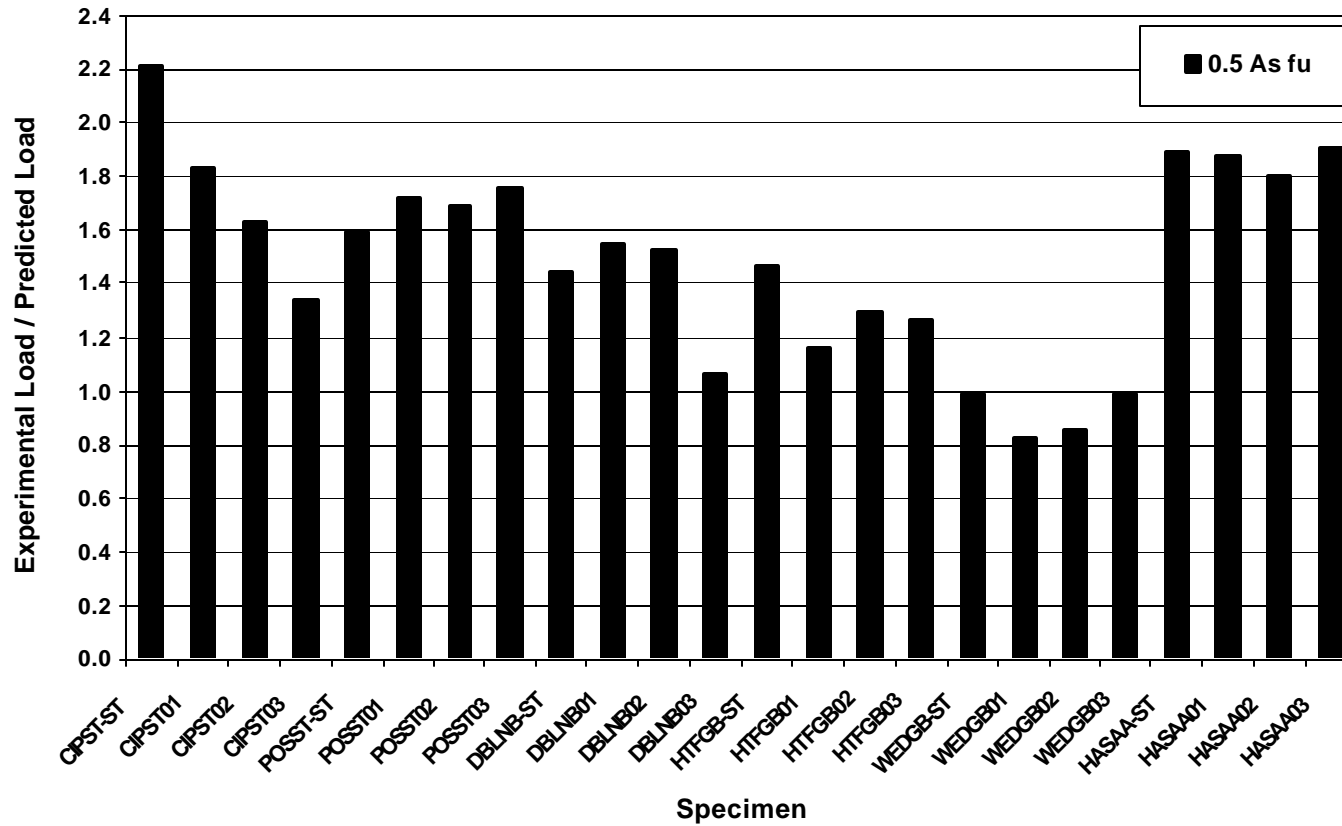*Figure 6.16: Comparison of load ratios for strength predicted by Eq. 6.5 with specified values for f_u*
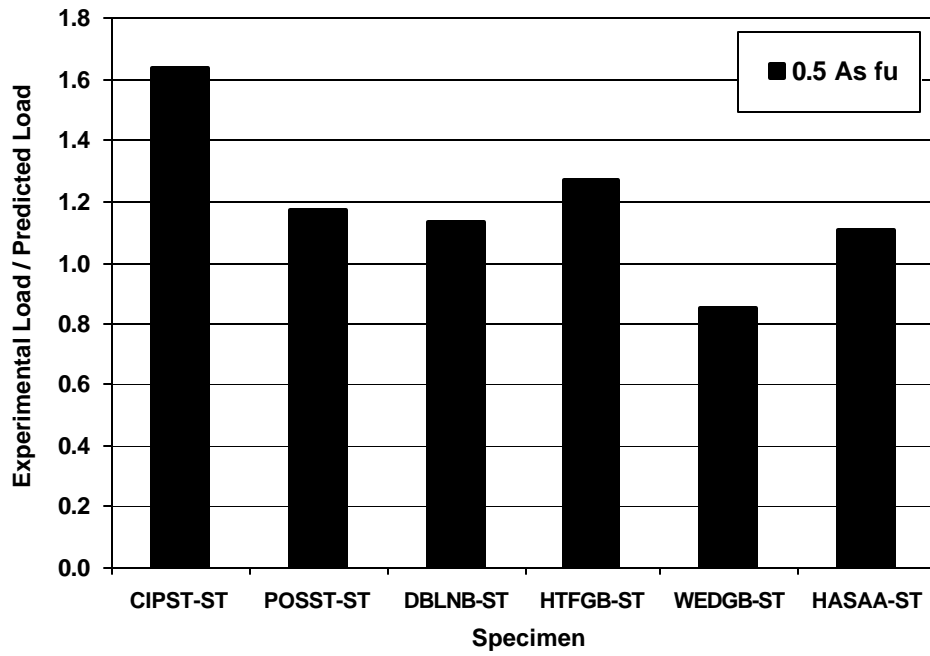
Figure 6.17: Comparison of load ratios for strength predicted by Eq. 6.5 with measured values for f_u

6.2.4 Choice of Connectors for High-Cycle Fatigue Tests

Due to the time and cost of high-cycle fatigue tests, it was not possible to conduct fatigue tests on all of the shear connector types that were tested statically in this research program and in the previous work by Schaap (2004) and Hungerford (2004). Consequently, at the completion of static testing, some shear connector types were eliminated from further consideration in this research program.

The 3MEPX method (epoxy plate) was eliminated from further consideration. Although this connection method exhibited the highest ultimate shear strength, it also had problematic aspects, including its brittle nature (essentially zero ductility), the potential difficulties and cost of construction, and concerns regarding its long-term durability. Although this method still shows promise and may merit additional research in the future, it was eliminated from further consideration in the current research program

In static testing, Specimen POSST-ST (post-installed welded shear stud) failed in a brittle manner due to a defective weld, raising questions regarding the reliability of this method. Welding the stud in a hole made in the concrete slab does not permit testing the stud weld using the conventional bend test used in new construction. Despite these concerns, however, the POSST was included in the program of high-cycle fatigue testing, with the intent of evaluating its feasibility and reliability after its behavior under fatigue loading had been studied.

As a result of static tests, the POSST, DBLNB, HTFGB, HASAA, and WEDGB methods were chosen for further testing under high-cycle fatigue. The CIPST method was also tested under high-cycle fatigue to provide a benchmark against which to compare other methods.

188

6.3   DISCUSSION OF HIGH-CYCLE FATIGUE TESTS

This section contains a discussion of the high-cycle fatigue data presented in Chapter 5. Results from 20 high cycle fatigue tests were used to plot S-N curves, in which the stress range applied to each connector is plotted as the ordinate and the number of cycles to failure is plotted as the abscissa using a logarithmic scale. Stress ranges were calculated based on the effective tensile stress area of each connector at the steel-concrete interface.

The following are comparisons made between results from this investigation and from past fatigue tests, as well as the design S-N curve provided by AASHTO. S-N curves for retrofit shear connectors are compared with that of the CIPST specimens and their relative performance is evaluated.

6.3.1   Comparison of S-N Curves of Test Results, Past Research for the Cast-in-Place Welded Stud

In Figure 6.18, all data for the CIPST specimens are plotted with data from past fatigue tests conducted on push-out type specimens. Data from past tests published in the literature were previously presented in Chapter 2. Data from past tests were used to draw curves of the mean, and plus and minus one standard deviation curve.
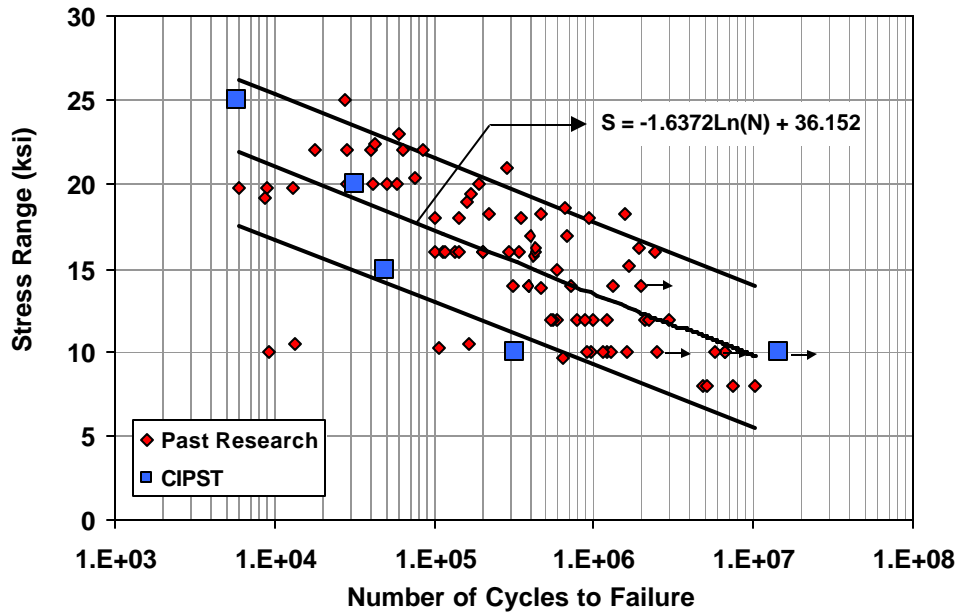
Figure 6.18: Comparison of S-N curve of past research with current data for the cast-in-place welded stud

Data from the current fatigue tests for the cast-in place welded stud are generally similar results to data from past research. It is clear from Figure 6.18 that S-N data from past tests show considerable scatter. In general, data from the current tests fall within the overall scatter band of the data from past tests. Thus, even though the current tests were not conducted on push-out type specimens, the direct-shear single connector test setup used for the current tests gives fatigue results comparable to push-out type specimens. The data shown in Figure 6.18 for the cast-in-place welded stud will be used in this study as a benchmark for comparison with the fatigue data for retrofit shear connectors.

Scatter in fatigue life is evident at every level of stress range in the past data. This scatter may be the result of many factors, including variability in material properties, variability in stud weld quality, and intrinsic variability in

190

fatigue life. Data for the CIPST specimens of this study shows similar scatter. The presence of scatter suggests that many tests are needed to adequately characterize the fatigue behavior of shear connectors.

6.3.2 Comparison of High-Cycle Fatigue Data for CIPST Specimens and for Specimens with Retrofit Shear Connectors

All specimens with retrofit shear connectors had improved fatigue life compared to the CIPST specimens. In Figure 6.19 through Figure 6.23, S-N curves for the retrofit shear connectors are compared to that for CIPST specimens. In these figures, a mean curve is plotted through data points for CIPST specimens along with lines indicating one standard deviation above and below the mean line. A fatigue endurance limit is also suggested in the figure, based on the data point of Specimen CIPST10, which did not fail after more than 10 million cycles of loading. Lines representing one standard deviation above and below the endurance limit are also shown.
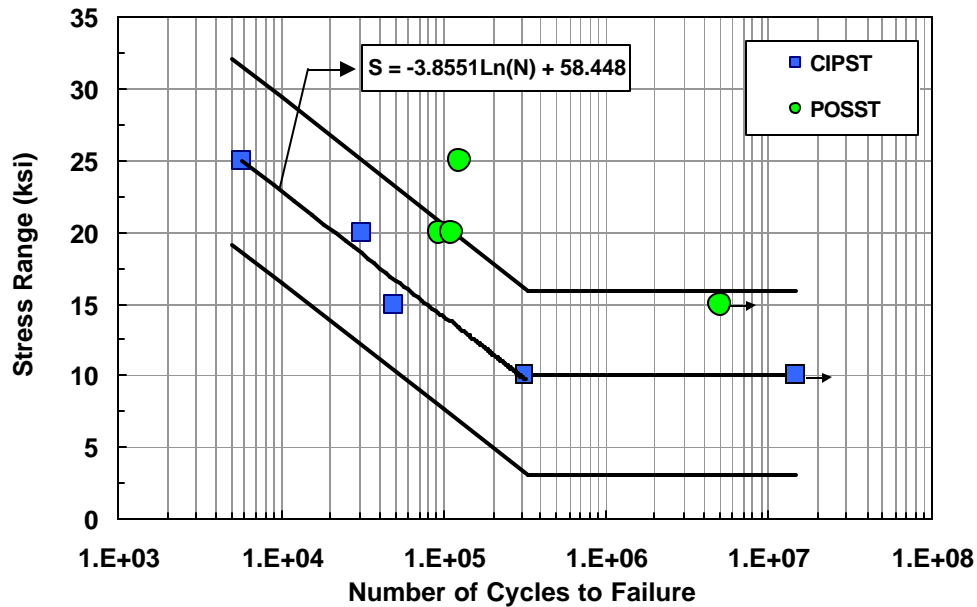
Figure 6.19: Comparison of fatigue data for POSST and CIPST specimens

In Figure 6.19 the fatigue performance of POSST specimens is compared to that of CIPST specimens. It can be observed from this figure that POSST specimens had longer fatigue lives than the CIPST specimens at every stress range. Although POSST specimens performed better than CIPST specimens, the improvement was not significant. All data except that for Specimen POSST25 fell above the mean curve for the CIPST specimens, within one standard deviation. Specimen POSST25 was beyond one standard deviation from the mean. Specimen POSST15(F), which had a fillet weld, had a significantly longer fatigue life than Specimen CIPST15 and did not fail.

192
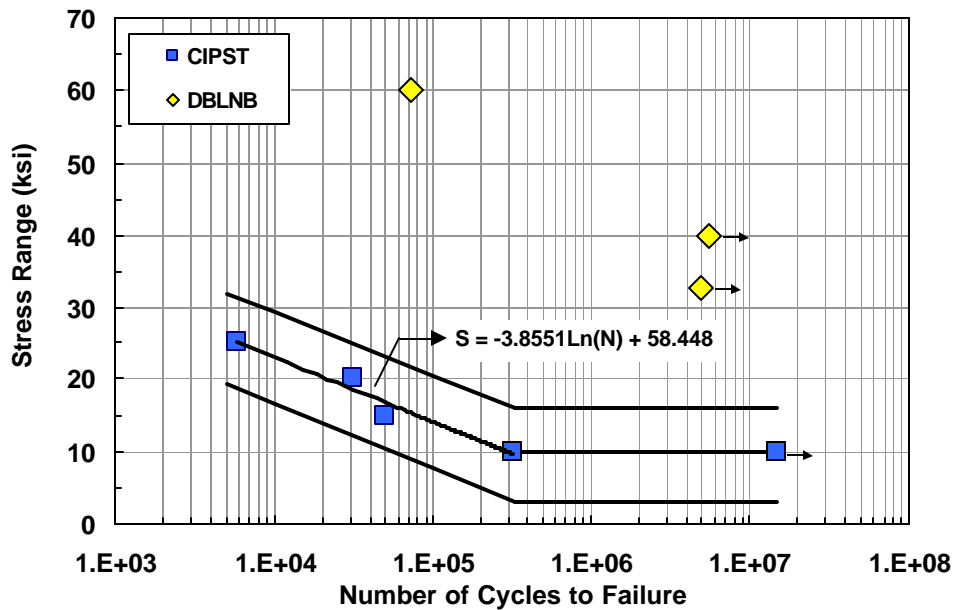
Figure 6.20: Comparison of fatigue data for DBLNB and CIPST specimens

In Figure 6.20, fatigue data for DBLNB specimens are compared to that of CIPST specimens. The superior fatigue performance of DBLNB specimens is readily apparent in this figure. The data of all three DBLNB specimens fall several standard deviations above the mean curve for the CIPST specimens. Failure was achieved for DBLNB specimens only at a stress range of 60 ksi. Specimens DBLNB40 and DBLNB33 did not fail and are shown as runout specimens with arrows next to the corresponding data points.
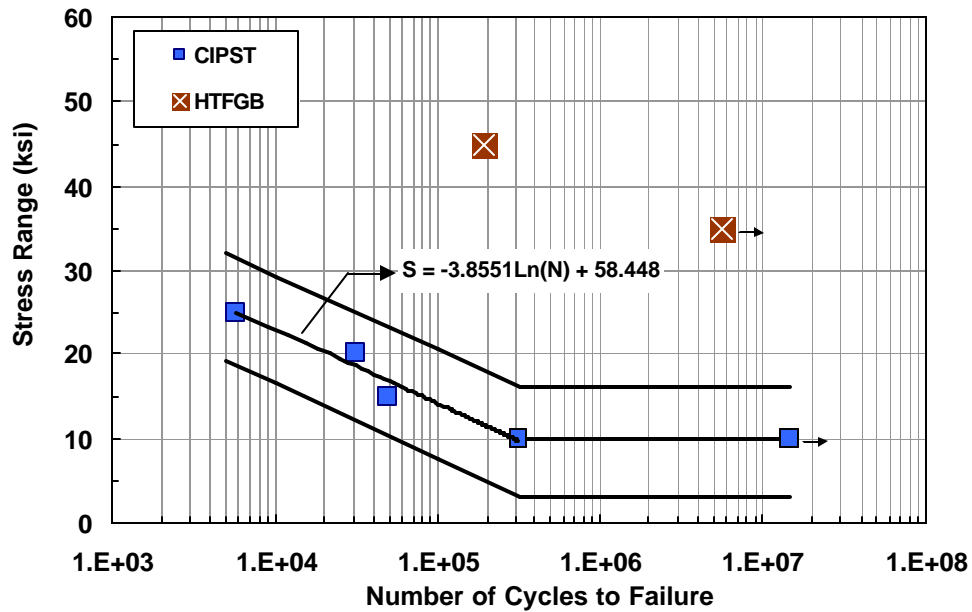
Figure 6.21: Comparison of fatigue data for HTFGB and CIPST specimens

Like the DBLNB specimens, the HTFGB specimens had better high-cycle fatigue performance than the CIPST specimens. This is shown in Figure 6.21. Failure of HTFGB specimens was obtained only at a 45-ksi stress range. Specimen HTFGB35 did not fail, and is shown as a runout specimen with an arrow adjacent to the corresponding data point. Data from the HTFGB specimens lie several standard deviations above the mean curve for CIPST specimens.

194
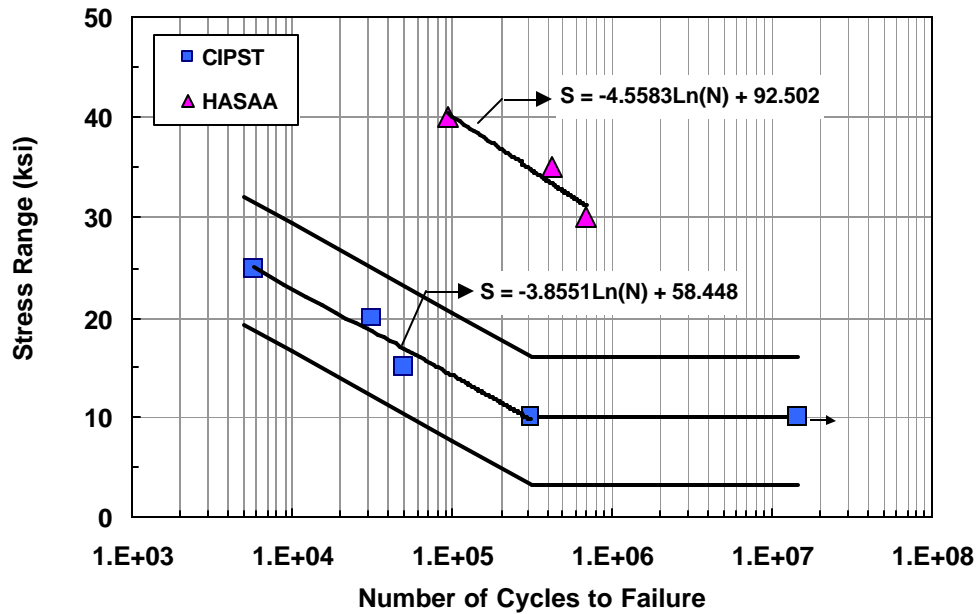
Figure 6.22: Comparison of fatigue data for HASAA and CIPST specimens

Failure was obtained for all HASAA specimens in high-cycle fatigue at a larger number of cycles than for the CIPST specimens. The resulting data for both types of specimens are shown in Figure 6.22, along with a mean curve shown for the HASAA specimens. This mean curve is parallel to and several standard deviations above the mean curve for CIPST specimens.

The data for WEDGB and CIPST specimens are shown in Figure 6.23. A longer fatigue life of WEDGB specimens is apparent compared to CIPST specimens. At a stress range of 25 ksi, Specimen CIPST25 failed at 5815 cycles, while Specimen WEDGB25 withstood 543133 cycles. The mean curve for the WEDGB specimens is shown and falls more than one standard deviation above the mean curve for CIPST specimens.
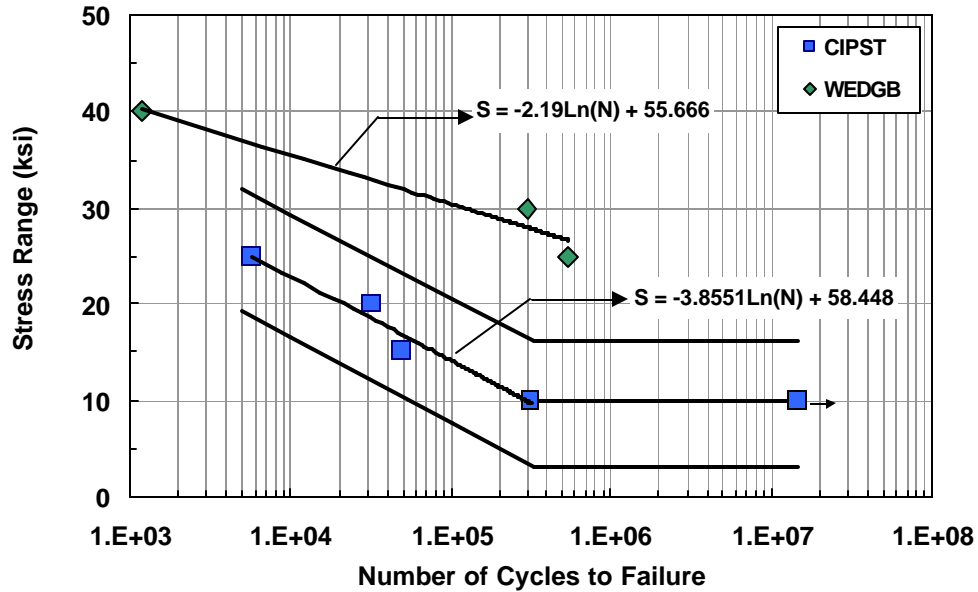
Figure 6.23: Comparison of fatigue data for WEDGB and CIPST specimens

In Figure 6.24, data for all tested specimens are compared with data from past push-out tests. This figure shows that DBLNB, HTFGB, HASAA, and WEDGB specimens performed significantly better in high-cycle fatigue than CIPST specimens and those from early push-out tests. While the POSST specimens had slightly longer fatigue lives, the improvement was not significant. It is important to note, however, that additional data are needed to better understand the fatigue behavior of these connectors and to develop representative S-N curves for use in design.

196
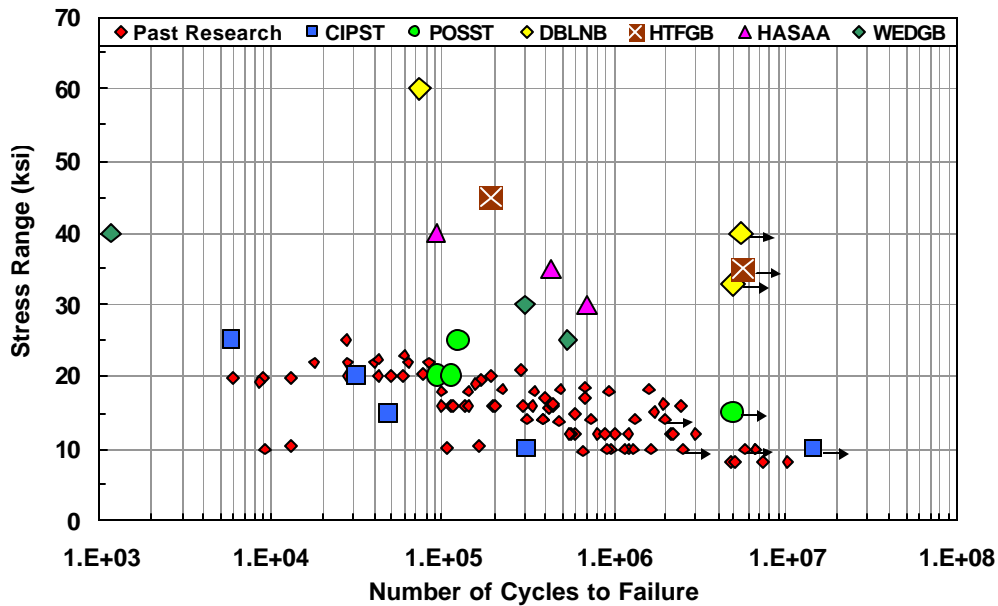
Figure 6.24: Comparison of fatigue data for retrofit shear connectors, CIPST specimens, and past research

6.3.3   Effect of Fatigue Loading on Subsequent Ultimate Strength

Several specimens with retrofit shear connectors did not fail under fatigue loading. To determine the effect of fatigue loading on the ultimate strength, these runout specimens, after fatigue loading, were loaded statically to failure. In Table 6.13, ultimate strengths obtained from residual static tests (that is, static tests conducted after fatigue loading) are compared, along with the corresponding load ratios (residual ultimate load divided by ultimate load from initial static test). The load ratios are all essentially unity, suggesting that the application of 5 million or more high-cycle fatigue cycles did not reduce the ultimate strength of the connectors. This is a significant observation, since similar tests on cast-in-place welded studs have shown a reduction in ultimate strength after the application of fatigue loading (i.e., Oehlers 1990, Mainstone and Menzies 1971).

197

Table 6.13: Comparison of static strength to residual strength for connectors previously subjected to fatigue loading

Specimen	Residual Ultimate Load (kips)	Ultimate Load from Initial Static Test (kips)	Load Ratio
POSST15(F)	29.0	28.8	1.00
DBLNB40	29.0	28.9	1.00
DBLNB33	29.4	28.9	1.01

6.4 DISCUSSION OF LOW-CYCLE FATIGUE TESTS

As discussed in Chapter 2, loads applied to shear connectors beyond their elastic limit are best evaluated from a standpoint of imposed displacement. This approach takes the view that the demands placed on the shear connectors in a composite beam can be viewed as a displacement (slip) demand at the steel-concrete interface rather than as a shear force demand. Consequently, the low-cycle fatigue tests were conducted by applying selected displacement cycles to the connectors, rather than applying load cycles, as was done in the high-cycle fatigue tests.

Fatigue failure was not obtained for specimens tested under low-cycle fatigue, except for Specimen HTFGB1, which had been previously subjected to 5 million loading cycles in the high-cycle fatigue tests. Also, Specimen CIPST1 could not be properly tested under low-cycle fatigue due to a defective weld. As discussed in Chapter 5, with the application of each displacement cycle the load sustained by each connector reduced until it reached a constant value. This is evident in load-time plots presented in Appendix E.

After 4000 displacement cycles were applied, the residual static strength of each specimen was evaluated and the load-slip curves were captured. Values for ultimate strength and slip, and load at 0.2 in. of slip, are reported in Table 6.14. These values are compared to those obtained from initial static tests (values reported in Chapter 5) and the load and slip ratios are given (the residual static test value divided by the initial static test value). Load and slip ratios are compared in a bar chart form in Figure 6.25.

Table 6.14: Comparison of values obtained in residual static tests and initial static tests

Specimen	Residual Ultimate Load		Slip at Residual Ultimate Load		Load at 0.2 in.	
	Exp. Load (kips)	Load Ratio	Exp. Slip (in)	Slip Ratio	Exp. Load (kips)	Load Ratio
DBLNB1	32.5	1.12	0.29	0.91	9.3	0.34
DBLNB2	34.6	1.20	0.30	0.94	11.1	0.41
HTFGB1	18.0	0.46	0.72	1.18	4.9	0.17
HTFGB2	37.5	0.97	0.97	1.59	4.7	0.16
HASAA1	23.6	1.03	0.30	0.91	6.9	0.31
HASAA2	21.8	0.95	0.29	0.88	4.6	0.21
WEDGB1	28.4	1.03	0.68	0.97	1.7	0.12
WEDGB2	27.8	1.01	0.64	0.91	2.5	0.17
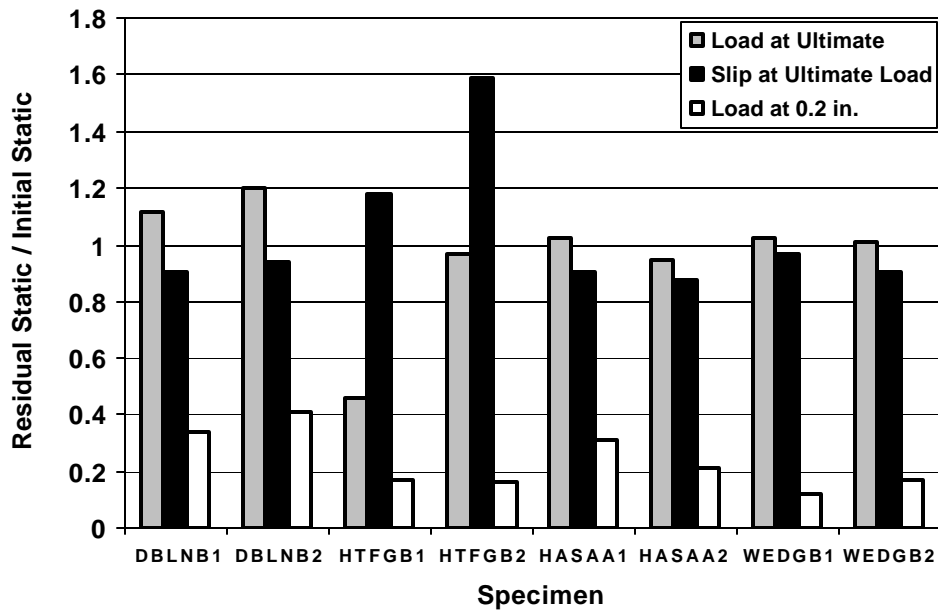
Figure 6.25: Ratios of values obtained in residual static tests divided by values obtained in initial static tests

It can be seen in Figure 6.25 that the residual static capacities of the DBLNB and WEDGB specimens exceeded the initial static capacities, while the failure mode remained the same. The HASAA specimens failed at the steel-concrete interface as in initial static tests. Specimen HASAA1 slightly exceeded and Specimen HASAA2 fell short of the initial static load at ultimate. This likely reflects the inherent variability in ultimate strength for a given failure mode.

Two different failure modes were observed for HTFGB specimens. For Specimen HTFGB2, the connector failed inside the steel plate, whereas for Specimen HTFGB3, the concrete block split before the connector could fail. Specimen HTFGB-ST, on the other hand, failed by shearing of the connector below the steel-concrete interface. The differences in failure modes were reflected in the residual ultimate loads. Specimen HTFGB2 experienced the

201

highest reduction in ultimate load and Specimen HTFGB3 experienced only a slight reduction. The residual ultimate load of Specimen HTFGB3 also includes the load necessary to split the concrete block, and therefore is higher than expected.

The corresponding ultimate slip experienced by each specimen almost matched the values observed in initial static tests. Only Specimen HTFGB3 showed a significant increase in ultimate slip, which can be attributed to the splitting of concrete. Any decrease in slip may be due to the higher strength of the concrete at the time low-cycle fatigue specimens were tested.

At a slip of 0.2 in., a significant decrease in sustained load is apparent for all specimens. The slip of 0.2 in. coincides with the maximum displacement applied to each specimen during fatigue cycles.

Initial static and residual load-slip curves are compared for each specimen in Figure 6.26 through Figure 6.29. The residual load-slip curves show that each connector had a zero load-carrying capacity at a slip of 0.15 in., corresponding to the mean value of the displacement range applied to each connector

In general, the slope of the loading branch (stiffness) of the load-slip curves is similar for the residual test and the initial static test specimens. This suggests that no significant degradation occurred in the shear connectors during fatigue cycles.

It appears that a high number of displacement cycles had no significant effect on the ultimate strength of a shear connector. Increasing damage of the concrete in front of the connector with each displacement cycle may have reduced the confinement around the connector, and, as the connector deformed inelastically, resulted in less load applied to the connector with each displacement cycle. As a result, the possibility of degradation in the connector material and a low-cycle fatigue failure could have been reduced.
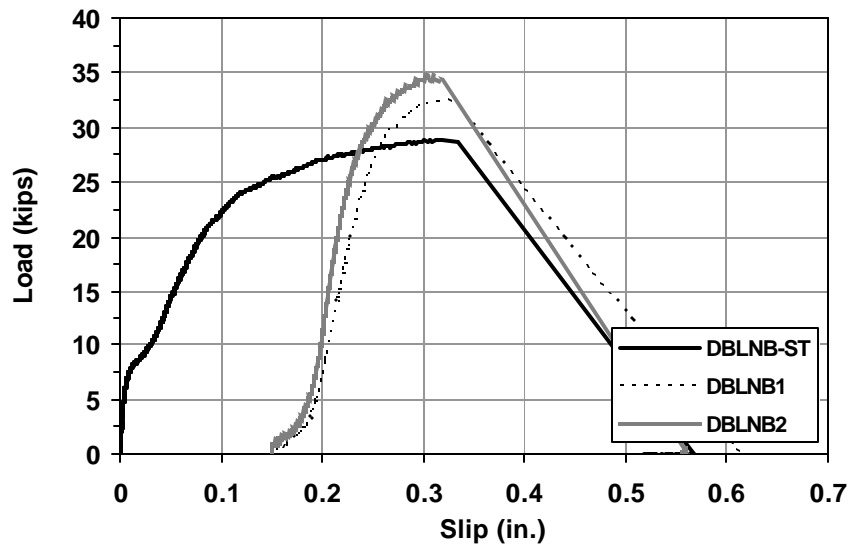
Figure 6.26: Comparison of initial static and residual load-slip curves for DBLNB specimens
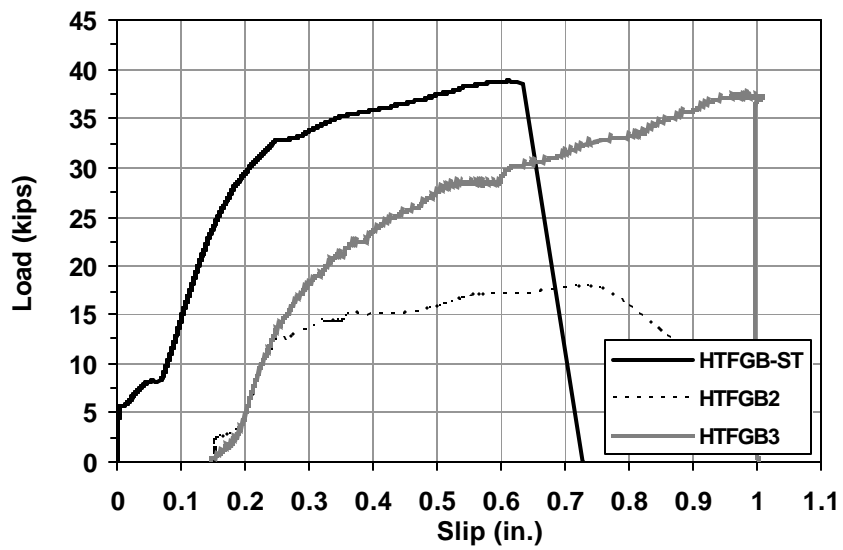

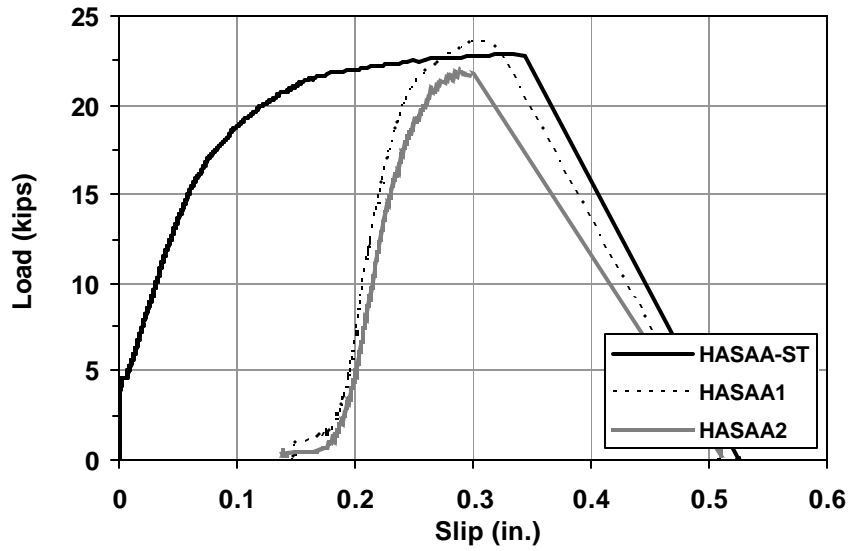*Figure 6.27: Comparison of initial static and residual load-slip curves for HTFGB specimens*

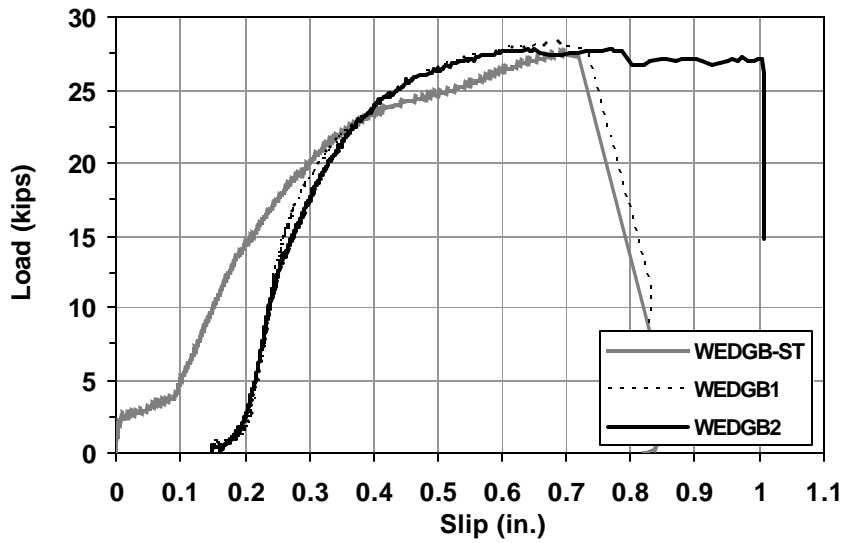*Figure 6.28: Comparison of initial static and residual load-slip curves for HASAA specimens*

Figure 6.29: Comparison of initial static and residual load-slip curves for WEDGB specimens

204

6.5 DISCUSSION ON THE CONSTRUCTABILITY OF RETROFIT SHEAR CONNECTORS

Thus far, the structural effectiveness of retrofit shear connectors has been evaluated and results from static and fatigue tests have been discussed. The objective of this thesis, however, was not just to evaluate the structural performance of retrofit shear connectors, but also to evaluate the connectors from the perspective of constructability and cost. These issues are discussed in this section. This discussion is based primarily on experience gained with the connectors in constructing the test specimens, combined with consideration of how these experiences may be related to connector installation in an actual bridge.

The POSST method is the only retrofit method using a welded shear stud, and also the only method that can be installed completely from the top of a bridge. Static and fatigue tests, however, showed that the behavior of this connection depends heavily on the quality of the stud weld. This prompts the need for inspections of the weld quality in a field application. For welded studs in new construction, stud welds are typically inspected by a non-destructive "bend test" in which a number of shear studs are bent a certain amount. Those shear studs that break during this procedure are replaced. This technique is not easy to use for the POSST method, since no room is available to bend the stud inside a 3.5-in. diameter hole. Consequently, some other stud weld inspection technique would be needed, and it is unclear if another practical method is available. Another issue related to the POSST method is that too much time may be required to core a large-diameter hole through the bridge deck. Also, different weathering characteristics of the grout and the concrete may result in cracks that might permit water seepage down to the steel girder.

Like the Post-Installed Welded Stud (and Stud Welded to Plate) method, the Double-Nut Bolt requires coring holes through the concrete slab. Unlike the

Post-Installed Welded Stud, however, installation of this connector requires access to under the bridge as well as on. The smaller diameter hole (2-in.) used with the Double-Nut Bolt may require less time and effort to drill than the 3.5-in. core used with the Post-Installed Welded Stud.

The High-Tension, Friction Grip Bolt was found to be the hardest of all tested connectors to install, even in a laboratory setting. Drilling concentric countersunk holes was a challenge, and could be even more difficult on a real bridge, especially for holes farther away from the edge of the slab. This method also requires several installation steps. First, a hole must be cored through the concrete from both the top; next, a hole also must be match-drilled from under the bridge; and finally, the cored hole must be grouted.

The Adhesive Anchor was found to be one of the easiest connectors to install in a laboratory setting. This connector can be installed in a bridge with minimal damage to the concrete slab from under the bridge. The only drawback of the installation process is the time needed for the adhesive to cure. For a $68^{o}F$ temperature a 50 min. curing time is required for the adhesive used in the tests. During this time the adhesive should not be disturbed, which may require traffic to be stopped on a bridge.

The Concrete Screw was the easiest connector to install. This one-piece screw requires drilling only from the bottom of the bridge. The concrete screw can be easily installed while the bridge is in service; it can resist load immediately after installation; and it can be re-installed in case of placement error.

The Epoxy Plate method has several installation disadvantages. First, a long curing time of 7 days is required for the epoxy used in the tests. During this time, it may be necessary to restrict traffic on the bridge. Second, the epoxy is brittle, which means no slip can be observed between the steel girder and concrete deck prior to failure. This would require high safety factors to be used in design.

206

Finally, the effects of weathering and extreme temperature on epoxy durability are also unknown for this type of application.

Schaap (2004) compares the expected material costs of different types of retrofit shear connectors, and identifies the Post-Installed Welded Shear Stud as having the lowest material cost, and the Epoxy Plate, the highest. The remaining shear connection methods can be listed in ascending material cost as: the Concrete Screw, the Stud Welded to Plate, the Adhesive Anchor, and the Double-Nut Bolt. This comparison does not include equipment and labor costs. In an actual bridge retrofit project, the labor, equipment, and traffic control costs may significantly outweigh the material costs.

6.6 FURTHER DISCUSSION ON THE SELECTION OF RETROFIT SHEAR CONNECTORS FOR FULL-SCALE BEAM TESTS

The next stage of the overall research program, as described in Chapter 1, is to conduct full-scale tests on composite beams constructed with retrofit shear connectors. Because only a small number of large-scale tests can be conducted, only a limited number of retrofit shear connectors can be evaluated in those tests. This section includes recommendations on which retrofit shear connectors should be considered for further consideration in the full-scale beam tests. These recommendations are based on evaluations of the structural performance and constructability of retrofit shear connectors performed as part of this current study, as well as by Schaap (2004) and Hungerford (2004).

6.6.1 Post-Installed Welded Stud

As a result of tests conducted and evaluations made on the Post-Installed Shear Stud method, it was found that the structural behavior of this connection is governed by the quality of the weld. In this study, the typical static capacity of this connection was not captured due to a brittle failure of a specimen from a

207

defective weld.   Although POSST specimens performed better than CIPST specimen under high-cycle fatigue, the improvement was not significant.   The construction of this connection is also difficult due to the many large diameter holes that are required to be cored through a bridge slab.   As a result, the POSST method is not recommended for full-scale testing unless weld quality can be easily inspected.

6.6.2   Double-Nut Bolt

The Double-Nut Bolt a strong candidate for full-scale beam tests, because it has higher strength at early slip than the cast-in-place welded stud, comparable ultimate strength, and superior high-cycle and low-cycle fatigue life. The Double-Nut Bolt has the longest high-cycle fatigue life of all connectors investigated in this study. Constructability issues discussed for the Post-Installed Welded Stud also apply to the Double-Nut bolt. For the Double-Nut Bolt, however, a smaller diameter hole through the slab and less grout is required, which makes this method more constructible.

6.6.3   High-Tension, Friction Grip Bolt

The High Tension, Friction Grip bolt displayed adequate strength and ductility under static loading compared to the cast-in-place welded stud, and also displayed good high-cycle fatigue behavior. This connector is not recommended for use in the full-scale beam tests, however, due to the many steps and difficulty associated with its installation.

6.6.4   Adhesive Anchor

Static tests on the Adhesive Anchor showed slightly higher strength at early slip, lower ultimate strength and less ultimate slip than the cast-in-place welded stud. Specimens tested under high and low-cycle tests showed better

fatigue performance, as well. In high-cycle fatigue the Adhesive Anchor had the third-longest fatigue life of all retrofit shear connectors. This anchor is easy to install from under the bridge and its installation is minimally destructive to the concrete slab. Except for the time needed for the adhesive to cure, fast installation with minimum traffic disruption is possible. Due to its satisfactory structural performance, easy construction and reasonable cost, the Adhesive Anchor is recommended for full-scale beam tests.

6.6.5   Concrete Screw

The Concrete Screw had a load-slip behavior that was fundamentally different from other connectors tested. The concrete screw required a substantial amount of slip before coming into bearing with the steel plate. It is unclear how this load-slip behavior may affect the overall performance of a composite beam constructed with this connector. Specimens tested under high and low-cycle fatigue showed longer fatigue lives compared to the cast-in-place welded stud. Further, this connector was the simplest to install and can be installed in a bridge without closing the bridge to traffic. Due to the uncertainties over the structural consequences of the unusual load-slip behavior of this connector, however, it is not recommended for further testing at this time. Nonetheless, because of its many important advantages noted above, this connector may merit future consideration.

6.6.6   Epoxy Plate

Although the Epoxy Plate showed very high ultimate strength compared to all connectors investigated, it was not tested further in fatigue and is not recommended for further consideration in the large-scale beam tests. This recommendation is based on this connection's brittle behavior, uncertain

durability and potentially high cost. Like the concrete screw, however, the use of epoxy adhesives to develop composite action may merit future consideration

CHAPTER 7

Summary, Conclusions, and Recommendations

7.1 SUMMARY

This thesis documents the continuation of a study intended to identify possible retrofitting methods to create composite action in non-composite bridge decks. Previous work of Schaap (2004) and Hungerford (2004) identified possible post-installed shear connection methods and their behavior under static loading. Connection methods that showed adequate shear strength and ductility were evaluated, as described in this thesis, on their performance under cyclic loads. The goal of these evaluations was to identify at least one structurally sound, constructible, practical, and cost-effective post-installed shear connector to be tested in large-scale beam tests.

Using a direct-shear test setup, the structural effectiveness of candidate post-installed shear connectors was evaluated through cyclic tests. Tests in high-cycle and low-cycle fatigue indicated the comparative behavior of these shear connectors subjected to repeated service loads and overloads, respectively. Additional static tests were conducted to examine the load-slip behavior of shear connectors under monotonically increasing shear loads. The performance of shear connectors under fatigue and static loading was compared to that of the cast-in-place welded shear stud, which is the reference connector for this application. Those that performed adequately under fatigue and static loading were selected to be used in full-scale beam tests. The installation processes of each shear connection method were also evaluated and their feasibility in a field application was determined.

The following types of shear connectors were investigated in this study:

1) Cast-in-Place Welded Shear Stud (benchmark)

2) Post-Installed Welded Shear Stud

3) Stud Welded to Plate

4) Double-Nut Bolt

5) High-Tension, Friction Grip Bolt

6) Adhesive Anchor

7) Concrete Screw

8) Epoxy Plate

The following sections address the principal conclusions from 8 static tests, 20 high-cycle fatigue tests, and 10 low-cycle fatigue tests, and also make recommendations for those connections to be used in final full-scale testing.

7.2 CONCLUSIONS REGARDING CANDIDATE SHEAR CONNECTORS TESTED AS RETROFIT OPTIONS

1) Structurally sound, constructible, and cost-effective post-installed shear connectors exist for retrofitting non-composite bridge decks.

2) A direct-shear test setup can be used to assess the behavior of shear connectors under static and cyclic loading.

7.2.1 Conclusions from Static Tests

3a) Specimens with non-welded shear connectors, except the High-Tension Friction Grip Bolt and the Epoxy Plate, had lower ultimate shear loads than the cast-in-place welded stud, because a welded stud has a larger effective tensile stress area at the critical shear plane.

212

3b)   Load-slip curves obtained for each shear connection method were comparable to those obtained by Schaap (2004) and Hungerford (2004).

3c)   Specimens using the Concrete Screw showed the lowest connection stiffness and largest slip at ultimate load.

3d)   The Epoxy Plate method, while sufficiently strong, was not studied further because of its brittleness.

3e)   Current design equations do not conservatively predict the ultimate load of cast-in-place or post-installed shear connectors.

3f)   A design equation is proposed that gives a shear capacity equivalent to one-half of the specified ultimate tensile strength of a shear connector.

7.2.2   Conclusions from High-Cycle Fatigue Tests

4a)   Results for Cast-in-Place Welded Stud specimens showed good agreement with data from past research. This confirmed the reliability of the direct-shear testing assembly, specimen design, and testing procedures.

4b)   Based on the S-N curves reported in Chapter 5, all alternative shear connection methods exhibited longer fatigue lives under high-cycle fatigue than the Cast-in-Place Welded Stud.

4c)   In descending order of high-cycle fatigue performance (best first) were the Double-Nut Bolt, the High-Tension Friction Grip Bolt, the Adhesive Anchor, the Concrete Screw, and the Post-Installed Welded Stud.

4c)   Connection methods with welded connectors had shorter fatigue lives than those with non-welded connectors, due to occlusions common in stud welds.

4d)   The Double-Nut Bolt, which includes a rod with rolled threads, had a longer fatigue life than the Adhesive Anchor which consists of a rod with cut threads.

4e)   The application of high-cycle fatigue did not influence the ultimate capacity of the Double-Nut Bolt under subsequent static testing.

4f)   Additional high-cycle fatigue testing would be useful to create more accurate S-N (stress range versus cycles to failure) curves for cast-in-place and post-installed shear connectors.

7.2.3   Conclusions from Low-Cycle Fatigue Tests

5a)   No fatigue failure was obtained for retrofit shear connectors tested under low-cycle fatigue.

5b)   The low-cycle fatigue performance of the Cast-in-Place Welded Stud could not be assessed due to a defective stud weld. This emphasizes the importance of weld inspection.

5c)   Low-cycle fatigue did not significantly influence the ultimate strength of shear connectors under subsequent static loading.

7.2.4 Conclusions regarding the Constructability of Candidate Post-Installed Shear Connectors

6a)   The Adhesive Anchor and the Concrete Screw are alternative retrofit shear connectors that can be easily installed in a bridge with little damage to the bridge deck and with minimal traffic disruption.

6b)   The High-Tension, Friction Grip bolt has several installation steps that are potentially cumbersome to perform on a bridge.

6c)   The structural behavior of connection methods that use welded shear connectors (Cast-in-Place Welded Stud, Post-Installed Welded Stud, and Stud Welded to Plate) is highly dependent on weld quality. These connectors may not be feasible in a retrofit application due to difficulties in weld inspection.

6d)   Shear connection methods that require grouting (the Post-Installed Welded Stud and the Double-Nut Bolt) may introduce problems related to water seepage due to the different weathering rates of the grout material and the concrete slab.

7.3 RECOMMENDATIONS FOR FURTHER TESTING

1)   Full-scale beam tests should be conducted to evaluate the validity of extending these results to real bridge girders.

2)	The Double-Nut Bolt and the Adhesive Anchor are structurally efficient and constructible post-installed shear connectors and should be further tested in full-scale beam tests.

3)	The constructability of recommended shear connectors should be evaluated further during the construction of the full-scale beams.

4)	Selected retrofit shear connectors should be implemented in an existing bridge to finalize evaluations on their structural effectiveness, constructability, practicality, and cost.

APPENDIX A

Test Parameters

Table A.1: Concrete strength of specimens on the day of testing

Specimen	Concrete Strength (psi)
CIPST-ST	3170
POSST-ST	3480
POSST-ST(F)	3620
DBLNB-ST	3520
HTFGB-ST	3620
HASAA-ST	3580
WEDGB-ST	3700
3MEPX-ST	3680

Table A.2: Parameters for high-cycle fatigue tests

Specimen	Stress Range (ksi)	Load Range (kips)	Min. Load (kips)	Max. Load (kips)	Loading Frequency (Hz)	Concrete Strength (psi)
CIPST25	25	11.0	0.9	11.9	2.5	3250
CIPST20	20	8.8	2.0	10.8	2-3.5	3220
CIPST15	15	6.6	3.1	9.7	3-3.5	3380
CIPST10	10	4.4	4.2	8.6	3-5	3240
CIPST10a	10	4.4	4.2	8.6	5	3250
POSST25	25	11.0	0.9	11.9	2-3	3490
POSST20	20	8.8	2.0	10.8	3	3490
POSST20a	20	8.8	2.0	10.8	3	3490
POSST15(F)	15	6.6	3.1	9.7	3.5-5	3620
DBLNB60	60	20.0	0.9	20.9	3	3520
DBLNB40	40	13.4	0.9	14.3	3	3590
DBLNB33	33	11.0	0.9	11.9	2.5	3680
HTFGB45	45	19.9	0.9	20.8	2.5	3680
HTFGB35	35	15.5	0.9	16.4	3-3.5	3680
WEDGB40	40	15.4	0.9	16.3	3	3700
WEDGB30	30	11.5	0.9	12.4	3	3700
WEDGB	25	9.6	1.6	11.2	3	3700
HASAA40	40	13.4	0.9	14.3	3	3590
HASAA35	35	11.2	0.9	12.1	3-3.5	3680
HASAA30	30	10.0	0.9	10.9	3	3700

Table A.3: Parameters for low-cycle fatigue tests

Specimen	Loading Frequency (Hz)	Concrete Strength (psi)
CIPST1	-	3700
DBLNB1	0.5	3700
DBLNB2	0.5	3700
HTFGB1	0.5	3700
HTFGB2	0.5	3700
HTFGB3	0.5	3700
HASAA1	1	3700
HASAA2	1	3700
WEDGB1	1	3700
WEDGB2	1	3700

APPENDIX B

Photos of Failed Specimens in High-Cycle Fatigue Tests

a)

b)
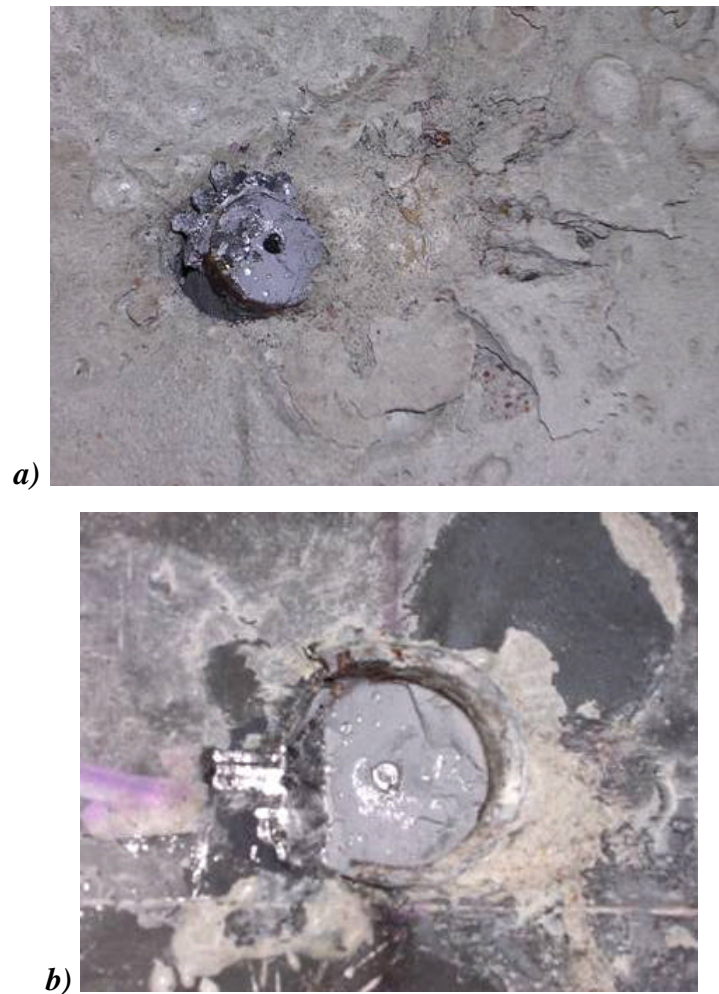
Figure B.1: Failed Specimen CIPST25: a) concrete block, b) steel plate

a)
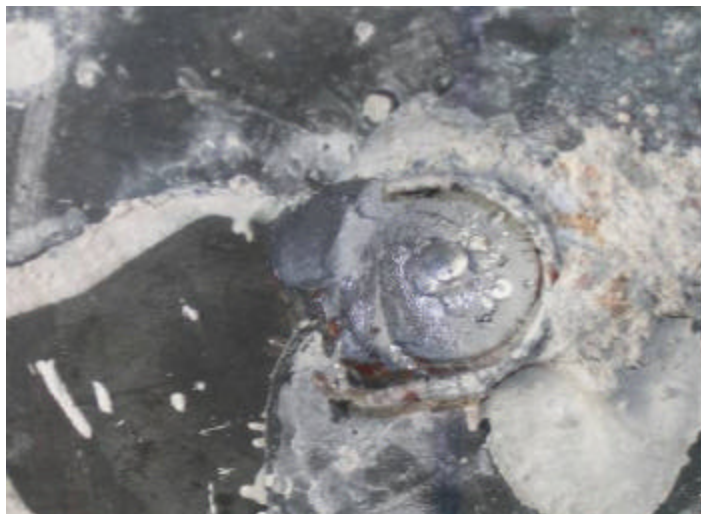
b)

Figure B.2: Failed Specimen CIPST20: a) concrete block, b) steel plate

a)

b)

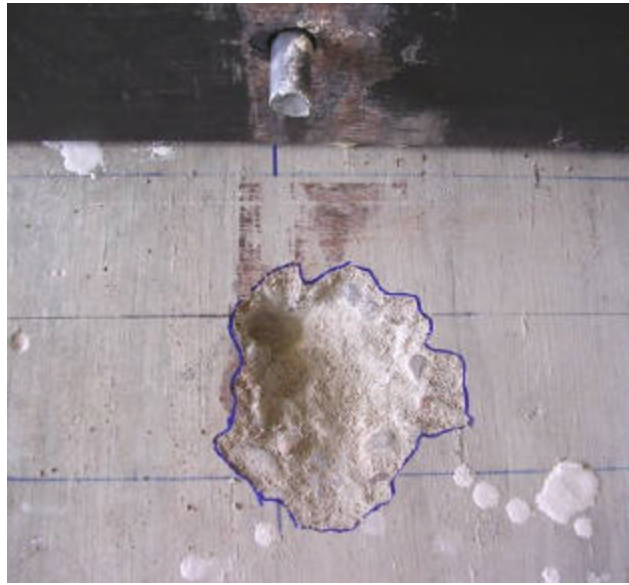**Figure B.3: Failed Specimen CIPST10: a) concrete block, b) steel plate**

a)

b)

Figure B.4: Failed Specimen POSST20a: a) concrete block, b) steel plate

a)

b)

Figure B.5: Failed Specimen DBLNB33: a) concrete block, b) steel plate

a)

b)

Figure B.6: Failed Specimen HASAA35: a) concrete block, b) steel plate

Figure B.7: Failed Specimen WEDGB30

APPENDIX C

Load versus Slip Graphs for High-Cycle Fatigue Tests
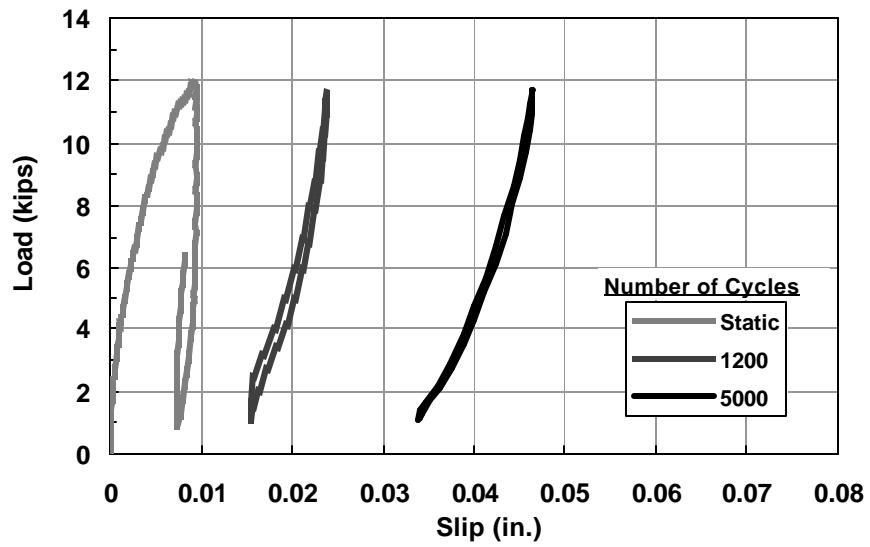
Figure C.1: Static and cyclic load-slip curves for Specimen CIPST25
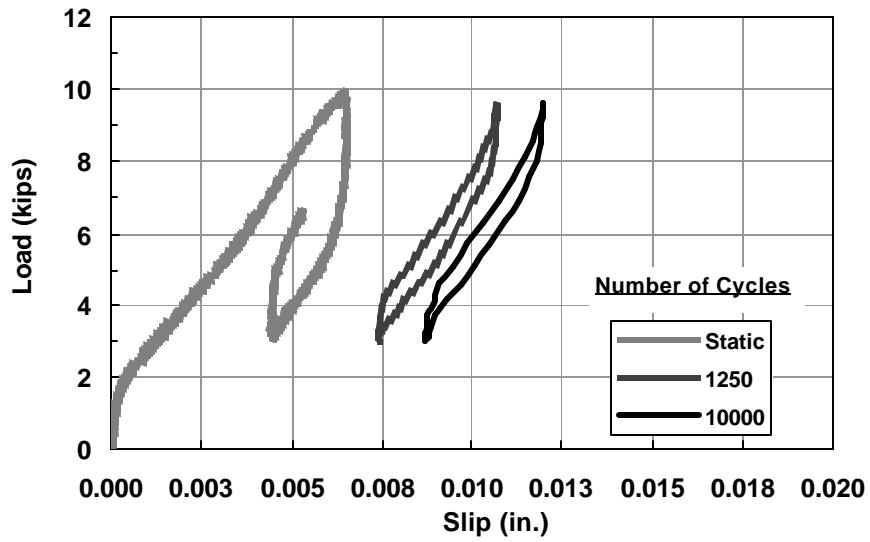
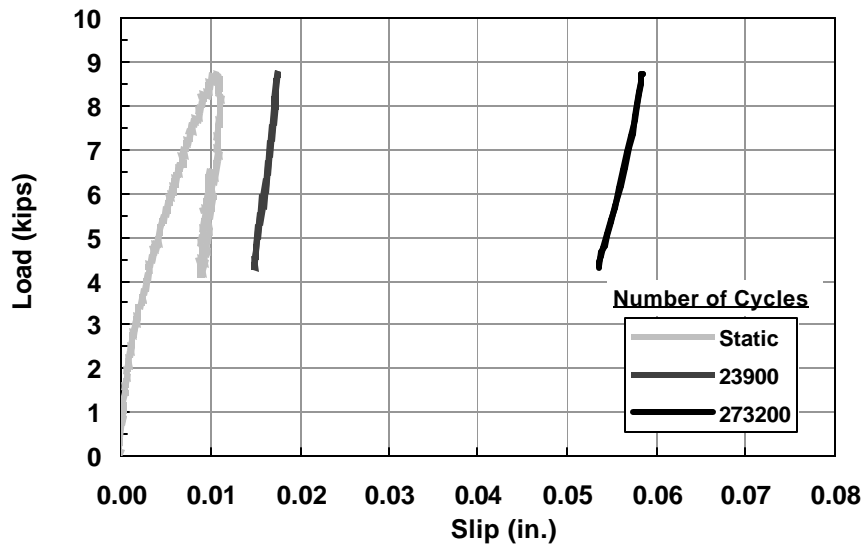*Figure C.2: Static and cyclic load-slip curves for Specimen CIPST15*

Figure C.3: Static and cyclic load-slip curves for Specimen CIPST10
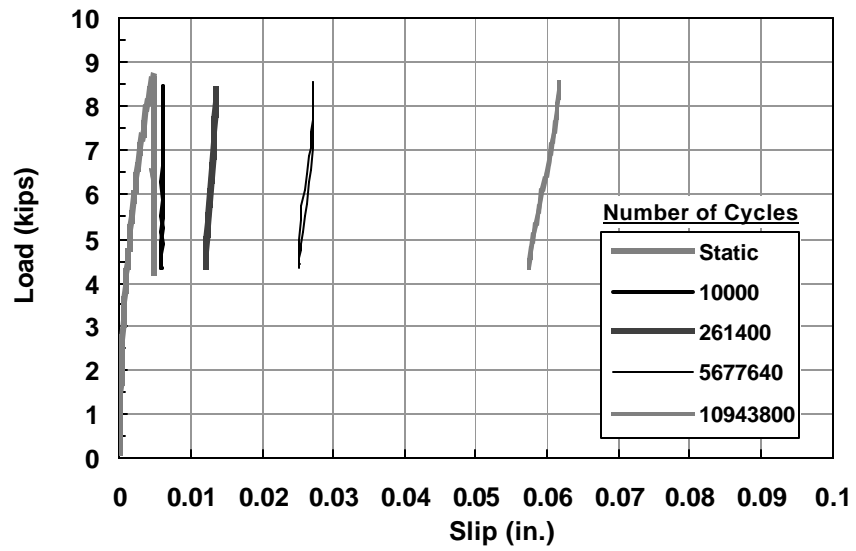
228

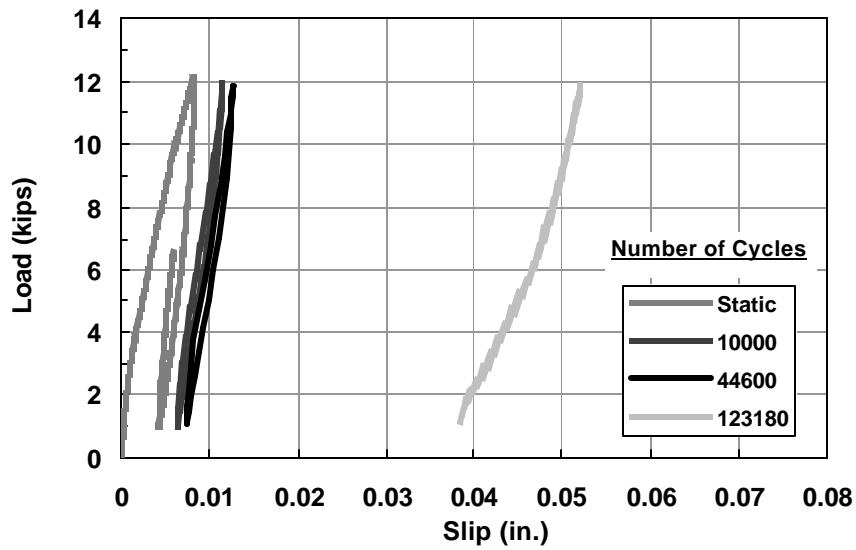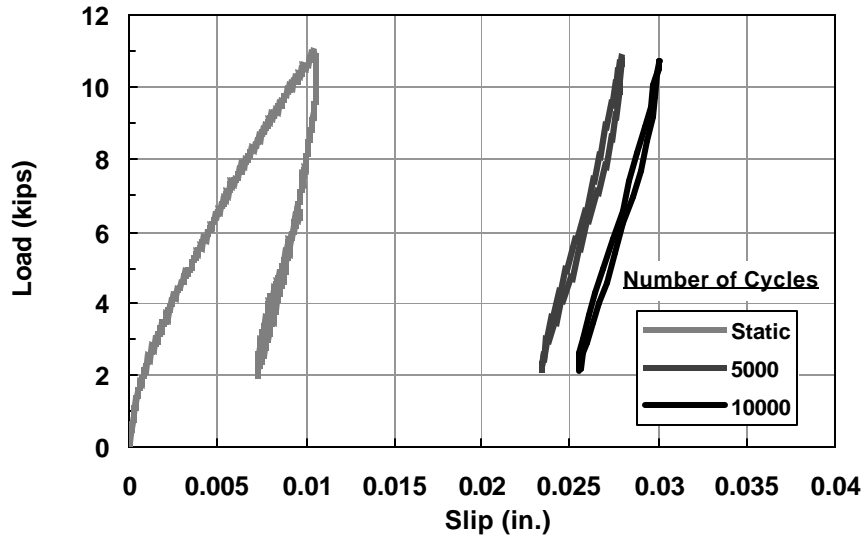*Figure C.4: Static and cyclic load-slip curves for Specimen CIPST10a*

Figure C.5: Static and cyclic load-slip curves for Specimen POSST25

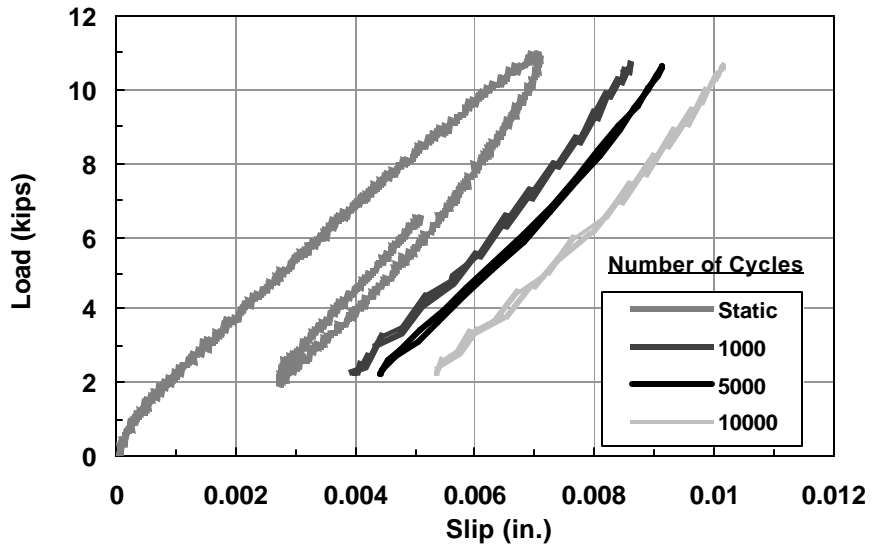*Figure C.6: Static and cyclic load-slip curves for Specimen POSST20*

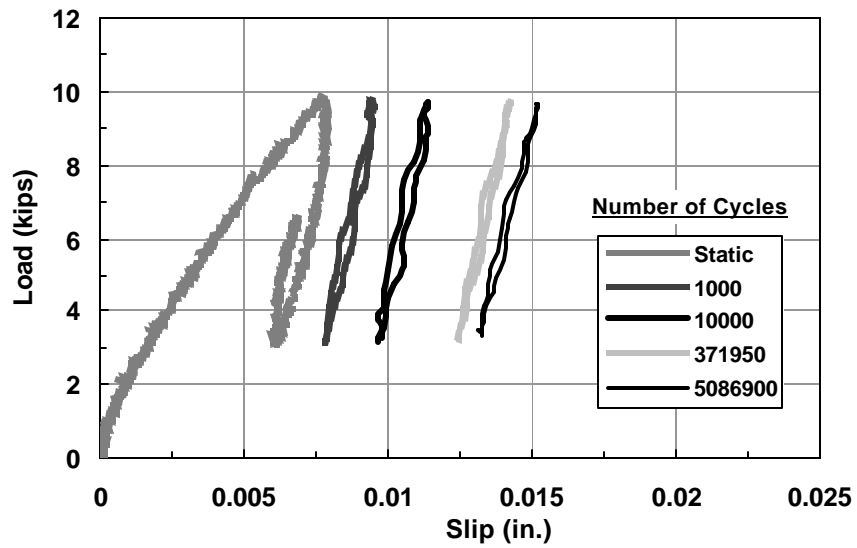*Figure C.7: Static and cyclic load-slip curves for Specimen POSST20a*

230

Figure C.8: Static and cyclic load-slip curves for Specimen POSST15
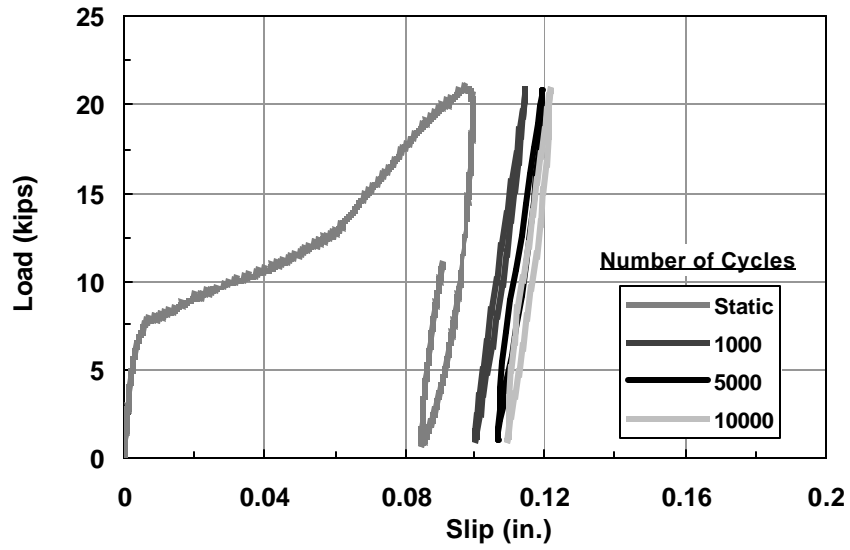

Figure C.9: Static and cyclic load-slip curves for Specimen DBLNB60

Figure C.10: Static and cyclic load-slip curves for Specimen DBLNB40

Figure C.11: Static and cyclic load-slip curves for Specimen DBLNB33
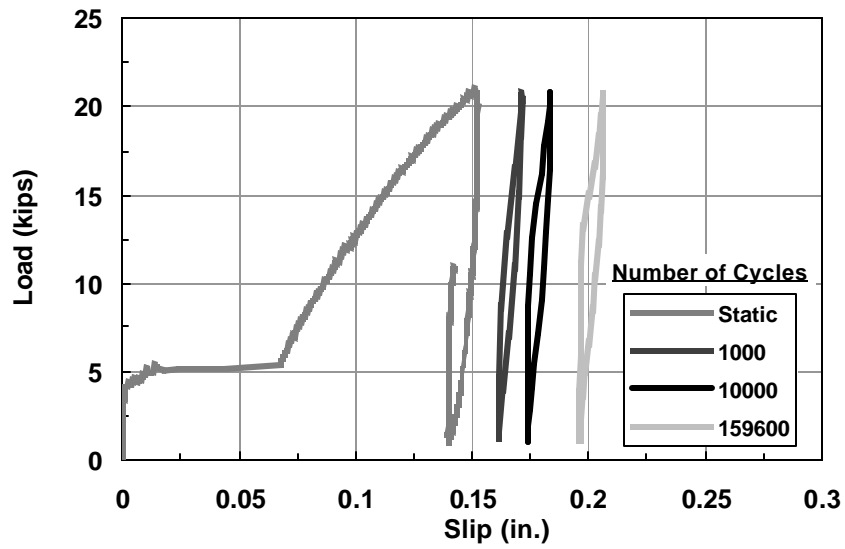
Figure C.12: Static and cyclic load-slip curves for Specimen HTFGB45
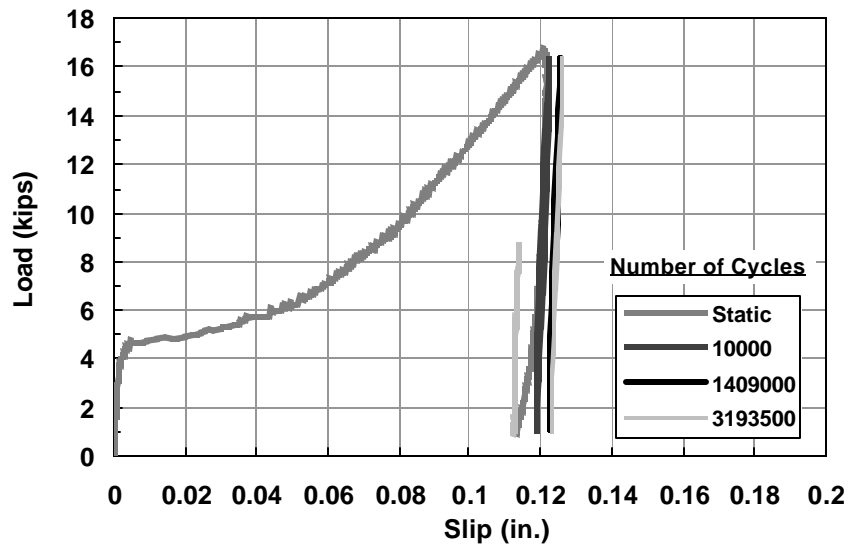
Figure C.13: Static and cyclic load-slip curves for Specimen HTFGB35

233
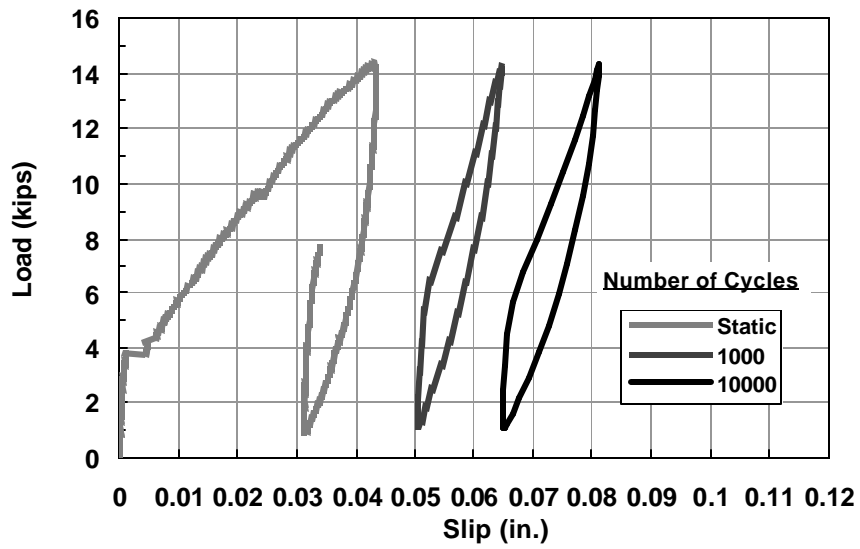
Figure C.14: Static and cyclic load-slip curves for Specimen HASAA40
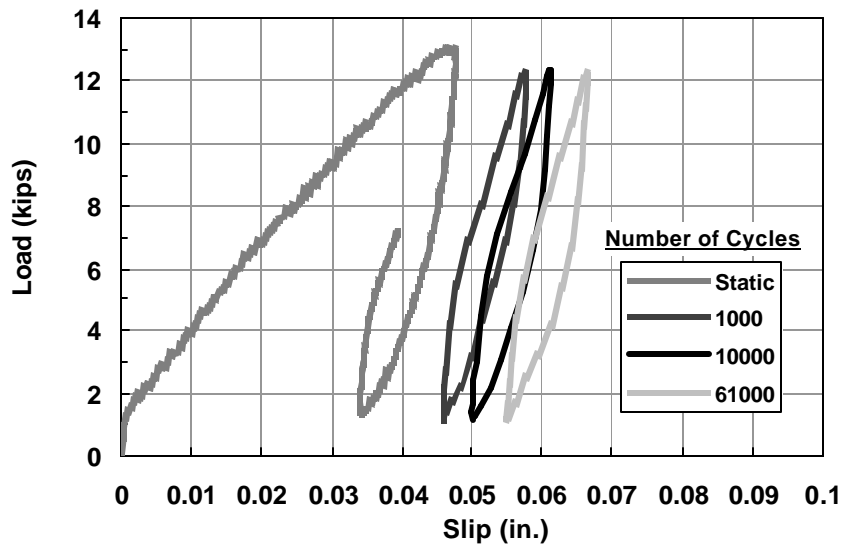
Figure C.15: Static and cyclic load-slip curves for Specimen HASAA35

234
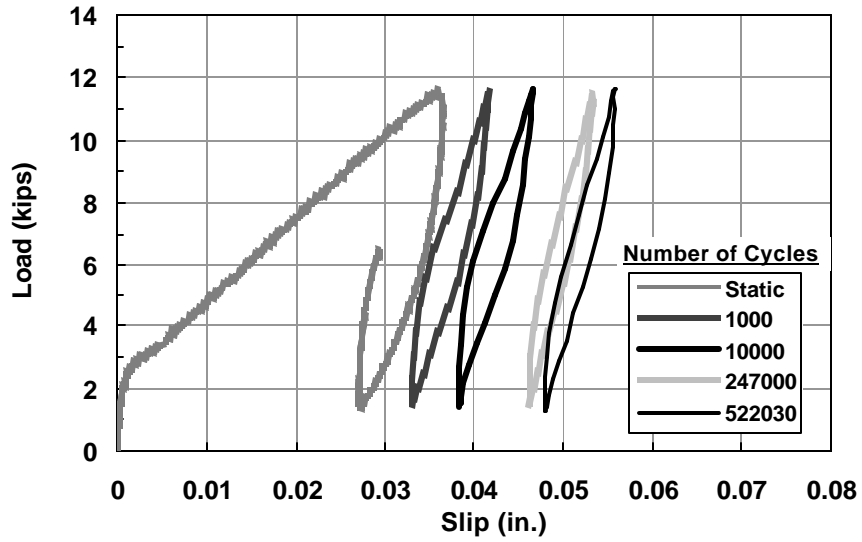
Figure C.16: Static and cyclic load-slip curves for Specimen HASAA30
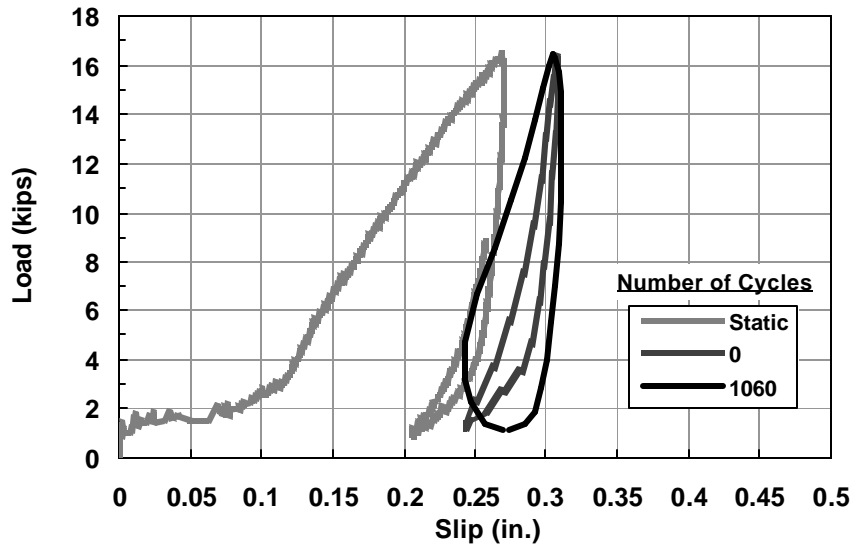
Figure C.17: Static and cyclic load-slip curves for Specimen WEDGB40

235
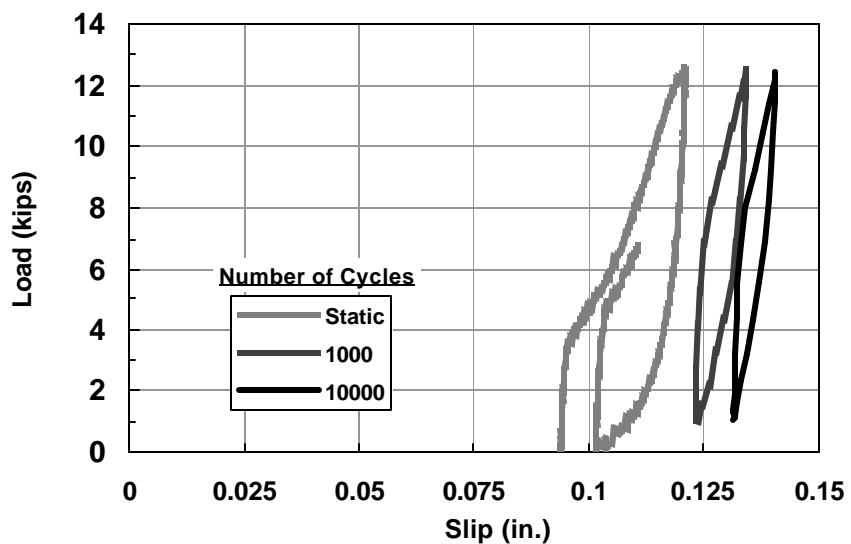
* Initial monotonic cycle was not captured. A second static load was applied.

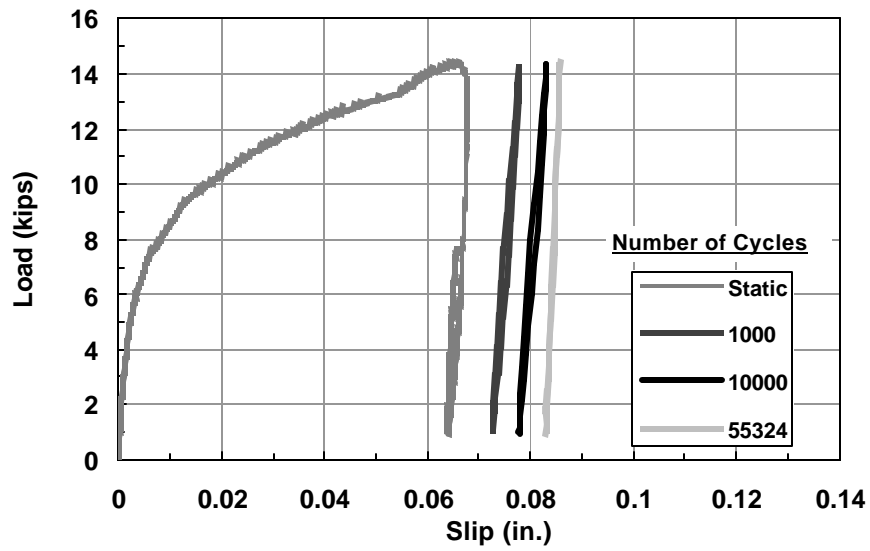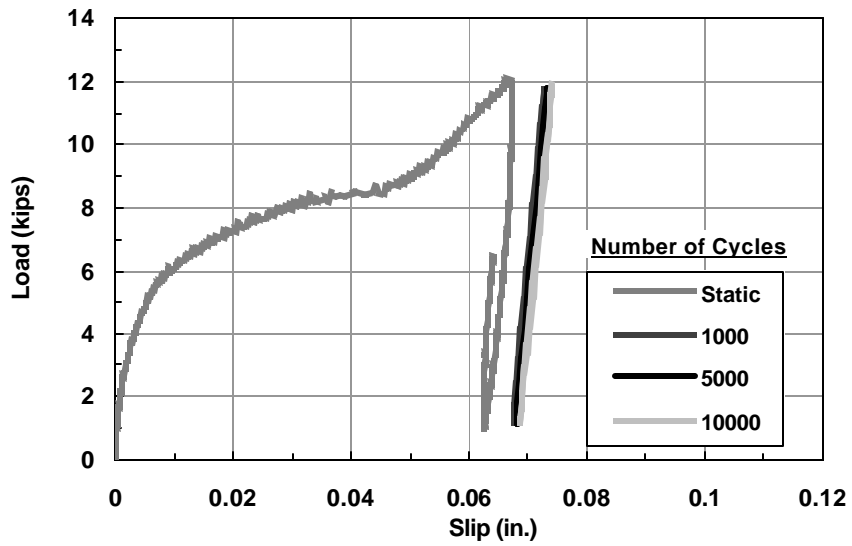*Figure C.18: Static and cyclic load-slip curves for Specimen WEDGB30*
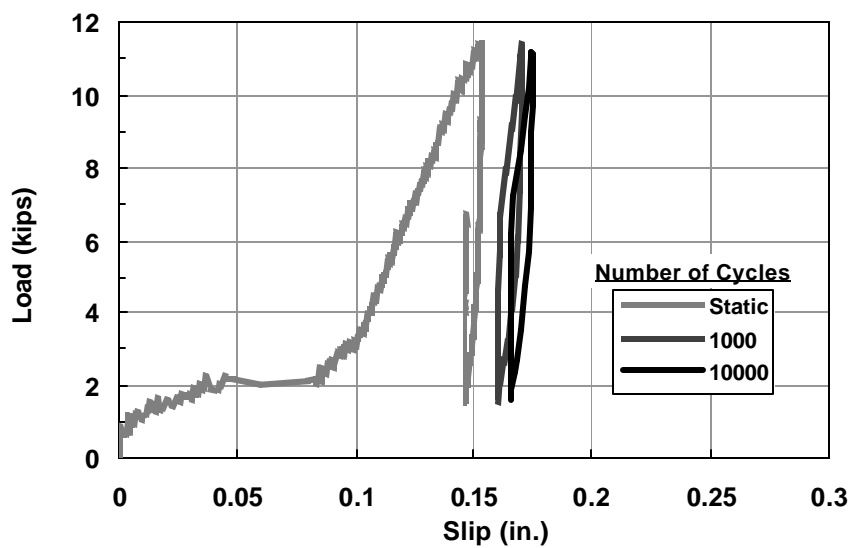
Figure C.19: Static and cyclic load-slip curves for Specimen WEDGB25

APPENDIX D

Photos of Failed Specimens in Low-Cycle Fatigue Tests

a)

b)

Figure D.1: Failed Specimen CIPST1: a) concrete block, b) steel plate

a)

b)
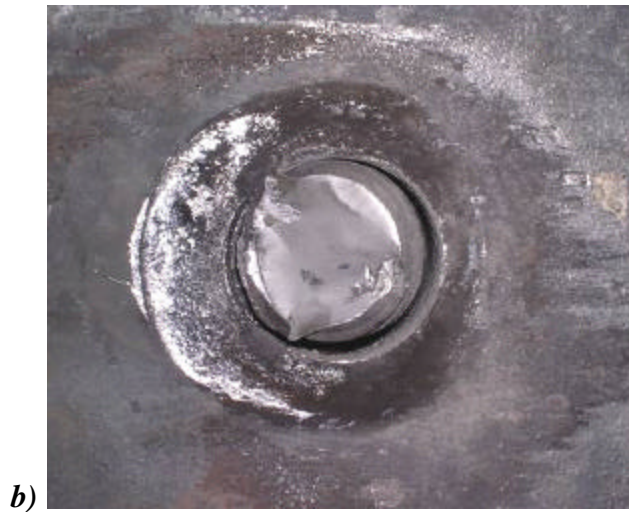
Figure D.2: Failed Specimen DBLNB1: a) concrete block, b) steel plate
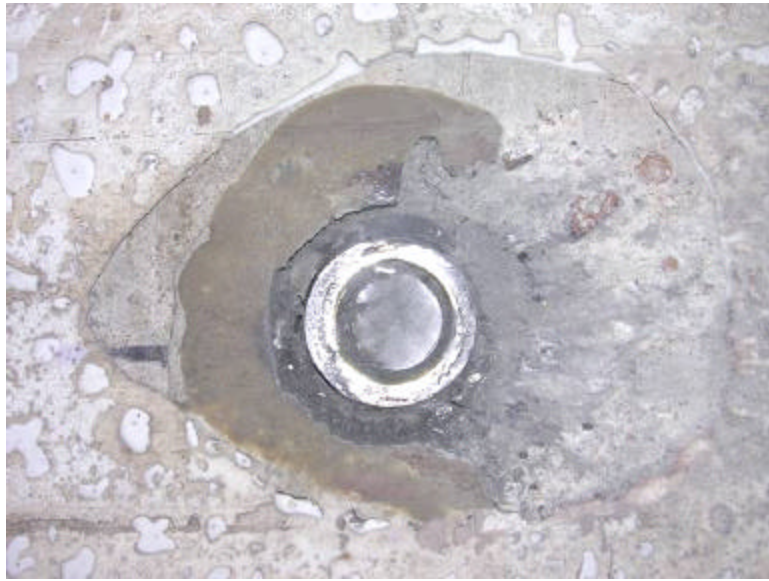
a)

b)

Figure D.3: Failed Specimen DBLNB2: a) concrete block, b) steel plate

Figure D.4: Failed Specimen HTFGB1

Figure D.5: Failed Specimen HTFGB2

Figure D.6: Failed Specimen HTFGB3

Figure D.7: Concrete failure of Specimen HTFGB3

a)

b)

Figure D.8: Failed Specimen WEDGB1: a) concrete block, b) steel plate

APPENDIX E

Load versus Time Graphs for Low-Cycle Fatigue Tests
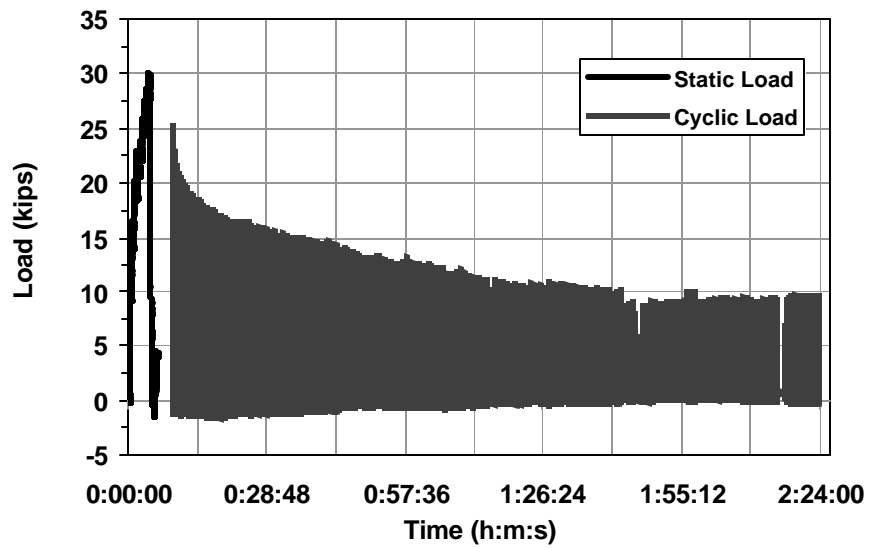
Figure E.1: Change in load sustained by connector over time (Specimen DBLNB1)
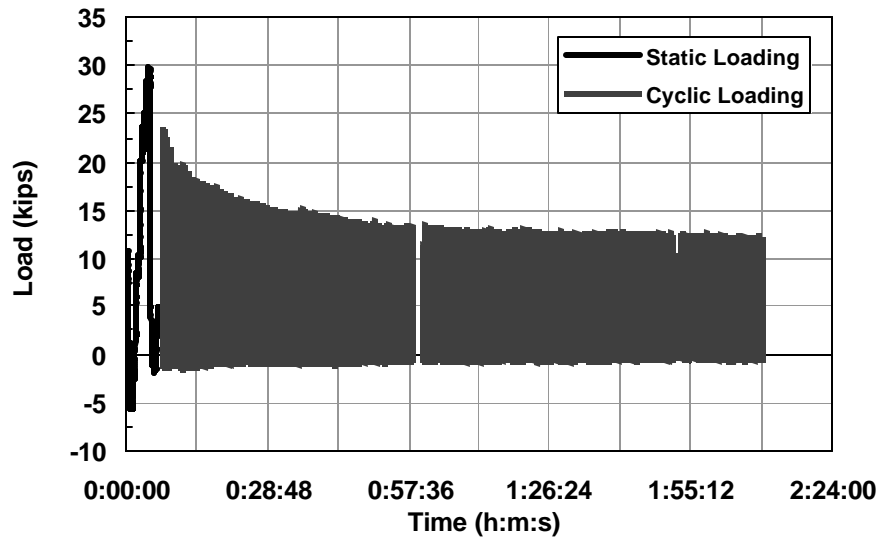
Figure E.2: Change in load sustained by connector over time (Specimen DBLNB2)
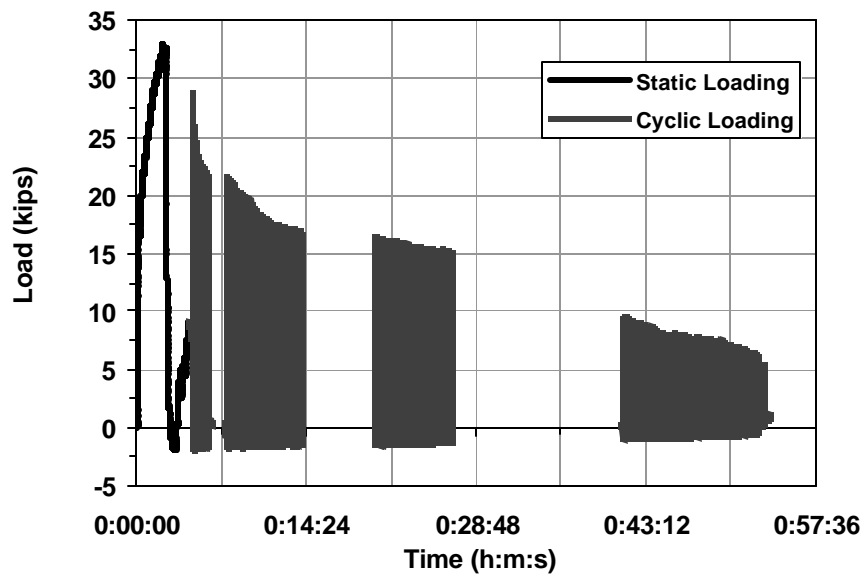
Figure E.3: Change in load sustained by connector over time (Specimen HTFGB1)
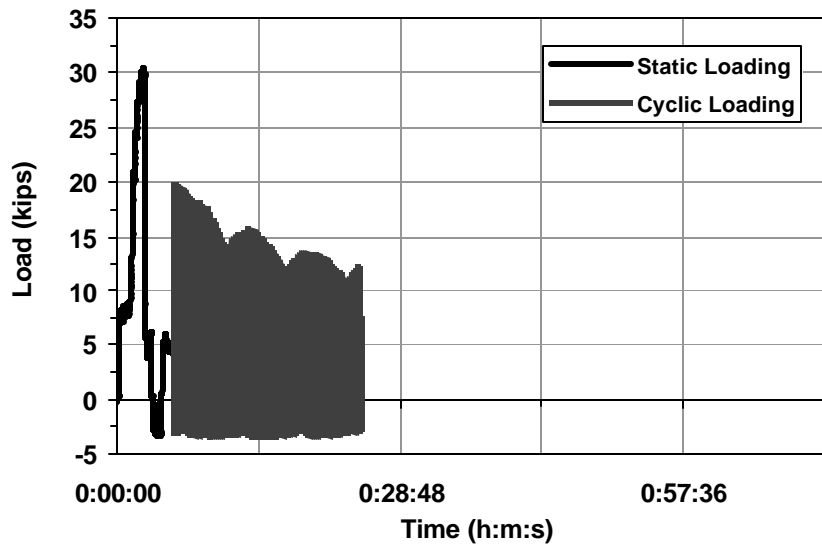
Figure E.4: Change in load sustained by connector over time (Specimen HTFGB2) (up to 600 cycles)
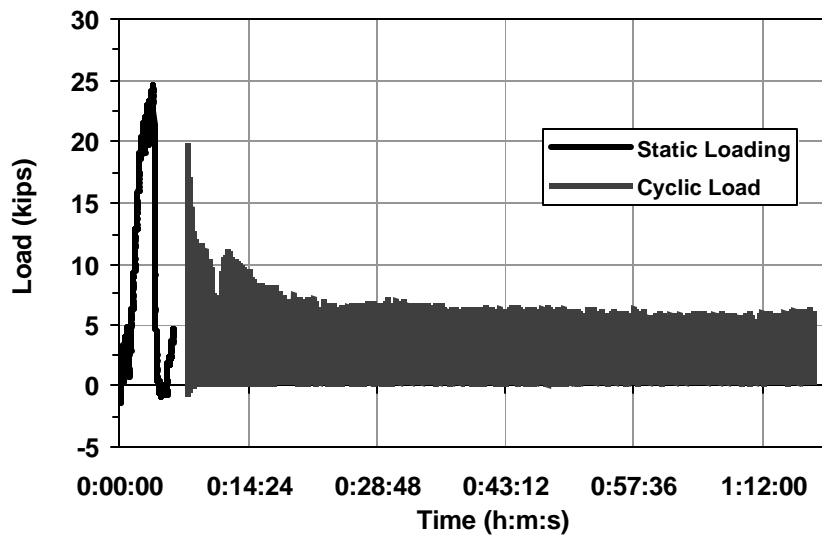
Figure E.5: Change in load sustained by connector over time (Specimen HTFGB3)
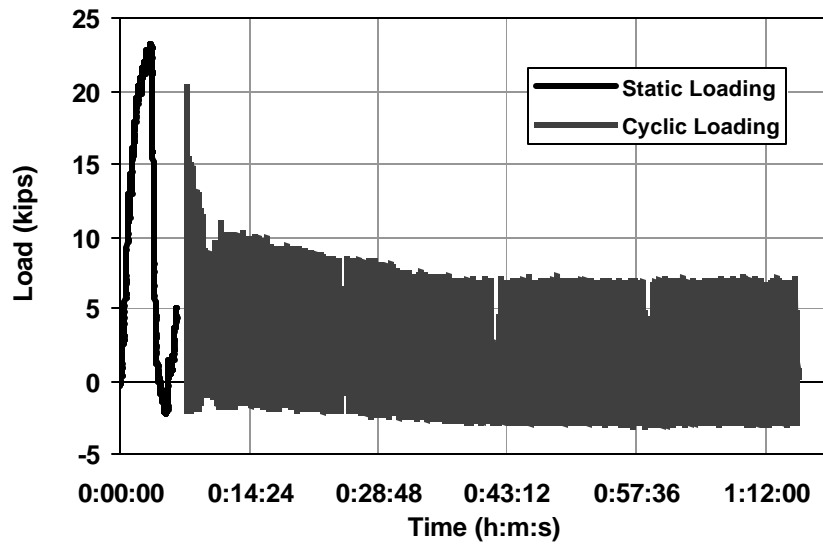
Figure E.6: Change in load sustained by connector over time (Specimen HASAA1)
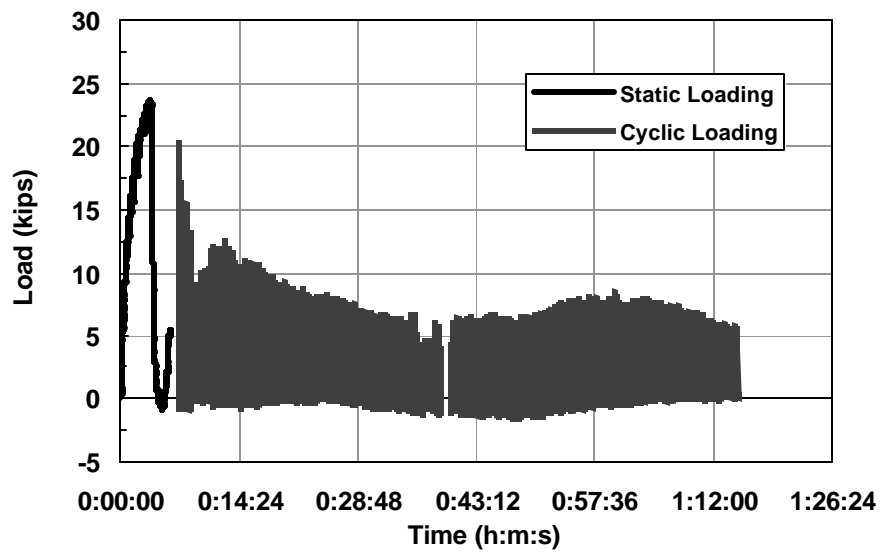
Figure E.7: Change in load sustained by connector over time (Specimen HASAA2)

248
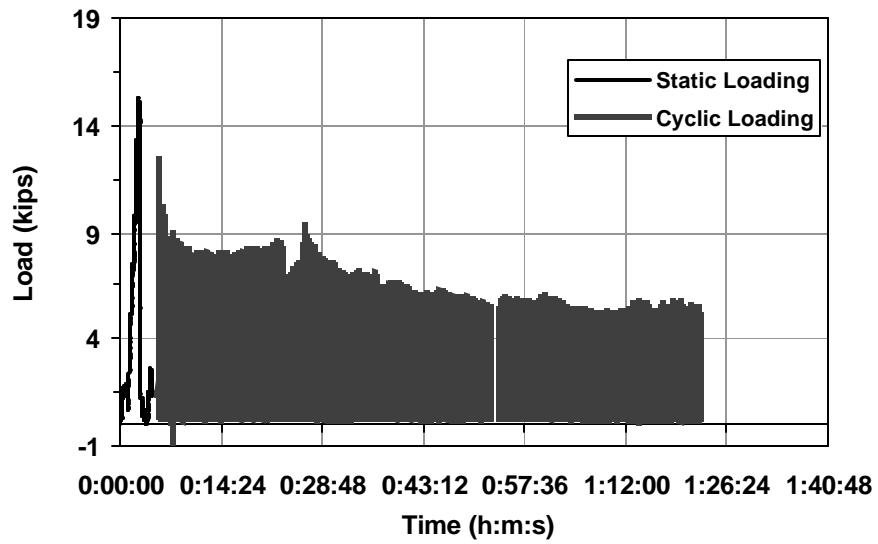
Figure E.8: Change in load sustained by connector over time (Specimen WEDGB1)
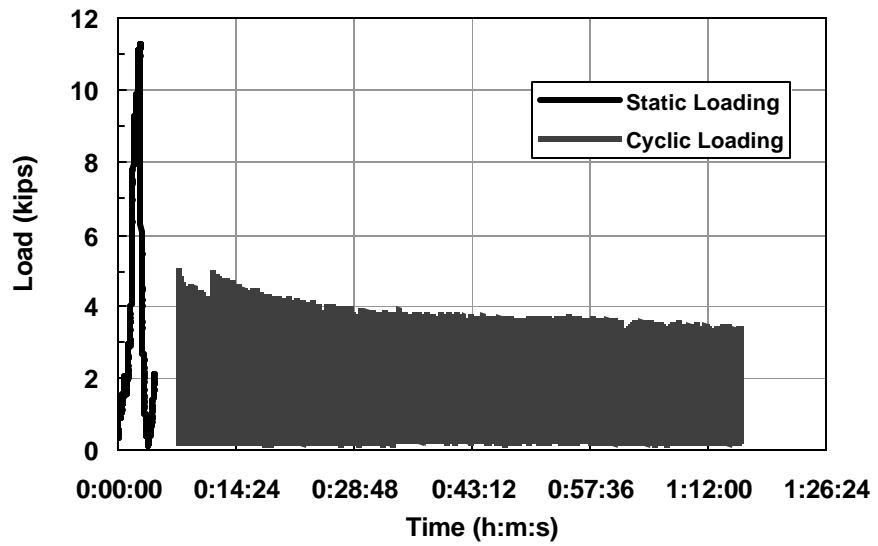
Figure E.9: Change in load sustained by connector over time (Specimen WEDGB2)

249

APPENDIX F

Parameters used for Calculations in Section 6.2.3

Table F.1: Parameters used for equations in Table 6.3 and 6.11

Specimen	A_s (in^2)	f_u (ksi)
CIPST-ST	0.442	60
CIPST01	0.442	60
CIPST02	0.442	60
CIPST03	0.442	60
POSST-ST	0.442	60
POSST01	0.442	60
POSST02	0.442	60
POSST03	0.442	60
DBLNB-ST	0.334	120
DBLNB01	0.334	120
DBLNB02	0.334	120
DBLNB03	0.443	120
HTFGB-ST	0.442	120
HTFGB01	0.442	120
HTFGB02	0.442	120
HTFGB03	0.442	120
WEDGB-ST	0.385	145
WEDGB01	0.385	145
WEDGB02	0.385	145
WEDGB03	0.385	145
HASAA-ST	0.334	72.5
HASAA01	0.334	72.5
HASAA02	0.334	72.5
HASAA03	0.334	72.5

Table F.2: Parameters used for equations in Table 6.4 and 6.12

Specimen	A_s (in^2)	f_u (ksi)
CIPST-ST	0.442	81.2
POSST-ST	0.442	81.2
DBLNB-ST	0.334	152.8
HTFGB-ST	0.442	137.8
WEDGB-ST	0.385	167.7
HASAA-ST	0.334	123.7

Table F.3: Parameters used for equations in Table 6.5

Specimen	A_s (in^2)	f'_c (psi)	f'_g (psi)	f'_{avg} (psi)	E_c^* (ksi)
CIPST-ST	0.442	3170	-	3170	3271
CIPST01	0.442	3200	-	3200	3286
CIPST02	0.442	3200	-	3200	3286
CIPST03	0.442	3200	-	3200	3286
POSST-ST	0.442	3480	7281	6582	4713
POSST01	0.442	3200	4500	4200	3765
POSST02	0.442	3200	5250	4770	4012
POSST03	0.442	3250	5370	4870	4054
DBLNB-ST	0.334	3520	9788	7965	5185
DBLNB01	0.334	3440	3170	3370	3372
DBLNB02	0.334	3440	3180	3380	3377
DBLNB03	0.443	3440	3180	3380	3377
HTFGB-ST	0.442	3620	-	3620	3495
HTFGB01	0.442	3320	-	3320	3347
HTFGB02	0.442	3320	-	3320	3347
HTFGB03	0.442	3320	-	3320	3347
WEDGB-ST	0.385	3700	-	3700	3534
WEDGB01	0.385	3480	-	3480	3427
WEDGB02	0.385	3480	-	3480	3427
WEDGB03	0.385	3480	-	3480	3427
HASAA-ST	0.334	3580	-	3580	3476
HASAA01	0.334	3302	-	3302	3338
HASAA02	0.334	3302	-	3302	3338
HASAA03	0.334	3302	-	3302	3338

* $E_c = w^{3/2} *$sqrt (f'_{avg}), w= unit weight of concrete

Table F.4: Parameters used for equations in Table 6.6

Specimen	A_s (in^2)	f'_c (psi)	f'_g (psi)	f'_{avg} (psi)	E_c^* (ksi)
POSST-ST	0.442	3480	7281	6582	4957
POSST01	0.442	3200	4500	4200	3897
POSST02	0.442	3200	5250	4770	4209
POSST03	0.442	3250	5370	4870	4257
DBLNB-ST	0.334	3520	9788	7965	5748
DBLNB01	0.334	3440	3170	3370	3271
DBLNB02	0.334	3440	3180	3380	3276
DBLNB03	0.443	3440	3180	3380	3276

* $E_c = w^{3/2}*$sqrt (f'_{avg}), w= unit weight of concrete

Table F.5: Parameters used for equations in Table 6.7

Specimen	A_s (in^2)	f_u (ksi)	f¢$_c$ (psi)	f¢$_g$ (psi)	f¢$_{avg}$ (psi)	f¢$_{cu}$ (psi)	E_c^* (ksi)	E_s (ksi)
CIPST-ST	0.442	60	3170	-	3170	3804	3209	29000
CIPST01	0.442	60	3200	-	3200	3840	3220	29000
CIPST02	0.442	60	3200	-	3200	3840	3220	29000
CIPST03	0.442	60	3200	-	3200	3840	3220	29000
POSST-ST	0.442	60	3480	7281	6582	7898	4624	29000
POSST01	0.442	60	3200	4500	4200	5040	3690	29000
POSST02	0.442	60	3200	5250	4770	5724	3940	29000
POSST03	0.442	60	3250	5370	4870	5844	3980	29000
DBLNB-ST	0.334	120	3520	9788	7965	9558	5087	29000
DBLNB01	0.334	120	3440	3170	3370	4044	3309	29000
DBLNB02	0.334	120	3440	3180	3380	4056	3314	29000
DBLNB03	0.443	120	3440	3180	3380	4056	3314	29000
HTFGB-ST	0.442	120	3620	-	3620	4344	3429	29000
HTFGB01	0.442	120	3320	-	3320	3984	3284	29000
HTFGB02	0.442	120	3320	-	3320	3984	3284	29000
HTFGB03	0.442	120	3320	-	3320	3984	3284	29000
WEDGB-ST	0.385	145	3700	-	3700	4440	3467	29000
WEDGB01	0.385	145	3480	-	3480	4176	3363	29000
WEDGB02	0.385	145	3480	-	3480	4176	3363	29000
WEDGB03	0.385	145	3480	-	3480	4176	3363	29000
HASAA-ST	0.334	72.5	3580	-	3580	4296	3410	29000
HASAA01	0.334	72.5	3302	-	3302	3962	3275	29000
HASAA02	0.334	72.5	3302	-	3302	3962	3275	29000
HASAA03	0.334	72.5	3302	-	3302	3962	3275	29000

* $E_c = 57*sqrt (f^{'}_{avg})$

Table F.6: Parameters used for equations in Table 6.8

Specimen	A_s (in^2)	f_u (ksi)	f'_c (psi)	f'_g (psi)	f'_{avg} (psi)	f'_{cu} (psi)	E_c^* (ksi)	E_s (ksi)
CIPST-ST	0.442	81.2	3170	-	3170	3804	3209	29000
POSST-ST	0.442	81.2	3480	7281	6582	7898	4624	29000
DBLNB-ST	0.334	152.8	3520	9788	7965	9558	5087	29000
HTFGB-ST	0.442	137.8	3620	-	3620	4344	3429	29000
WEDGB-ST	0.385	167.7	3700	-	3700	4440	3467	29000
HASAA-ST	0.334	123.7	3580	-	3580	4296	3410	29000

* $E_c = 57 * \text{sqrt} (f'_{avg})$

Table F.7: Parameters used for equations in Table 6.9

Specimen	A_s (in^2)	f_u (ksi)	f′$_c$ (psi)	f′$_g$ (psi)	f′$_{avg}$ (psi)	f′$_{cu}$ (psi)	E_c^* (ksi)	E_s (ksi)
POSST-ST	0.442	60	3480	7281	6582	8737	4624	29000
POSST01	0.442	60	3200	4500	4200	5400	3690	29000
POSST02	0.442	60	3200	5250	4770	6300	3940	29000
POSST03	0.442	60	3250	5370	4870	6444	3980	29000
DBLNB-ST	0.334	120	3520	9788	7965	11746	5087	29000
DBLNB01	0.334	120	3440	3170	3370	3804	3309	29000
DBLNB02	0.334	120	3440	3180	3380	3816	3314	29000
DBLNB03	0.443	120	3440	3180	3380	3816	3314	29000

* $E_c = 57*$sqrt (f′$_{avg}$)

Table F.8: Parameters used for equations in Table 6.10

Specimen	A_s (in^2)	f_u (ksi)	f′$_c$ (psi)	f′$_g$ (psi)	f_{avg} (psi)	f′$_{cu}$ (psi)	E_c^* (ksi)	E_s (ksi)
POSST-ST	0.442	81.2	3480	7281	6582	8737	4624	29000
DBLNB-ST	0.334	152.8	3520	9788	7965	11746	5087	29000

* $E_c = 57*$sqrt (f′$_{avg}$)

References

3M (2003). <u>3M Scotch-Weld™ Epoxy Adhesive DP-460 NS</u>, Technical Data, 3M Engineered Adhesives Division.

AASHTO (2005). <u>LRFD Bridge Design Specifications Interim Customary U.S. Units, 3rd Edition</u>, American Association of State Highway and Transportation Officials, Washington, D.C.

AASHTO (2002). <u>Standard Bridge Design Specifications (2002) 17th Edition</u>, American Association of State Highway and Transportation Officials, Washington, D.C.

AISC (2005). <u>Steel Construction Manual Thirteenth Edition</u>, American Institute of Steel Construction, U.S.A., 2005.

Badie, S.S, Tadros, M.K., Kakish, H.F., Splittgerber, D.L., Baishya, M.C. (2000). "Large Shear Studs for Composite Action in Steel Bridge Girders." *Journal of Bridge Engineering*, 7(3), 195-203.

Dogan, O., Roberts, T.M. (1997). "Fatigue of Welded Stud Shear Connectors in Steel-Concrete-Steel Sandwich Beams." *Journal of Constructional Steel Research*, 45(3), 301-320.

Five Star Products Online (2006). "Five Star® Highway Patch Data Sheet". January 2006. < http://www.fivestarproducts.com/html/f1b7e.html>.

Hilti Online (2004). "Hilti Anchoring Systems, HIT HY 150/HIT-ICE Injections Adhesive Anchor". Hilti Product Technical Guide. March 2006 <http://www.hilti.com>.

Hilti Online (2006). Picture for HIT-HY 150 Curing Injection System. January 2006. <http://www.hilti.com/holcom/modules/prcat/prca_navigation.jsp? OID=9822&fview=1>.

Hungerford, B. E. (2004). *Methods to Develop Composite Action in Non-Composite Bridge Floor Systems: Part II*, MS Thesis, Department of Civil Engineering, The University of Texas at Austin.

Johnson, R. P. (1999). "Resistance of Stud Shear Connectors to Fatigue." *Journal of Constructional Steel Research,* (56), 101-116.

Lehman, H.G., Lew, H.S., Toprac, A.A. (1965). "Fatigue Strength of 3/4 in. Studs in Lightweight Concrete." Center for Highway Research, The University of Texas at Austin

Mainstone, R.J., Menzies, J.B. (1967). "Shear Connectors in Steel-Concrete Composite Beams for Bridges: part 1: Static and Fatigue Tests on Push-out Specimens." *Concrete*, 291-302.

MTS Systems Division (2000). Model 407 Controller Product Manual, Firmware Version 5.3.

N. Gattesco, Giuriani, E. (1996). "Experimental Study on Study Shear Connectors Subjected to Cyclic Loading." *Journal of Constructional Steel Research,* 38(1), 1-21.

N. Gattesco, Giuriani, E., Gubana, A. (1996). Low-Cycle Fatigue Test on Stud Shear Connectors. *Journal of Structural Engineering,* 123(2), 145-115-.

Nakajima, A., Saiki, I., Kokai, M., Doi, K., Takabayashi, Y., Ooe, H. (2003). "Cyclic Shear Force-Slip Behavior of Studs under Alternating and Pulsating Load Condition." *Journal of Engineering Structures* (25), 537-545.

National Bridge Inventory website (2006). NBI Report 2003. February 2006. <http://www.nationalbridgeinventory.com/nbi_report_200322.htm>.

National Bridge Inventory website (2006). NBI Report 2003. February 2006. <http://www.nationalbridgeinventory.com/new_page_30.htm>.

Oehlers, D. J., Bradford, M.A. (1999). *Elementary Behaviour of Composite Steel & Concrete Structural Members*, Butterworth Heinemann, England.

Oehlers, D. J., Seracino, R. (1998). "Low-Cycle Fatigue Test on Stud Shear Connectors." *Journal of Structural Engineering*, 124(5), 599.

Oehlers, D.J. (1990). "Deterioration in Strength of Stud Connectors in Composite Bridge Beams." *Journal of Structural Engineering,* 116(12), 3417-3431.

Oehlers, D.J. (1995). "Design and Assessment of Shear Connectors in Composite Bridge Beams." *Journal of Structural Engineering,* 121, 214-224.

Oehlers, J., Foley, L. (1985). "The Fatigue Strength of Stud Shear Connections in Composite Beams." *Institution of Civil Engineers*, 349-365.

Ollgaard, J.G., Slutter, R.G., Fisher, J.W. (1971). "Shear Strength of Stud Shear Connectors in Lightweight and Normal-Weight Concrete." *AISC Engineering Journal,* 8, 55-64.

Powers Fasteners (2000). Powers Fasteners Wedge-Bolt™ Catalog, Cat. No. 00200, Powers Fasteners, Inc.

Powers Fasteners Online (2006). Powers Fasteners Online Product Specifications, Mechanical Anchors, WedgeBolt™. January 2006. <http://www.powers. com/product_07246.html>.

Schaap, B. A. (2004). *Methods to Develop Composite Action in Non-Composite Bridge Floor Systems: Part I*, MS Thesis, Department of Civil Engineering, The University of Texas at Austin.

Skidmore-Wilhelm Manufacturing Company Online (2006). "Model MS Bolt Tension Calibrator". January 2006. < http://www.skidmorewilhelm.com /products/ms_112_2. asp>.

Slutter, R.G., Fisher, J.W. (1966). "Fatigue Strength of Shear Connectors." *Highway Research Record* (147).

Thurlimann, B. (1959). "Fatigue and Static Strength of Stud Shear Connectors." *Journal of the American Concrete Institute*, 1287-1301.

Viest I.M., R. S. F., R.C. Singleton (1958). Composite Construction in Steel and Concrete for Bridges and Buildings. New York, Toronto, London, McGraw-Hill.

Viest, Ivan M. et al. (1997), Composite Construction: Design for Buildings, McGraw--Hill, New York, NY.

VITA

Hulya Kayir was born on September 29, 1982 in Washington, D.C to parents Ilhami and Sahika Kayir. She attended Purdue University in West Lafayette, Indiana where she graduated with a B.S.C.E in December 2003. In January 2004, she attended The University of Texas as a Graduate Research Assistant, and completed her M.S.E. in May 2006.

Permanent Address: 5235 Kester Ave.

Sherman Oaks, CA 91411

This thesis was typed by the author.